Homo- and heteroaggregation processes involving colloidal particles in the presence of various charged species

Cao, Tianchi

UNIVERSITÉ DE GENÈVE
FACULTÉ DES SCIENCES
Section de chimie et biochimie
Département de chimie minérale et analytique
Professeur Michal Borkovec

Homo- and Heteroaggregation Processes Involving Colloidal Particles in the Presence of Various Charged Species

THÈSE

présentée à la Faculté des sciences de l'Université de Genève
pour obtenir le grade de Docteur ès sciences, mention chimie

par
Tianchi CAO
De
Chine

Thèse N^{o} 5366

GENÈVE
Atelier ReproMail
2019

UNIVERSITÉ DE GENÈVE

FACULTÉ DES SCIENCES

DOCTORAT ÈS SCIENCES, MENTION CHIMIE

Thèse de Monsieur Tianchi CAO

intitulée :

«Homo- and Heteroaggregation Processes Involving Colloidal Particles in the Presence of Various Charged Species»

La Faculté des sciences, sur le préavis de Monsieur M. BORKOVEC, professeur ordinaire et directeur de thèse (Département de chimie minérale et analytique), Monsieur G. HOPFGARTNER, professeur ordinaire (Département de chimie minérale et analytique), Monsieur I. SZILAGYI, professeur (Department of physical chemistry and material science, University of Szeged, Hungary), autorise l'impression de la présente thèse, sans exprimer d'opinion sur les propositions qui y sont énoncées.

Genève, le 15 juillet 2019

Thèse - 5366 -

Le Doyen

N.B. - La thèse doit porter la déclaration précédente et remplir les conditions énumérées dans les "Informations relatives aux thèses de doctorat à l'Université de Genève".

Contents

Abstract

In this thesis, particle aggregation including homo- and heteroaggregaion in different ionic environments was investigated using electrophoresis and light scattering techniques combined with DLVO theory calculations. *Chapter 1* presents a detailed introduction to particle aggregation, the experimental techniques involved, and the outline of the thesis.

In *Chapter 2*, homoaggregation of amidine-modified polystyrene latex (AL) and sulfate-modified polystyrene latex (SL) particles in the presence of salts containing multivalent co-ions was studied. It was observed that the critical coagulation concentration (CCC) of AL particles or SL particles is inversely proportional to the valence of co-ions. Calculation within the theory of Derjaguin, Landau, Verwey and Overbeek (DLVO) also reflects the same behavior. But this dependence is much weaker than that of the CCC on the valence of counterions. The latter is known as the *Schulze-Hardy rule*, which suggests that CCC is inversely proportional to the sixth power of the valence (z) of the counterions. For the present case of co-ions, an analogous *inverse Schulze–Hardy rule* was proposed, which suggests an inverse dependence on the co-ion valence.

Chapter 3 presents homoaggregation of positive AL particles and negative SL particles in the presence of hydrophobic anions—tetraphenylborate (Ph_4B^-)and NaCl as background. Electrophoresis measurements showed that AL particles undergo charge reversal because of the adsorption of Ph_4B^- anions. This charge reversal induced a narrow fast aggregation region, followed by an intermediate regime of slow aggregation. For SL particles, the Ph_4B^- anions also adsorbed onto like-charged particle surfaces, making the particles more negative charged. This accumulation of negative charge leads to an intermediate slow regime. This aggregation behavior can be explained with classical DLVO theory. However, another regime of fast aggregation was observed at intermediate Ph_4B^- concentrations for both types of particles. The occurrence of this regime can be only rationalized when incorporating an additional attractive non-DLVO force is considered. This additional force is probably induced by surface charge heterogeneities.

In *Chapter 4*, heteroaggregation process between AL particles (300 nm in diameter) and SL particles (600 nm in diameter) was studied in two sets of solution systems. One was in inorganic salts containing multivalent anions. In this solution system, AL particles reversed their charge as increasing the salt concentration, while SL particles always kept the same

charge sign. The stability of heteroaggregation went through a maximum at the intermediate salt concentrations where both of AL particles and SL particles are highly negatively charged. The other was in an aliphatic polyamine (N6) and monovalent salt. In this system, the charge of AL particles was hardly affected, while SL particles underwent a significant charge reversal with increasing concentration of N6. Similarly, a pronounced maximum in the stability ratio of heteroaggregation was observed at the intermediate region where both types of particles are highly positively charged. The DLVO theory calculations based on the potentials from electrophoresis measurements can predict this aggregation behavior rather well.

Chapter 5 demonstrates a strategy to measure the heteroaggregation rate over a wider range with the multi-angle light scattering technique. The previously measured heteroaggregation rates with light scattering technique were in a narrow range, over one order of magnitude or less. Herein, specific pair of particles—AL particles (302 nm in diameter) and SL particles (250nm in diameter) were chosen for increasing the contrast of scattering profiles between the different aggregates. The anionic surfactant—sodium n-octyl sulfate (SOS) was used to suppress the homo-aggregates (SL-SL) formed by homoaggregation between SL particles since its scattering profile has similar characteristic peak as that of the formation of hetero-aggregates (AL-SL). As a result, the stability ratios of heteroaggregation were measured over a much wider range, namely more than two orders of magnitude.

Résumé

Dans cette thèse, l'agrégation de particules, y compris l'homo- et l'hétéroagrégaion dans différents environnements ioniques a été étudiée en utilisant des techniques d'électrophorèse et de diffusion de la lumière combinées à des calculs théoriques DLVO. Le chapitre 1 présente une introduction détaillée à l'agrégation de particules, les techniques expérimentales utilisées et les grandes lignes de la thèse.

Au chapitre 2, l'homoagrégation de particules de latex de polystyrène modifié à l'amidine (AL) et de particules de latex de polystyrène modifié au sulfate (SL) en présence de sels contenant des co-ions multivalents a été étudiée. On a observé que la concentration critique de coagulation (CCC) des particules AL ou des particules SL est inversement proportionnelle à la valence des co-ions. Le calcul dans la théorie de Derjaguin, Landau, Verwey et Overbeek (DLVO) reflète également le même comportement. Mais cette dépendance est beaucoup plus faible que celle du CCC sur la valence des contre-ions. Cette dernière est connue sous le nom de règle de Schulze-Hardy, qui suggère que CCC est inversement proportionnelle à la sixième puissance de la valence (z) des contre-ions. Dans le cas présent des co-ions, une règle de Schulze-Hardy inverse analogue a été proposée, ce qui suggère une dépendance inverse de la valence des co-ions.

Le chapitre 3 présente l'homoagrégation des particules AL positives et des particules SL négatives en présence d'anions hydrophobes - tétraphénylborate (Ph_4B^-) et NaCl comme fond. Les mesures d'électrophorèse ont montré que les particules d'AL subissent une inversion de charge en raison de l'adsorption des anions Ph_4B^-. Cette inversion de charge a induit une région d'agrégation rapide étroite, suivie d'un régime intermédiaire d'agrégation lente. Pour les particules SL, les anions Ph_4B^- sont également adsorbés sur des surfaces de particules chargées de la même manière, ce qui rend les particules plus chargées négativement. Cette accumulation de charges négatives conduit à un régime intermédiaire lent. Ce comportement d'agrégation peut être expliqué par la théorie DLVO classique. Cependant, un autre régime d'agrégation rapide a été observé à des concentrations intermédiaires de Ph_4B^- pour les deux types de particules. L'existence de ce régime ne peut être rationalisée que si l'on tient compte de l'incorporation d'une force supplémentaire attrayante qui n'est pas une force de DLVO. Cette force supplémentaire est probablement induite par l'hétérogénéité des charges de surface.

Au chapitre 4, le processus d'hétéroagrégation entre les particules AL (300 nm de diamètre) et les particules SL (600 nm de diamètre) a été étudié dans deux ensembles de systèmes de solution. L'un était dans des sels inorganiques contenant des anions multivalents. Dans ce système de solution, les particules d'AL ont inversé leur charge en augmentant la concentration en sel, tandis que les particules de SL ont toujours gardé le même signe de charge. La stabilité de l'hétéroagrégation est passée par un maximum aux concentrations intermédiaires de sel où les particules AL et les particules SL sont fortement chargées négativement. L'autre était dans une polyamine aliphatique (N6) et un sel monovalent. Dans ce système, la charge des particules d'AL était à peine affectée, tandis que les particules de SL subissaient une inversion de charge significative avec une concentration croissante de N6. De même, un maximum prononcé du rapport de stabilité de l'hétéroagrégation a été observé dans la région intermédiaire où les deux types de particules sont fortement chargées positivement. Les calculs théoriques DLVO basés sur les potentiels des mesures d'électrophorèse permettent de prédire assez bien ce comportement d'agrégation.

Le chapitre 5 présente une stratégie pour mesurer le taux d'hétéroagrégation sur une plus grande plage avec la technique de diffusion de lumière multi-angle. Les taux d'hétéroagrégation mesurés précédemment avec la technique de diffusion de la lumière se situaient dans une plage étroite, sur un ordre de grandeur ou moins. Une paire spécifique de particules - particules AL (302 nm de diamètre) et particules SL (250 nm de diamètre) - a été choisie pour augmenter le contraste des profils de diffusion entre les différents agrégats. Le tensioactif anionique-sodium n-octyl sulfate (SOS) a été utilisé pour supprimer les homo-agrégats (SL-SL) formés par homo-agrégation entre particules de SL puisque son profil de diffusion a un pic caractéristique similaire à celui de la formation des hétéroagrégats (AL-SL). En conséquence, les rapports de stabilité de l'hétéroagrégation ont été mesurés sur une plage beaucoup plus large, à savoir plus de deux ordres de grandeur.

CHAPTER 1

Introduction

Particle suspensions, also generally known as colloids, colloidal systems or colloidal suspensions, consist of dispersed insoluble particles distributed in a liquid medium. The size of these particles is in the range of 1-1000 nanometers. From a broader viewpoint, the dispersed phase can be a gas or a liquid, and the dispersion medium can also be a gas or a solid. Colloidal systems exist ubiquitously in nature and various industrial applications. Examples are smoke and fog, which are formed when fine solid particles or liquid droplets are dispersed in air, ink and paint, which are dispersions of small solid particles in a liquid.

The scientific study of colloids can be traced back to the early nineteenth century.[1] Robert Brown, a British botanist, found that pollen particles suspended in water move around in continuous and random fashion, which was later called Brownian motion. This behavior is the result of the collisions between particles and the surrounding fast-moving water molecules. During the late 1840s Francesco Selmi, an Italian chemist and toxicologist, first systematically studied inorganic particles such as silver chloride and Prussian blue and demonstrated that these particles aggregated by adding salts. Subsequently, Michael Faraday investigated destabilization process of gold suspensions through their color change. He demonstrated that the color of the suspension changed from red (absorption of light by individual gold particles) to blue (absorption of light by gold aggregates) by adding salts.[2] In 1861, Thomas Graham introduced the term “colloid” to describe substances which would not diffuse through a membrane.[3] Graham and Selmi are generally regarded as the founders of colloid science. Initiated by the studies of Selmi and Faraday, tremendous work was conducted on particle aggregation in the following years. However, general theoretical framework to explain these aggregation behaviors was still missing until the 1940s. Two Russian scientists, Derjaguin and Landau, and two Dutch scientists, Verwey and Overbeek, independently established the theory of colloidal stability suggesting that particle aggregation is governed by the interactions between particles, which result from the combination of attractive van der Waals and repulsive double layer forces.[4,5] This theory is referred to as the DLVO theory, which currently is the key to understand the stability of colloids and the interaction between colloidal particles.

Aggregation in particle suspensions is important in material manufacturing as well as in environmental and industrial processes.[3,6-10] In these processes, different behavior of particle aggregation can be established, including rapid particle aggregation, stable particle suspensions and controlled aggregation. In wastewater treatment, to remove the suspended solid particles efficiently, rapid particle aggregation must be induced by adding organic polymer or multivalent metal ions. The resulting large particle aggregates can be removed easily by the subsequent sedimentation or filtration. Papermaking process is another case involving particle aggregation. The raw material is obtained by the aggregation of cellulose fibers and filler particles in a suspension. By contrast, in paint products, stable suspensions of pigments particles are needed. Aggregation of these particles must be avoided for the long-term use of the product. In the field of material science, materials with desired properties can be targeted by control the aggregation of particles. For instance, the architectures of silica-core gold satellites nanoclusters can be precisely controlled by tuning the aggregation/deposition of gold nanoparticles onto the silica nanoparticle.[8] As a result, the optical properties of these core-satellite nanostructures are successfully tailored.

Due to the importance and relevance of particle aggregation in a wide range of applications described previously, aggregation of particles in suspension needs to be well understood.

1.1 Early stages of the aggregation in particle suspensions

Particles suspended in water usually get charged because of the ionization of surface groups or other mechanisms (like ion adsorption). This process will induce that an electrical double layer (EDL) forms around the particles. This EDL force, which can be screened by adding salts, makes the particles repel each other. At the same time, the ubiquitously attractive van der Waals force, which is almost independent of ionic strength, tends to drive the particles together. The overall effect is determined by the combination of EDL repulsion and van der Waals attraction, as suggested by the DLVO theory. Therefore, the particles undergo fast aggregation at high salt concentrations since the EDL force vanishes, while the aggregation rates are small at low electrolyte concentrations. The transition between these two regimes is called the critical coagulation concentration (CCC).

The aggregation of particles in suspension can be induced by adding proper chemicals including simple or complex electrolytes, surfactants or polymers. Initially, one obtains particle doublets or dimers, which is referred to as the early stages of the aggregation process. As the irreversible aggregation process proceeds forward, triplets and larger aggregates form,

which refers to the late stages of the aggregation. At the end, sedimentation due to gravitational forces occurs. Particle aggregation can be divided into homoaggregation, occurring between similar or identical particles, and heteroaggregation, involving dissimilar particles. In the following, they will be discussed separately.

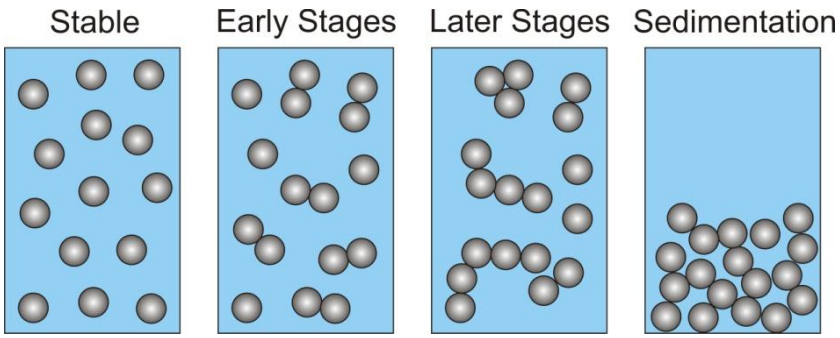

Figure 1. Illustration of stable and unstable colloidal suspensions.

1.1.1 Homoaggregation

Homoaggregation of colloidal particles in the presence of mono- and multivalent electrolytes has been widely studied for a long time and is understood quite well. The DLVO theory was also established based on findings from homoaggregation processes. Accordingly, particle suspension is stable due to the strong EDL repulsion between particles at low electrolyte concentrations. At high salt concentrations, the aggregation of particles is fast since the repulsive EDL force is screened and the attractive van der Waals force dominates. For monovalent salts, the DLVO theory takes into account only the concentration, regardless of their chemical characteristics such as the composition and hydrophobicity. Thus, all the monovalent salts are supposed to give rise to the same CCCs without ion specificity. However, in some situations, the monovalent ions (counterions) may absorb specifically to particle surfaces, which will alter the surface charge and thus modify the double layer force.[11-13]

As a result, the CCCs of particle suspensions may be different in the presence of monovalent ions.[14-18] The Hofmeister series, which is an order of ions based on their absorption ability to surfaces and to their extent of hydration,[19-21] gives a good explanation to this shift in the CCCs. The effect, proposed by Franz Hofmeister, was first used to describe the effects of ion species (anions and cations) on the solubility of proteins.[21] The original Hofmeister series involved ions of higher valence, but only the monovalent ions are discussed here. The case of higher valent ions will be addressed in terms of the Schulze-Hardy rule.

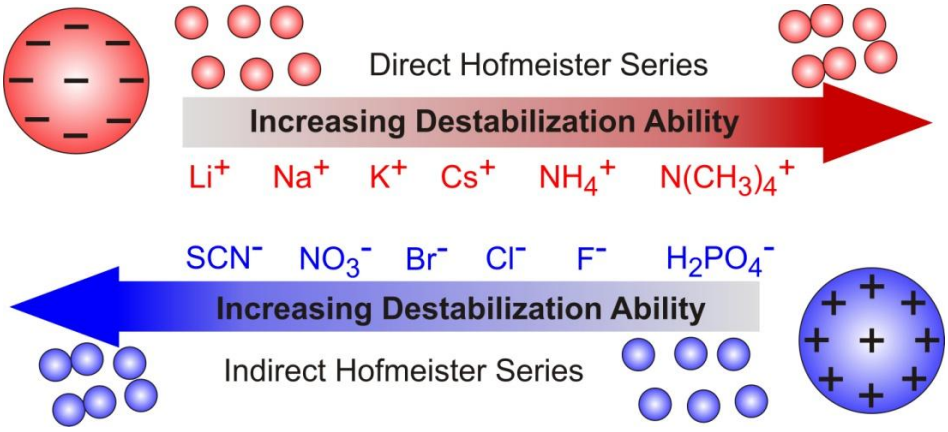

Figure 2. Position of cations and anions in the Hofmeister series for hydrophobic surfaces. Reproduction from reference 14.

As shown as in Figure 2, the CCCs of charged hydrophobic particles in monovalent salts reflect the direct and indirect Hofmeister series.[14] For negatively charged hydrophobic particles, the stabilization ability of cations goes along with the direct Hofmeister series. The ions on the right side give rise to lower CCC, while the ions on the left cause higher one. Oppositely, in the case of hydrophilic particles, the CCCs for positively charged particles obey the direct Hofmeister series, while the CCCs for negatively charged particles reflect the indirect series.[22] In the case of positively charged hydrophobic particles, stabilization ability of anions follows the indirect Hofmeister series. Specifically, the ions on the right side (e.g., $H_2PO_4^-$) tend to cause higher CCC, while the ones on the left side (e.g., SCN^-) can induce the aggregation at low concentration resulting in lower CCC. Although the mechanism of the Hofmeister effect hasn't been understood completely, it is generally believed that the above shift in the CCCs results from the size of the ions and their hydration degree of ions. The anions on the right side (e.g., $H_2PO_4^-$) are small in size and strongly hydrated, while the anions appearing on the left (e.g., SCN^-) with large size are poorly hydrated. The cations are presented in the reverse manner, that large and poorly hydrated ones are situated on the left side while small and strongly hydrated ones on the right. Therefore, in the case of positively charged hydrophobic particles, the strongly hydrated anions (e.g., $H_2PO_4^-$) prefer to stay in the bulk solutions, inducing aggregation at high concentrations. The poorly hydrated ones (e.g., SCN^-) adsorb on the hydrophobic surface more strongly and thus decrease the surface charge, resulting in the lower CCCs. Therefore, the aggregation behavior of positively charged hydrophobic particles follows the indirect Hofmeister series. Regarding the negatively charged hydrophobic particles, the poorly hydrated cations on the left side adsorb to the hydrophobic surface more strongly than the ones on the right side, which leads to the

aggregation of negatively charged hydrophobic particles following the direct Hofmeister series.

As mentioned above, Hofmeister effect considers the composition and hydrophobicity of the monovalent salts. When it comes to the situation of the multivalent salts, Schulze-Hardy rule as well as the classical DLVO theory will be used. Accordingly, multivalent ions are much more effective in destabilizing particle suspensions than monovalent ions.[23,24] For this reason, trivalent salts of iron and aluminum are commonly used inorganic coagulants in wastewater treatment and water purification.[25] The dependence between the CCCs of particle suspensions and the valence of counterions (z) can be shown as:[26-28]

$$CCC \propto \frac{1}{z^n} \tag{1}$$

This dependence has been discovered by Schulze and Hardy more than one hundred years ago when they studied the aggregation of lyophobic sol particles in the presence of various salts. They found that the dependence is followed up to n = 6, which is nowadays known as the Schulze–Hardy rule. This strong dependence can be derived from the DLVO theory only under the assumption that colloidal particles process high surface charge density (more than 1000 mC/m^2). Under the situation of low surface charge density, such as in the range of 10-100 mC/m^2, the dependence of n = 2 is obtained. Actually, the charge density of many colloidal particles is located in this range. In addition to the Schulze–Hardy rule addressing the influence of counterions on CCCs, the dependence of CCCs on the valence of co-ions is also investigated experimentally and theoretically.[29,30] The results show this dependence (n = 1) on the valence of co-ions is relatively weak, which will be discussed in detail in Chapter 2.

Tremendous work has been conducted on the aggregation behavior of various types of particles, such as polystyrene latex, hematite, arsenic sulfide, montmorillonite, silver bromide and layered double hydroxides. [31-36] The dependence of their CCCs on valence of counterions is summarized in Figure 3. The relative CCC decreases with the valence of the counterion in all cases, in spite of the face that the values exhibit substantial system specificity. In some cases, the dependence is even stronger than Schulze–Hardy rule, which is incompatible with DLVO theory. The possible reason is that additional interactions in these colloidal systems exist.

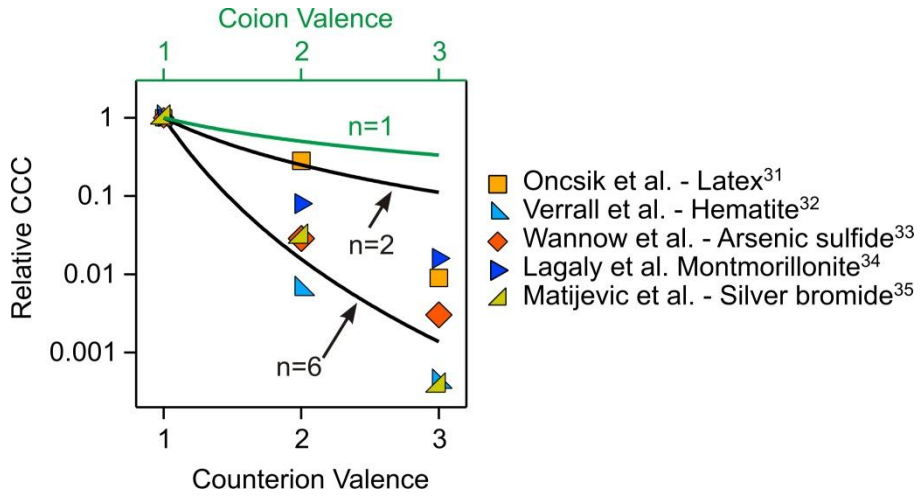

Figure 3. The dependence of relative CCCs of colloidal particles on the valence of counterions and co-ions.

The previous discussion on homoaggregation between colloidal particles focuses on the situation of mono- and multivalent inorganic salts. However, the different types of coagulants are not limited to them. Let us now move to another commonly used ones—oligomer and polyelectrolyte. Oligomer and polyelectrolytes, including polycations and polyanions, are charged macromolecules bearing repeating ionizable or ionized groups. They can be strongly charged when dissolved in aqueous solutions under appropriate pH conditions. Polyelectrolytes with long molecule chains and high charge density are widely used as coagulant or stabilizer for colloidal particles. One of most commonly used oligomers is linear oligoamine. Negatively charged polyelectrolytes include poly(sodium styrene sulfonate) (PSS), poly(acrylic acid) (PAA) and heparin, while the positively charged ones involve polyethylenimine (PEI), linear oligoamine and poly(amidoamine) dendrimer.

The application of oligomers or polyelectrolytes as coagulants or stabilizers for colloidal particles is based on their strong adsorption on particle surfaces.[37] Generally, the strong adsorption of oligomers or polyelectrolytes can make particles undergo charge neutralization and then charge reversal. To demonstrate the influence of oligomers on the charging and aggregation behavior of colloidal particles, the system involving negatively charged polystyrene latex and cationic pentaethylenehexamine (N6) are taken from the literature (Figure 4).[38] At low N6 concentrations, zeta potential is still negative due to the fact that the negatively charged particles are only partially neutralized by the adsorbed cationic N6. With increasing concentration of N6, zeta potential becomes less negative and reaches the isoelectric point (IEP), at which particles are neutralized. After IEP, particles become positively charged due to additional adsorption of N6. Zeta potential reaches a maximum at a

certain N6 concentration, followed by the decrease at highest concentrations. This decrease is due to the screening of the charge by the counterions. The corresponding aggregation behavior as described by the stability ratio is consistent with the charging behavior. Around the IEP, the stability ratio has the lowest value, indicating that particles aggregate rapidly since electrical double layer forces vanish and van der Waals attractive forces are dominant. The stability ratio has very high values, which means particles are stable, at low N6 concentrations as well as at the intermediate region after the IEP. At highest concentrations, this ratio decreases again and reaches unity as feature of the fast aggregation regime. This characteristic behavior in aggregation, destabilization—stabilization— destabilization, has been observed in many colloidal systems.[36,39,40]

As stated above, colloidal particles exhibit characteristic homoaggregation in the presence of various ionic species, including mono- and multivalent salts, and polyelectrolytes. Extensive work has been preformed since more than one century ago. Classical DLVO theory can give a good explanation for these results. However, it is still challenging to predict the aggregation behavior of colloidal particles due to the diversity of particles and the ionic species, for instance, the shape, size and chemical nature of particles as well as their specific interactions with ionic species. More studies still need to be carried out to improve our understanding of particle aggregation in these situations.

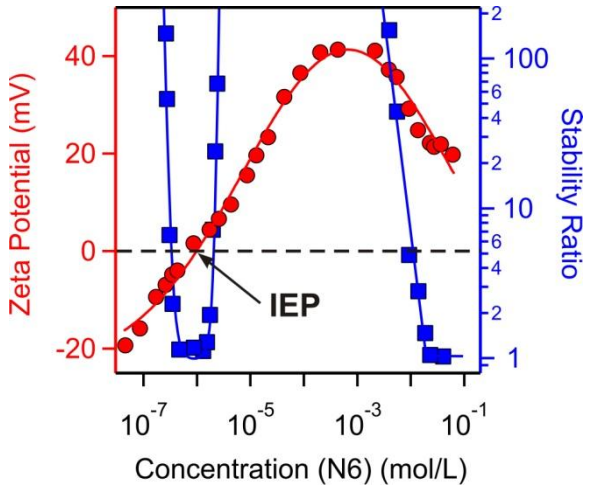

Figure 4. Zeta potential and stability ratio of negatively charged polystyrene latex versus the contentration of cationic pentaethylenehexamine (N6). The data are from reference 38.

1.1.2 Heteroaggregation

Compared to homoaggregation, heteroaggregation has been investigated to a much lesser extent, although it dominates many environmental and industrial processes. These applications include particles with different size and surface charge. For instance, in papermaking, the heteroaggregation between cellulose fibers and particle fillers is the central step to form the raw material. This aggregation process is tuned by adding appropriate amount of polymeric flocculants. Another example includes aggregate formation in water treatment or the preparation of composite materials. [41,42] Unlike homoaggregation, in which the involved system is simple with symmetric and equivalent surfaces, heteroaggregation is more rich and complicated from a conceptual point of view due to the asymmetric system with different particle size and surface charge densities. Therefore, in addition to heteroaggregation process, two homoaggregation processes may undergo simultaneously in the asymmetric system. These aspects make heteroaggregation more difficult to measure than homoaggregation since it needs separate these three aggregation processes properly to extract the heteroaggtregation rate.

Previous studies of such asymmetric systems containing two types of colloidal particles focused generally on two different situations.[43] In the first situation, the two sets of particles have a large disparity in size and opposite surface charges in aqueous solution. In this situation, heteraggregation process is analogous to that smaller particles adsorb onto the much larger ones. When reaching the limit of size ratio between two constituents, the special case for this situation is equivalent to deposition of particles on a planar substrate. In the second situation, the two kinds of particles have different or comparable sizes.

As discussed above, DLVO theory can be used to quantitatively explain homoaggregation. Some research has also been conducted to explore the predictions of this theory for heteroaggregation processes. Vincent and coworkers investigated mixtures of water-soluble polymers coated polystyrene latex particles with largely different sizes and opposite surface charges.[44-46] The adsorption isotherms of particles were used to demonstrate the interaction between small particles and larger ones. They found high-affinity and irreversible adsorption isotherms presented at low ionic strengths, while S-shaped and reversible adsorption at high ionic strengths. These findings can be rationalized within DLVO theory in terms of electrical double layer forces. Accordingly, two sets of forces are present in this system. One is the attractive adsorbing force normal to the interface between small and large particles. The other

is the lateral repulsive force between neighbouring adsorbed small particles. The magnitudes of these two forces are related to the electrolyte concentration. The balance between them results in the patterns of adsorption isotherms of particles. Hansen and Matijevic studied asymmetric systems composed of small latex particles (40 nm in radius) and larger meal oxide particles (250 nm in radius) by measuring the adsorption isotherms between them.[47] They compared the interaction energies obtained from experiments with the ones calculated theoretically. It was found that the electrostatic energy is greatly overestimated within the Hogg-Healy-Fuerstenau (HHF) model, while the values calculated from the two-dimensional Poisson-Boltzmann equation gives much better agreement with the experimental results.

Particle deposition, which is a special case of heteroaggregation, has also been studied by researchers using various techniques, such as reflectivity, optical microscopy or chromatography in a porous bed. [48-51] General understanding has been developed based on the findings. For example, Elimelech has studied deposition process of positively charged polystyrene latex particles onto the collector surface packed with negatively charged glass beads.[51] The experimental results showed that colloid deposition rates increase notably as decreasing the ionic strength of the aqueous solution. DLVO theory is capable to describe this behavior quantitatively. Thereby, the convective diffusion equation could be solved numerically.

The formation and morphology of heteroaggregates in binary mixtures of oppositely charged particles have also been investigated. Dumont *et al*. demonstrated that the structure of the formed heteroaggregates is dominated by the size ratio and the relative number of the interacting units, rather than the chemical nature of particles.[52] Moreover, Furusawa *et al*. have systematically investigated the effects of various synthesis conditions, such as pH, particle size ratio, particle number ratio and salt concentration, on composite particles. The resulting composite formed by heteroaggregation process presented the morphology, a "core" of large polymer particle surrounded by a "shell" of adsorbed small inorganic particles. This core-shell structure based on heteroaggregation or particle adsorption were further employed for materials manufacturing.[53,54]

The second situation of heteroaggregation, in which the particles have different but comparable sizes, has not been studied as much as heteroaggregation between particles with large size difference. The reason is the lack of reliable experimental techniques, which can separate efficiently the heteroaggregation and homoaggregation. Several researchers have

measured the heteroaggregation rate constants using time-resolved light-scattering techniques.[55-57] The systems they explored were limited to the cases in which only heteroaggregation process occurs. To expand the applicability, one can measure the overall apparent aggregation rate as a function of the particle fraction.[58,59] Heteroaggregation and homoaggregation rate constants can be extracted separately from this apparent aggregation rate, which is the weighted superposition of heteroaggregation and homoaggregation contributions. However, this technique still requires tremendous data analysis and restricted choice of particles. Borkovec and coworkers have further proposed the use of the angular-resolved static or dynamic light scattering technique, which is capable of measuring heteroaggregation in binary mixtures of colloidal particles with any size ratio.[60,61] This technique exploits the form factors of different particle doublets, which present specific angular dependence. On the basis of this featured dependence, one can distinguish heteroaggregation and homoaggregation in a single experiment. One of the key points of this technique is the theoretical prediction of form factors. For the small spherical particles, Rayleigh, Debye, and Gans (RDG) theory can be used. For particles of larger size, a more precise computational model, the so-called T-matrix theory, must be used. [62,63] Generally, this technique provides a straightforward separation of both heteroaggregation and homoaggregation processes for a wider range of particle sizes.

Despite the limitations in experimental techniques, researchers still achieved some significant understanding. An important one was that the heteroaggregation rate in the binary mixture of oppositely charged particles is always fast over the whole range of salt concentration, and decreases slowly with increasing the concentration of monovalent salt. This dependence is much weaker compared to that of homoaggregation. Although the surface charge of the particles changes substantially over the range of salt concentration, the corresponding heteroaggregation rate only has a slight change and is almost independent of the magnitude of surface charge. DLVO theory predicts these trends quantitatively. The similar observation was also obtained in the case of the deposition of polystyrene latex particles onto the collector surface packed with oppositely charged glass beads.[51] Furthermore, heteroaggragtion between oppositely charged particles in the presence of multivalent salts also was studied. The results show that the system presents two different patterns of heteroaggregation. The classical pattern corresponds to fast heteroaggregion under all conditions, while the novel pattern shows there is a slow heteroaggregaion regime in an intermediate region. These findings will be discussed in detail in *Chapter 4*.

In spite of the increasing understanding of the heteroaggregation, more studies still need to be conducted. For instance, the previous work mainly focuses on spherical particles. Actually, many particles present various shapes, such as rod-like or plate-like. Modification of current experimental techniques and theory should be pursued to measure and predict the heteroaggregation rates in such systems. Moreover, the concept of heteroaggregation is being growingly recognized in many processes. For example, when engineered nanoparticles are released into the environment, the fate of these materials is determined by their transport and heteroaggregation behavior in aqueous systems. However, the chemical conditions in aquatic environments are complex, including the presence of species of various charges (*e.g.*, mono- and multivalent ions), different pH, or the presence of biological matter and natural colloids with different size and shape. Investigating heteroaggregation process under such conditions would be of significance as well.

1.2 Light scattering methods to investigate particle aggregation

Considering that particle aggregation is of great importance in various applications and in fundamental research, many techniques have been developed to monitor particle aggregation.[64] Among these techniques, turbidity measurements and time-resolved light scattering methods are the widely used ones. In the turbidity measurements, the changes of the transmitted light are measured by a spectrophotometer. It needs a high particle concentration to obtain sufficient signal when particles are small. In this situation, it is difficult to monitor the early stages of particle aggregation.[65] In contrast, time-resolved light scattering methods, including static light scattering (SLS), dynamic light scattering (DLS), and simultaneous static and dynamic light scattering (SSDLS), are very powerful experimental techniques to monitor the particle aggregation kinetic. In SLS, the intensity of the light scattered by the particles is measured as a function of the scattering angle, which provides the structural information concerning the particles and aggregates. In DLS, the fluctuation in scattered light intensity due to Brownian motion is recorded, and is used to determine the particle size. Light scattering techniques are able to measure colloidal particles with a wide range of size, generally between 10 nm and 1000 nm.

Particle aggregation in the early stages leads to the formation of dimers or doublets, which is analogous to a chemical reaction. A or B refers to monomer, and AA, BB or AB refers to dimer.

$$A + A \rightarrow AA \qquad (2)$$

$$B + B \rightarrow BB \quad (3)$$

$$A + B \rightarrow AB \quad (4)$$

This formation of the symmetric and asymmetric dimers can be described in terms of the changes in particle number concentration by the following kinetic equations:

$$\frac{dN_{AA}(t)}{dt} = -\frac{1}{2}\frac{dN_A(t)}{dt} = \frac{1}{2}k_{AA}N_A{}^2(t) \quad (5)$$

$$\frac{dN_{BB}(t)}{dt} = -\frac{1}{2}\frac{dN_B(t)}{dt} = \frac{1}{2}k_{BB}N_B{}^2(t) \quad (6)$$

$$\frac{dN_{AB}(t)}{dt} = -\frac{dN_A(t)}{dt} = -\frac{dN_B(t)}{dt} = k_{AB}N_A(t)N_B(t) \quad (7)$$

where t is the time, N_A and N_B the number concentrations of monomers, and N_{AA}, N_{BB} and N_{AB} the number concentrations of dimers. The homoaggregation rate constants for the formation of dimers (AA and BB) are expressed as k_{AA} and k_{BB}, while k_{AB} is heteroaggregation rate constant.

These aggregation rates can be measured experimentally with light scattering. The classical setup of light scattering is demonstrated in Figure 5. When a coherent and monochromatic laser beam (incident light, I_0) passes through the colloidal suspension, the light will be scattered by particles in all directions and can be monitored at a certain angle by the photon counter detector. The scattered light interferes either constructively or destructively due to particles undergoing Brownian motion, which makes the intensity of the scattered light to fluctuate over time. The characteristics of the scattered light are directly related to the size and shape of particles. Thus, particle aggregation process will have an influence on these

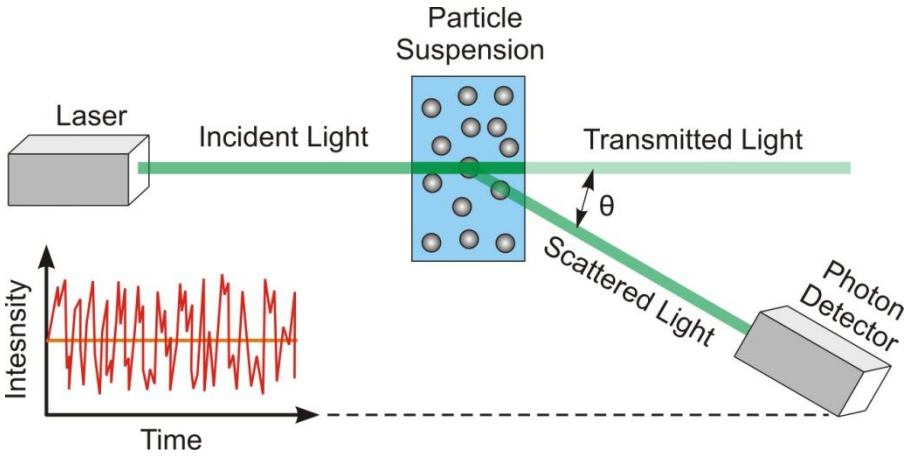

Figure 5. Illustration of light scattering setup.

characteristics. The aggregation rates can be determined by probing these changes in the scattered light over time.

1.2.1 Static light scattering

First using homoaggregation of particle A as an example, at the early stages of particle aggregation, where the suspension is dominated by monomers and dimers, the intensity of the total scattered light is the sum of that for monomers and dimers, and can be written as:[66]

$$I(q,t) = I_{\mathrm{A}}(q)N_{\mathrm{A}}(t) + I_{\mathrm{AA}}(q)N_{\mathrm{AA}}(t) \tag{8}$$

where $I_{\mathrm{A}}(q)$ and $I_{\mathrm{AA}}(q)$ are the scattered intensities of monomers and dimers, and $q = (4\pi n/\lambda)\sin(\theta/2)$ refers to the magnitude of the scattering vector in which θ is the scattering angle, n is the refractive index of the medium and λ is the wavelength of the light in vacuum. By differentiating equation (8) with respect to the time, one can obtain:

$$\frac{\mathrm{d}I(q,t)}{\mathrm{d}t} = \frac{\mathrm{d}N_{\mathrm{A}}(t)}{\mathrm{d}t} I_{\mathrm{A}}(q) + \frac{\mathrm{d}N_{\mathrm{AA}}(t)}{\mathrm{d}t} I_{\mathrm{AA}}(q) \tag{9}$$

By inserting equation (5), equation (9) becomes:

$$\frac{\mathrm{d}I(q,t)}{\mathrm{d}t} = -k_{\mathrm{AA}} {N_{\mathrm{A}}}^2 I_{\mathrm{A}}(q) + \frac{1}{2} k_{\mathrm{AA}} {N_{\mathrm{A}}}^2 I_{\mathrm{AA}}(q) \tag{10}$$

The apparent static rate (Σ) is defined as:[66]

$$\Sigma = \frac{1}{I(q,0)} \left(\frac{\mathrm{d}I(q,t)}{\mathrm{d}t} \right)_{t \to 0} = \left(\frac{I_{\mathrm{AA}}(q)}{2I_{\mathrm{A}}(q)} - 1 \right) k_{\mathrm{AA}} N_{\mathrm{A}} \tag{11}$$

where $I(q,0)$ is the total scattering intensity at the initial time ($t = 0$), and $I(q,0) = I_{\mathrm{A}}(q)N_{\mathrm{A}}(0)$ since there are only monomers in the system. According to the above equation, the values of the scattering intensities for monomers and dimers, $I_{\mathrm{A}}(q)$ and $I_{\mathrm{AA}}(q)$, should be known to calculate the aggregation rate k_{AA}. For small and spherical particles, Rayleigh–Gans–Debye (RGD) theory is commonly used to describe their light scattering properties. Based on RGD theory, the scattered intensity of particles or aggregates can be written as:

$$I_z(q) \propto {V_z}^2 P_z(q) \tag{12}$$

where z refers to the type of particle, such as monomers (A) and dimers (AA), V_z refers to the volume of the particle I, and $P_z(q)$ is the form factor. Within the RDG approximation, the expression of the form factor for a spherical particle A is written as:[68]

$$P_A(q) = \frac{9}{(qr)^6}\left[\sin(qr) - qr\cos(qr)\right]^2 \tag{13}$$

where r is the radius of the monomer A. The form factor of an z-fold aggregate formed by monomers A can be expressed as a sum over all particle centers in the aggregate, as follows:[66]

$$P_z(q) = \frac{P_A(q)}{z^2}\left[\sum_{i,j}\frac{\sin(r_{ij}q)}{r_{ij}q}\right] \tag{14}$$

where z is equal to 2 for doublets (AA), and r_{ij} is the distance between the particle i and j in the aggregate. Using equations (13) and (14), the value of $\left[I_{\mathrm{AA}}(q)/2I_{\mathrm{A}}(q)-1\right]$ in the equation (11) is approximately equal to $\left[\sin(2qr)/2qr\right]$. Thus, equation (11) containing the aggregation rate coefficient k_{AA} can be rewritten as:

$$\Sigma = \frac{1}{I(q,0)}\left(\frac{\mathrm{d}I(q,t)}{\mathrm{d}t}\right)_{t\to 0} = \frac{\sin(2qr)}{2qr}N_{\mathrm{A}}k_{\mathrm{AA}} \tag{15}$$

where $\left[\mathrm{d}I(q,t)/\mathrm{d}t\right]_{t\to 0}$ is the rate of the change in the scattering intensity at the initial time, which can be obtained from the slope of the measured intensity over time at a certain q (or

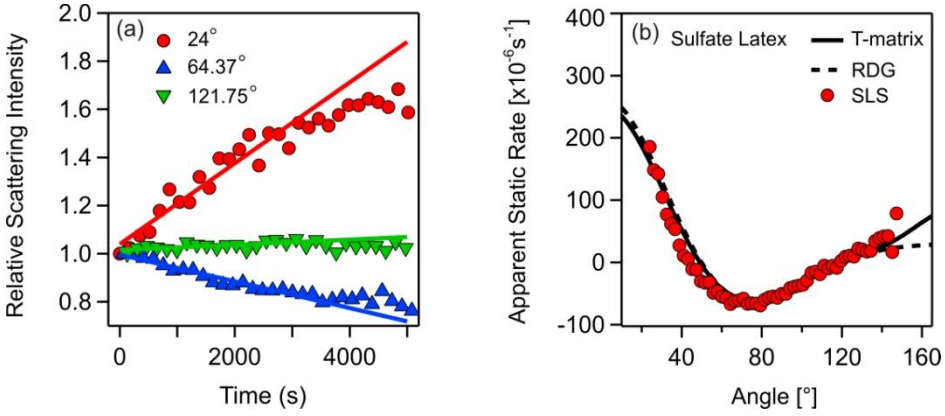

Figure 6. Relative change in scattering intensity (a) and apparent static rate as a function of the scattering angle (b) for homoaggregation of sulfate latex in 800 mM NaCl.

scattering angle θ), as shown as the straight lines in the Figure 6(a). Also, one can notice that the values of the slope depend on the scattering angle (or scattering vector). The dependence of Σ on the scattering angle is shown in Figure 6(b). This angular dependence can be fitted with the form factors calculated using RGD or T-matrix theory. The absolute fast aggregation rate coefficient k_{AA} is then the only adjustable parameter. By this way, the homoaggregation rate constant k_{AA} is measured by static light scattering.

For large particles, RDG approximation may be inaccurate in calculating the scattered intensity. To improve the accuracy, the Maxwell equations, which describe electromagnetic field of the scattered light must be solved exactly. The T-matrix method is very powerful in computing the scattered intensity of large particles or arbitrary aggregates composed of spherical particles.[63,69] This method generates accurate estimation of optical properties of colloidal particles with large size.

Now let us look at the situation of heteroaggregation in mixtures of particles A and B. The intensity of the total scattered light includes three contributions, namely two homoaggregations AA and BB, and one heteroaggregation AB. It can be written as:[38]

$$I(q,t) = \sum_{z} I_z(q) N_z(t) \tag{16}$$

where the letter *z* represents one of the elements A, B, AA, BB, and AB. The corresponding scattering intensities of monomers and dimers are expressed as $I_{\mathrm{A}}(q)$, $I_{\mathrm{B}}(q)$, $I_{\mathrm{AA}}(q)$, $I_{\mathrm{BB}}(q)$, and $I_{\mathrm{AB}}(q)$. Similarly, by differentiating equation (16) and inserting the result into equation (7), the apparent static rate (Σ) for the mixture can be written as:[38]

$$\Sigma = \frac{1}{I(q,0)}\left(\frac{\mathrm{d}I(q,t)}{\mathrm{d}t}\right)_{t\to 0} = k_{\mathrm{AA}}F_{\mathrm{AA}}(q) + 2k_{\mathrm{AB}}F_{\mathrm{AB}}(q) + k_{\mathrm{BB}}F_{\mathrm{BB}}(q) \tag{17}$$

where $I(q,0) = I_{\mathrm{A}}(q)N_{\mathrm{A}}(0) + I_{\mathrm{B}}(q)N_{\mathrm{B}}(0)$ is the total scattering intensity at the initial time ($t = 0$). The functions $F_{\mathrm{ij}}(q)$ are given by:[60]

$$F_{ij}(q) = N_0 x_i x_j \frac{I_{ij}(q) - I_i(q) - I_j(q)}{2\left[x_{\mathrm{A}} I_{\mathrm{A}}(q) + x_{\mathrm{B}} I_{\mathrm{B}}(q)\right]} \tag{18}$$

where *i* and *j* refers to particles A and B. N_0 is the initial particle number concentration and is given by $N_0 = N_{\mathrm{A}}(0) + N_{\mathrm{B}}(0)$. The particle number fraction is given by $x_i = N_{\mathrm{i}}(0) / N_0$.

Similarly, for small particles, the scattering intensities, $I_{\mathrm{A}}(q)$, $I_{\mathrm{B}}(q)$, $I_{\mathrm{AA}}(q)$, $I_{\mathrm{BB}}(q)$, and $I_{\mathrm{AB}}(q)$, can be calculated using equation (13) and (14) within the RDG approximation. For larger particles, the superposition T-matrix method must be used. The homoaggregaion rate coefficients k_{AA} and k_{BB} can be first measured from the pure systems containing only one type of particles. Then the heteroaggregation rate coefficient k_{AB} can be extracted based on equation (17) by fitting the angle dependent apparent static rate measured experimentally with the calculated one.

1.2.2 Dynamic light scattering

As mentioned above, in DLS measurements, the fluctuation of the scattered light over time is recorded by the photon detector. This fluctuation directly depends on the diffusion coefficient of the particles which is directly related to the hydrodynamic radius (R_{h}) by the Stokes-Einstein equation:

$$R_{\mathrm{h}} = \frac{k_B T}{6\pi\eta D} \tag{19}$$

where k_B is the Boltzmann constant, and η is viscosity of the medium. It means that small particles exhibiting higher diffusion coefficient will lead to faster fluctuations. To analyze the characteristics of the fluctuations in the scattered intensity, a signal processing technique, known as autocorrelation, is being used. The normalized intensity correlation function, $g^{(2)}(\tau)$, is given by:[70]

$$g^{(2)}(\tau) = \frac{\langle I(t)I(t+\tau)\rangle}{\langle I(t)\rangle^2} \tag{20}$$

$$\langle I(t)I(t+\tau)\rangle = \lim_{T\to\infty}\int_0^T I(t)I(t+\tau)d\tau \tag{21}$$

where *t* is actual time, τ is the delay time, and T is the total measurement time. Once the intensity correlation function is obtained, one can obtain electric-field correlation function, $g^{(1)}(\tau)$, by the Siegert relationship:[71]

$$g^{(2)}(\tau) = \alpha + \beta\left[g^{(1)}(\tau)\right]^2 \tag{22}$$

where α is the baseline, and β is spatial coherence factor . They are experimental constants. This electric-field correlation function can be used to determine the diffusion coefficient *D* from the following expression:

$$g^{(1)}(\tau) = \exp(-Dq^2\tau) \tag{23}$$

Thus, the hydrodynamic radius (R_h) can be achieved from the diffusion coefficient using Stokes-Einstein equation.

Again, let us first discuss homoaggregation of particles A. The average diffusion coefficient of the particles is calculated from the intensity-weighted average of the diffusion coefficients of the monomer D_A and of the dimer D_{AA} :

$$D(q,t) = \frac{D_A I_A(t) N_A(t) + D_{AA} I_{AA}(t) N_{AA}(t)}{I_A(t) N_A(t) + I_{AA}(t) N_{AA}(t)} \tag{24}$$

Based on Stokes-Einstein equation, the hydrodynamic radius is inversely proportional to the diffusion coefficient. Then we have:

$$\frac{1}{R_h(t)} = \frac{I_A(t) N_A(t) / R_{h,A} + I_{AA}(t) N_{AA}(t) / R_{h,AA}}{I_A(t) N_A(t) + I_{AA}(t) N_{AA}(t)} \tag{25}$$

where $R_{h,A}$ and $R_{h,AA}$ refer to are the hydrodynamic radius of monomers and dimers, respectively. Differentiating equation (25) with respect to time, and eliminating the number concentration of particles with equation (5), one can get the apparent dynamic rate:[66]

$$\Delta = \frac{1}{R_h(0)} \left(\frac{dR_h(t)}{dt} \right)_{t \to 0} = \frac{I_{AA}(q)}{2 I_A(q)} \left(1 - \frac{1}{\alpha_{AA}} \right) k_{AA} N_0 \tag{26}$$

where $R_h(0) = R_{h,A}$ is the average radius of monomers at the initial time, and the hydrodynamic factor $\alpha_{AA} = R_{h,AA} / R_{h,A} = 1.392$. Moreover, the apparent dynamic rate can be obtained from the slope of the measured hydrodynamic radius over time at a certain *q* (or scattering angle θ), as shown as the straight lines in the Figure 7(a). The optical factor $I_{AA}(q)/2I_A(q)$ in equation (26) can be calculated within the RDG approximation or the T-matrix method. Fitting the angular dependence of Δ, as shown in Figure 7(b), with the form factors calculated using RGD or T-matrix theory, and then the homoaggregation rate constant k_{AA} can also be extracted from the apparent dynamic rate measured.

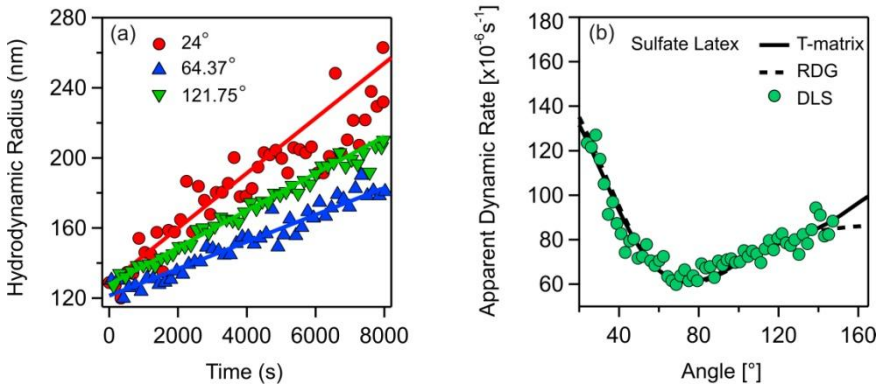

Figure 7. Change in hydrodynamic radius (a) and apparent dynamic rate (b) as a function of the scattering angle for homoaggregation of sulfate latex in 800 mM NaCl.

For the case of heteroaggregation in the mixture of the particle A and B, the determination of heteroaggregation rate k_{AB} is essentially similar to that of k_{AA} by modifying the above equations. Since two homoaggregation and one heteroaggregation processes occur in the system, the average diffusion coefficient of the particles is expressed as:[61]

$$D(q,t) = \frac{\sum_z N_z I_z(q) D_z}{\sum_z N_z I_z(q)} \tag{27}$$

where the subscript *z* represents a series of species, A, B, AA, BB, and AB. Similar to the situation in static light scattering, the apparent dynamic rate (Δ) for the mixture can be written as:[38]

$$\Delta = \frac{1}{R_h(0)}\left(\frac{dR_h(t)}{dt}\right)_{t\to 0} = k_{AA}H_{AA}(q) + 2k_{AB}H_{AB}(q) + k_{BB}H_{BB}(q) \tag{28}$$

where $H_{ij}(q) = F_{ij}(q) - G_{ij}(q)$, $F_{ij}(q)$ is given in equation , and $G_{ij}(q)$ is expressed as:

$$G_{ij}(q) = N_0 x_i x_j \frac{I_{ij}(q)/R_{h,ij} - I_i(q)/R_{h,i} - I_j(q)/R_{h,j}}{2\left[x_A I_A(q)/R_{h,A} + x_B I_B(q)/R_{h,B}\right]} \tag{29}$$

where *i* and *j* refer to particles A and B. All the elements have the same meaning as above. $R_{h,ij}$ is the hydrodynamic radius of the dimers, which can be obtained from the relative hydrodynamic radii of the dimers, α_{ij}, given by the empirical relation:[57]

$$\alpha_{ij} = \frac{2R_{ij}}{R_i + R_j} = 1.392 + 0.608\left(\frac{R_i - R_j}{R_i + R_j}\right)^2 \tag{30}$$

The above approximation agrees well with the values obtained from the hydrodynamics of a pair of unequal spheres in a fluid with low Reynolds numbers.

The analysis of apparent dynamic rate is similar to the static one. The homoaggregaion rate coefficients k_{AA} and k_{BB} are determined from systems containing only one type of particles. Then the measured apparent dynamic rate is fitted with the calculated one, which will result in the heteroaggregation rate coefficient k_{AB}.

1.2.3 Simultaneous static and dynamic light scattering

From the above discussion, one may notice that in order to get the aggregation rate coefficient, the form factor terms should be calculated theoretically either in SLS or in DLS technique. It makes the results highly depend on the accuracy of the theory used. With advanced light scattering instruments, the scattering intensity and hydrodynamic radius as a function of scattering angle can be measured simultaneously. Combining the above equations (15) and (29) for the apparent static rate (Σ) and the apparent dynamic rate (Δ), respectively, and eliminating the common term $I_{AA}(q)/2I_A(q)$, one can obtain a linear relationship:[66]

$$\Sigma = \left(1 - \frac{1}{\alpha_{AA}}\right)^{-1} \Delta - k_{AA} N_0 \tag{31}$$

Accordingly, the dependence of Σ on Δ follows a straight line, as shown as in Figure 8. The aggregation rate coefficient k_{AA} can be achieved from the intercept, while the slope gives the

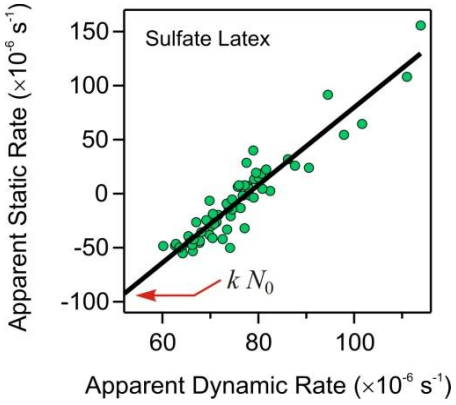

Figure 8. Apparent static rates as a function of apparent dynamic rate for homoaggregation sulfate latex particles (200 nm in diameter) in 800 mM NaCl.

information of the hydrodynamic factor α_{AA}. This technique avoids the calculation of optical factors of monomers and dimers.

1.3 DLVO theory to calculate aggregation rates

In addition to being measured experimentally, aggregation rates can also be calculated theoretically based on the DLVO theory. As mentioned above, charged colloidal particles present an electrical double layer around them, which will bring about repulsive forces due to the overlap of the double layers when particles get close. Meanwhile, the attractive van der Waals forces, which result from the instantaneous dipoles in atoms and molecules, are always present between particles. The DLVO theory suggests that particle aggregation is related to the result of these two surface forces balance.

This theory assumes that the total interaction energy (V) between two particles is the sum of the contributions from van der Waals (V_{vdW}) and electric double layer (V_{EDL}) interactions, as expressed as follows:

$$V(h) = V_{vdW}(h) + V_{EDL}(h) \tag{32}$$

where h is the distance between two particles. The van der Waals interaction energy between two identical spherical particles can be calculated using the Derjaguin approximation without the retardation effects, following the equation:[28,72]

$$V_{vdW}(h) = -\frac{HR}{12h} \tag{33}$$

where R is the radius of the particles, and H is the Hamaker constant which is a characteristic parameter depending on the particle surface. The double layer interaction is obtained by numerically solving the Poisson-Boltzmann (PB) equation, as given as:[72]

$$\frac{d^2\psi}{dx^2} = -\frac{q}{\varepsilon_0 \varepsilon} \sum_i z_i c_i e^{-z_i \beta q \psi} \tag{34}$$

where $\psi(x)$ is the electrical potential profile, q is the elementary charge, ε_0 is the dielectric permittivity of vacuum, ε is the dielectric permittivity of medium, q is the elementary charge, z_i is the ionic valence, c_i is the concentration of ion, and $\beta = 1/k_B T$ is the inverse thermal

energy. To solve above equation, the constant regulation (CR) boundary conditions at mid-plane can be applied. Then one will get the expression:[72]

$$\pm\varepsilon_0\varepsilon\left.\frac{d\psi}{dx}\right|_{x=\pm h/2} = \sigma^{(\pm)} - C_{\mathrm{I}}\left[\psi(\pm h/2) - \psi_{\mathrm{D}}\right] \tag{35}$$

where $x = +h/2$ and $x = -h/2$ refer to the location of right and left surfaces, respectively, σ is the surface charge density, C_{I} is the inner capacitance between the two isolated surfaces, and ψ_{D} is the diffuse layer potential of the isolated surface. The regulation parameter (p) is introduced to describe the regulation properties of each surface, and it is defined as:[73,74]

$$p = \frac{C_{\mathrm{D}}}{C_{\mathrm{D}} + C_{\mathrm{I}}} \tag{36}$$

where C_{D} refers to the diffuse layer capacitance. While $p = 1$ means constant charge (CC) boundary condition is used, and $p = 0$ means constant potential. The C_{D} is given as:

$$C_{\mathrm{D}} = \frac{d\sigma}{d\psi_{\mathrm{D}}} \tag{37}$$

Moreover, the surface charge density is connected to the diffuse layer capacitance by the following relation:[75]

$$\sigma = \pm\left[2k_B T\varepsilon_0\varepsilon\sum_i c_i(e^{-z_i\beta q\psi_{\mathrm{D}}} - 1)\right]^{1/2} \tag{38}$$

Once the electrical potential profile $\psi(x)$ at different separations h is obtained by solving PB equation (34), the disjoining pressure resulting from the electrical double layer overlap can be calculated by the following expression:

$$\Pi = k_B T\sum_i c_i(e^{-z_i\beta q\psi_{\mathrm{M}}} - 1) \tag{39}$$

where ψ_{M} is the value of the electrical potential (ψ) at the midplane ($x = 0$). When the disjoining pressure is known, using the Derjaguin approximation, the electrical double layer force can be obtained by integration as follows:[72]

$$F_{\mathrm{EDL}} = \pi R \int_{h}^{\infty} \Pi(h') dh' \tag{40}$$

The electrostatic potential energy will be achieved by a further integration of double layer force[72]

$$V_{\mathrm{EDL}} = \int_{h}^{\infty} F_{\mathrm{EDL}}(h') dh' \tag{41}$$

Thus, the total interaction energy between two particles can be known by combining equations (32), (33) and (41). The aggregation rate constant (k) can be calculated from the forced diffusion equation solved through steady state method, which is expressed as:[28,72]

$$k = \frac{4k_{\mathrm{B}}T}{3\eta R}\left[\int_{0}^{\infty} \frac{B(h/R)}{(2R+h)^2} \exp\left[\frac{V(h)}{k_{\mathrm{B}}T}\right] dh\right]^{-1} \tag{42}$$

where η refers to the viscosity of water, and $B(h)$ denotes the hydrodynamic resistance function, expressed as:[76]

$$B(h/R) = \frac{6(h/R)^2 + 13h/R + 2}{6(h/R)^2 + 4h/R} \tag{43}$$

Instead of the aggregation rate coefficient, researchers also use the stability ratio (W) to describe the aggregation behavior of particle suspension. It is defined as follows:

$$W = \frac{k_{fast}}{k} \tag{44}$$

where k_{fast} refers to the fast aggregation rate coefficient, which is obtained when the total interaction only includes the contribution of van der Waals forces and the electrical double forces vanish.

It has been demonstrated that DLVO theory is capable to describe the aggregation rate coefficient quantitatively in many systems, such as the amidine or sulfate latex particles in the presence of inorganic salts and oxyanions.[38,77] While in some cases, non-DLVO forces may also have a significant effect on the total interactions between particles. These non-DLVO interactions probably result from surface charge heterogeneities or hydrophobic effects.[78-80] Specifically, in the system of the amidine or sulfate latex particles in the presence sodium tetraphenylborate and NaCl, classic DLVO theory can only partially describe the aggregation behavior of the particels. An additional attractive non-DLVO force was

introduced to better rationalize the experimental results. These observations will be discussed thoroughly in Chapter 3.

1.4 Electrophoresis to study surface charge of particles

During the above calculation process, the diffuse layer potential of the isolated surface (ψ_D) should be known. We usually assume that its value is approximately equal to that of the electrokinetic potential (ζ potential) which can be obtained from electrophoresis.

When the charged colloidal particles dispersed in a solution, their surface charge properties are dominated by the spatial distribution of the surrounding ions. As shown as in Figure 9, the positive charge on the particle surface is balanced by the accumulation of anions (counterions) and the depletion of cations (coions). The surface potential (ψ_0) refers to the potential of the solid surface in the liquid-solid interface. The diffuse layer potential (ψ_D) refers to the potential at the orgin of the diffuse layer. The electrokinetic potential (ζ) is the potential at the location of slip plane (or shear plane). The stationary layer of the fluid inside the slip plane moves together with the particle when applying an external electrical field. Since this layer is extremely thin, the value of electrokinetic potential can be approximated with the diffuse

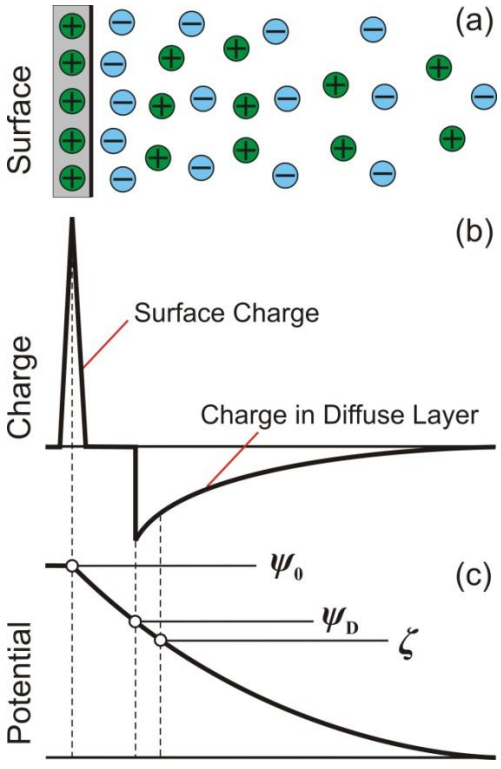

Figure 9. Illustration of electrical double layer. Reproduction from reference 37.

layer potential.

Electrophoresis is widely used to study the surface charge properties of colloidal particles in various ionic environments.[81,82] Principally, this technique investigates the motion of the charged particles in the liquid induced by an external electrical field. The positively charged colloidal particles move towards the cathode, while the negatively charged colloidal particles move towards the anode. The magnitude of velocity (v) of the particles is proportional to the magnitude of the applied electrical field (E). The resulting ratio is defined as the electrophoretic mobility (u_e), as follows:[82]

$$u_e = \frac{v}{E} \tag{45}$$

Obviously, the movement of the charged particles under an electric field is related to their surface charge. In other words, the electrophoretic mobility is proportional to the electrokinetic potential (ζ). Different models have been developed to convert the mobility to the ζ potential. The applicability of these models depends on the characteristics of the particle (the size R and the charge e) and the salt concentration. The concentration of electrolyte can be expressed in terms of Debye length (κ^{-1}) given by:

$$\kappa^{-1} = \sqrt{\frac{\varepsilon\varepsilon_0 k_B T}{\sum_{i=1}^{n} c_i z_i N_A e^2}} \tag{46}$$

where e, c_i and z_i are the elementary charge, the number concentration and charge number of the ion i, respectively. N_A refers to the Avogadro number.

The relation between ζ potential and the electrophoretic mobility u_e can be regulated by Henry's formula as follows:[82]

$$\zeta = \frac{2u_e\eta}{3\varepsilon\varepsilon_0} f(\kappa R) \tag{47}$$

where $f(\kappa R)$ refers to Henry' function. Its value varies smoothly from 1 to 1.5 depending on the salt concentration in the suspension. In the situation of $\kappa R \ll 1$(*e.g.*, small particles and low salt concentration), $f(\kappa R) = 1$ will be used. One can obtain the following relation:

$$\zeta = \frac{2u_e\eta}{3\varepsilon\varepsilon_0} \tag{48}$$

This relation agrees with the Hückel–Onsager equation.[83]

If $\kappa R \gg 1$ and the ζ value is low ($|\zeta| \leq 50\text{mV}$), $f(\kappa R) = 1.5$ will be applied. The expression becomes:

$$\zeta = \frac{u_e\eta}{\varepsilon\varepsilon_0} \tag{49}$$

This situation is corresponding to the model developed by Helmholtz and Smoluchowski.[84]

1.5 Outline of the thesis

The present PhD thesis focuses on the aggregation and charging behavior of colloidal polystyrene latex particles in various types of ionic environment. The techniques used are electrophoresis and light scattering, combined with model calculations within DLVO theory. The motivation and the main findings of the present studies are as follows.

Chapter 2 deals with the effect of multivalent co-ions on the homoaggregation of colloidal particles. More than a century ago, Schulze and Hardy found that multivalent ions were much more efficient than monovalent ones in destabilizing colloidal suspensions. This finding is known as the *Schulze-Hardy rule*, which states that the critical coagulation concentration (CCC) is inversely proportional to the sixth power of the valence (z) of the counterions ($CCC \propto 1/z^6$). In other words, multivalent anions can coagulate the positively charged particles more effectively, while multivalent cations negatively charged particles. According to DLVO theory, the explanation for this behavior is that repulsive electrical double layer forces between charged particles can be more easily screened by multivalent counterions. Surprisingly, researchers have always investigated situations in which the multivalent ions represent the counterions. Therefore, systems where multivalent ions represent the co-ions were investigated. The results showed that the corresponding CCC of the particles decreases with valence of the co-ions. This dependence was much weaker than that induced by multivalent counterions. Using the ionic strength to represent the salt concentration, the critical coagulation ionic strength (CCIS) decreased rapidly as increasing valence of counterions ($CCIS \propto 1/z^4$) in the case of the *Schulze-Hardy rule*. However, in the current situation of multivalent co-ions, the CCIS increased slowly with the valence of co-ions ($CCIS \propto z$). Therefore, an analogous *inverse Schulze–Hardy rule* was proposed to describe this effect of multivalent co-ions on particle aggregation.

In *Chapter 3*, homoaggregation of amidine-modified polystyrene latex (AL) and sulfate-modified polystyrene latex (SL) particles in solutions containing hydrophobic tetraphenylborate anions (Ph_4B^-) and NaCl is discussed. Classic DLVO theory is powerful in describing the aggregation behavior of colloidal particles in the presence of various ionic species, such as mono- and multivalent salts, ionic liquids and polyelectrolytes. Ph_4B^- anions are hydrophobic organic monovalent ions, which can strongly adsorb to hydrophobic surfaces and may result in a charge reversal. Moreover, the Ph_4B^- salts can freely dissolve in water and do not form micelles in solution. It is interesting to study the effect of this type of

monovalent ions on the charging and aggregation behavior of colloidal particles. AL particles are positively charged in monovalent NaCl salt solution due to the cationic amidine groups on the particle surface. As increasing the concentration of Ph_4B^- anions, AL particles became less positively charged due to the adsorption of anions. Further accumulation of Ph_4B^- anions on the particle surface first induced charge neutralization at a concentration of 0.030 mM, followed by a pronounced charge reversal. The electrokinetic potential went through a minimum around a concentration of 10 mM, and then the potential increased due to screening. Adding NaCl electrolyte as background, electrokinetic potential varied similarly with the concentration of Ph_4B^- anions, but the magnitudes of potential decrease. For SL particles, the potentials are negative at low concentration of Ph_4B^- anions, which reflects the negative charge of the anionic sulfate groups on the particle surface. Under the condition of NaCl electrolyte as background, the electrokinetic potentials decreased with increasing Ph_4B^- concentration and reach a minimum near 10 mM, which indicates that the Ph_4B^- anions also adsorb to the negatively charged SL particles. After going though a minimum, the potential increased again at higher concentrations because of screening. The electrokinetic potentials of AL and SL particles exhibited a similar trend. The above adsorption of Ph_4B^- anions onto the like-charged particle surfaces, including negative SL particle surfaces and negative AL particle surfaces in the charge reversal stage, strongly indicates that other forces than electrostatic ones drive this adsorption process. If looking at the molecular structures of polystyrene latex particles and the Ph_4B^- anions, both of them present the phenyl rings. These features make the surfaces of hydrophobic nature. Therefore, the forces probably result from strong hydrophobic and π–π stacking effects.

The corresponding aggregation behavior was described in terms of the stability ratio. For AL particles, stability ratios were unity near the charge neutralization point, which means that fast aggregation happens. Increasing the Ph_4B^- concentration further, the stability ratio increased strongly and the system became stable. At very high Ph_4B^- concentrations, the stability ratio decreased rapidly with the concentration and became unity again for Ph_4B^- concentrations above 790 ± 20 mM due to the screening. However, at intermediate Ph_4B^- concentrations and NaCl background, the stability ratio went through another minimum. For SL particles, at very high Ph_4B^-concentrations, fast aggregation was also observed because of screening. At intermediate NaCl and Ph_4B^-concentrations, again a minimum in the stability ratio was present, which is similar to the case of AL particles. DLVO theory was first used to interpret the observed stability ratios. The calculations can capture the aggregation behavior

at low and very high Ph_4B^-concentrations. The theory entirely failed to predict the observed intermediate minimum in the stability ratio. Considering that additional hydrophobic forces are responsible for the adsorption of Ph_4B^- anions onto the like-charged particle surfaces, these non-DLVO attractive forces were included in the calculation. Such calculations including the non-DLVO interactions reproduced the experimental stability ratios quite well. Especially, the intermediate minimum of stability ratio was predicted.

Heteroaggregation has been studied much less than homoaggregation. To improve the understanding of heteroaggregation processes, we investigated the heteroaggregaton in the binary mixture of oppositely charged colloidal particles in the presence of multivalent ions by multi-angle light scattering, as described in *Chapter 4*. The particles used included positive AL particles (300 nm in diameter) and negative SL particles (600 nm in diameter). Two types of electrolyte systems were used. One included simple inorganic electrolytes—KCl, K_2SO_4, $K_3Fe(CN)_6$ and $K_4Fe(CN)_6$. The other included an organic polycation—pentaethylenehexamine (N6) with the chemical formula $H_2N(CH_2CH_2NH)_4CH_2CH_2NH_2$. In the system of two types of particles and inorganic salts, the charge of AL particles became less positive as increasing the salt concentration, and even became neutral followed by negative because of the charge reversal effect when the salts were multivalent. However, the charge of SL particles was still negative over all the concentrations. In the presence of KCl, and K_2SO_4, the corresponding stability ratios of heteroaggregation between AL particles and SL particles were always fast over all the concentrations since these two types of particles were oppositely charged. In the presence of $K_3Fe(CN)_6$ and $K_4Fe(CN)_6$, except for the fast heteroaggregation at the low and very high concentrations, slow heteroaggregation was present at the intermediate concentrations because of the charge reversal of AL particles. In presence of N6 with different KCl background, AL particles always presented a positive charge over all the conditions, while the charge of SL particles changed from negative to positive with increasing the N6 concentration. The fast heteroaggregation occurred at low and very high concentrations, while slow heteroaggregation regime was present at intermediate N6 concentrations due to the charge reversal of SL particles. The pattern of fast heteroaggregation was observed by previous researchers. The novel pattern of heteroaggregation containing a slow aggregation regime is reported here for the first time. These findings can be described quite well by DLVO theory. The calculated stability ratio was very sensitive to the boundary conditions used when solving the Poisson-Boltzmann equation.

Heteroaggregation rate can be extracted from the angular-dependence of the scattering profiles of different aggregates, which are measured by multi-angle light scattering technique. However, because the contrast of these scattering signals between the different aggregates was poor, the obtained heteroaggregation rates could be only measured in a narrow range, over one order of magnitude or less. *Chapter 5* presents a strategy, by which the contrast between the different aggregates can be enhanced. In this fashion, the heteroaggregation rate can be monitored over a wider range. The system involved was a binary mixture of AL particles (302 nm in diameter) and SL particles (250nm in diameter) in the presence of sodium n-octyl sulfate (SOS). The size of the particles was important to increase the contrast of scattering profiles between different aggregates. The characteristic peak of the scattering profiles of hetero-aggregates (AL-SL) is located in the similar region than the one of homo-aggregates (SL-SL), but in a different region than the one of homo-aggregates (AL-AL). The charge of AL particles changed from positive to negative with increasing concentration of SOS, while the SL particles still presented a highly negative charge. Thus, the homoaggregation of SL particles could be suppressed. The contrast between different aggregates could be largely optimized. By this approach, the stability ratios of heteroaggregation were measured in a much wider range, namely over more than two orders of magnitude.

References

(1) Vincent, B.: Early (pre-DLVO) studies of particle aggregation. *Advances In Colloid And Interface Science* **2012**, *170*, 56-67.

(2) Faraday, M.: On the color of colloidal gold. *Phil. Trans. R. Soc. London* **1857**, *147*, 145-181.

(3) Everett, D. H.: *Basic principles of colloid science*; Royal society of chemistry, 2007.

(4) Derjaguin, B.; Landau, L. D.: Theory of the stability of strongly charged lyophobic sols and of the adhesion of strongly charged particles in solutions of electrolytes. *Acta Phys. Chim.* **1941**, *14*, 633-662.

(5) Verwey, E. J. W.; Overbeek, J. T. G.: *Theory of stability of lyophobic colloids*; Elsevier: Amsterdam, 1948.

(6) Bolto, B.; Gregory, J.: Organic polyelectrolytes in water treatment. *Water Research* **2007**, *41*, 2301-2324.

(7) Nasser, M. S.; Twaiq, F. A.; Onaizi, S. A.: Effect of polyelectrolytes on the degree of flocculation of papermaking suspensions. *Separation and Purification Technology* **2013**, *103*, 43-52.

(8) De Silva Indrasekara, A. S.; Norton, S. J.; Geitner, N. K.; Crawford, B. M.; Wiesner, M. R.; Vo-Dinh, T.: Tailoring the Core–Satellite Nanoassembly Architectures by Tuning Internanoparticle Electrostatic Interactions. *Langmuir* **2018**, *34*, 14617-14623.

(9) Hotze, E. M.; Phenrat, T.; Lowry, G. V.: Nanoparticle aggregation: challenges to understanding transport and reactivity in the environment. *Journal of environmental quality* **2010**, *39*, 1909-1924.

(10) Elimelech, M.; Gregory, J.; Jia, X.: *Particle deposition and aggregation: measurement, modelling and simulation*; Butterworth-Heinemann, 2013.

(11) Sprycha, R.: Electrical double layer at alumina/electrolyte interface: I. Surface charge and zeta potential. *J Colloid Interface Sci* **1989**, *127*, 1-11.

(12) Morag, J.; Dishon, M.; Sivan, U.: The governing role of surface hydration in ion specific adsorption to silica: An AFM-based account of the Hofmeister universality and its reversal. *Langmuir* **2013**, *29*, 6317-6322.

(13) Dishon, M.; Zohar, O.; Sivan, U.: From repulsion to attraction and back to repulsion: the effect of NaCl, KCl, and CsCl on the force between silica surfaces in aqueous solution. *Langmuir* **2009**, *25*, 2831-2836.

(14) Oncsik, T.; Trefalt, G.; Borkovec, M.; Szilagyi, I.: Specific ion effects on particle aggregation induced by monovalent salts within the Hofmeister series. *Langmuir* **2015**, *31*, 3799-3807.

(15) López‐León, T.; Ortega‐Vinuesa, J. L.; Bastos‐González, D.: Ion‐Specific Aggregation of Hydrophobic Particles. *CHEMPHYSCHEM* **2012**, *13*, 2382-2391.

(16) Tian, R.; Yang, G.; Li, H.; Gao, X.; Liu, X.; Zhu, H.; Tang, Y.: Activation energies of colloidal particle aggregation: towards a quantitative characterization of specific ion effects. *Physical Chemistry Chemical Physics* **2014**, *16*, 8828-8836.

(17) Peula-García, J. M.; Ortega-Vinuesa, J. L.; Bastos-Gonzalez, D.: Inversion of Hofmeister series by changing the surface of colloidal particles from hydrophobic to hydrophilic. *The Journal of Physical Chemistry C* **2010**, *114*, 11133-11139.

(18) López-León, T.; Santander-Ortega, M. J.; Ortega-Vinuesa, J. L.; Bastos-González, D.: Hofmeister effects in colloidal systems: influence of the surface nature. *The Journal of Physical Chemistry C* **2008**, *112*, 16060-16069.

(19) Parsons, D. F.; Salis, A.: Hofmeister effects at low salt concentration due to surface charge transfer. *Current Opinion in Colloid & Interface Science* **2016**, *23*, 41-49.

(20) Jungwirth, P.; Cremer, P. S.: Beyond hofmeister. *Nature Chemistry* **2014**, *6*, 261.

(21) Kunz, W.; Henle, J.; Ninham, B. W.: 'Zur Lehre von der Wirkung der Salze'(about the science of the effect of salts): Franz Hofmeister's historical papers. *Current Opinion in Colloid & Interface Science* **2004**, *9*, 19-37.

(22) Schwierz, N.; Horinek, D.; Sivan, U.; Netz, R. R.: Reversed Hofmeister series—the rule rather than the exception. *Current Opinion in Colloid & Interface Science* **2016**, *23*, 10-18.

(23) Schulze, H.: Schwefelarsen in wässriger Lösung. *J. Prakt. Chem.* **1882**, *25*, 431-452.

(24) Hardy, W. B.: A preliminary investigation of the conditions which determine the stability of irreversible hydrosols. *Proc. Roy. Soc. London* **1900**, *66*, 110-125.

(25) Nowicki, W.; Nowicka, G.: Verification of the Schulze-Hardy rule: a colloid chemistry experiment. *Journal of Chemical education* **1994**, *71*, 624.

(26) Russel, W. B.; Saville, D. A.; Schowalter, W. R.: *Colloidal Dispersions*; Cambridge University Press: Cambridge, 1989.

(27) Trefalt, G.; Szilagyi, I.; Borkovec, M.: Poisson-Boltzmann description of interaction forces and aggregation rates involving charged colloidal particles in asymmetric electrolytes. *J Colloid Interface Sci* **2013**, *406*, 111-120.

(28) Elimelech, M.; Gregory, J.; Jia, X.; Williams, R. A.: *Particle Deposition and Aggregation: Measurement, Modeling, and Simulation*; Butterworth-Heinemann Ltd.: Oxford, 1995.

(29) Cao, T.; Szilagyi, I.; Oncsik, T.; Borkovec, M.; Trefalt, G.: Aggregation of colloidal particles in the presence of multivalent co-ions: The inverse Schulze–Hardy rule. *Langmuir* **2015**, *31*, 6610-6614.

(30) Trefalt, G.: Derivation of the inverse Schulze-Hardy rule. *Physical Review E* **2016**, *93*, 032612.

(31) Oncsik, T.; Trefalt, G.; Csendes, Z.; Szilagyi, I.; Borkovec, M.: Aggregation of negatively charged colloidal particles in the presence of multivalent cations. *Langmuir* **2014**, *30*, 733-741.

(32) Verrall, K. E.; Warwick, P.; Fairhurst, A. J.: Application of the Schulze-Hardy rule to haematite and haematite/humate colloid stability. *Colloids And Surfaces A-Physicochemical And Engineering Aspects* **1999**, *150*, 261-273.

(33) Wannow, H. A.: Über eine neue Methode zur quantitativen Koagulationsmessung. *Kolloidchem. Beih.* **1939**, *50*, 367-472.

(34) Lagaly, G.; Ziesmer, S.: Colloid chemistry of clay minerals: the coagulation of montmorillonite dispersions. *Adv Colloid Interface Sci* **2003**, *100*, 105-128.

(35) Matijevic, E.; Kerker, M.: The charge of some heteropoly anions in aqueous solutions as determined by coagulation effects. *Journal of Physical Chemistry* **1958**, *62*, 1271-1276.

(36) Pavlovic, M.; Huber, R.; Adok-Sipiczki, M.; Nardin, C.; Szilagyi, I.: Ion specific effects on the stability of layered double hydroxide colloids. *Soft Matter* **2016**, *12*, 4024-4033.

(37) Szilagyi, I.; Trefalt, G.; Tiraferri, A.; Maroni, P.; Borkovec, M.: Polyelectrolyte adsorption, interparticle forces, and colloidal aggregation. *Soft Matter* **2014**, *10*, 2479-2502.

(38) Cao, T.; Sugimoto, T.; Szilagyi, I.; Trefalt, G.; Borkovec, M.: Heteroaggregation of oppositely charged particles in the presence of multivalent ions. *Physical Chemistry Chemical Physics* **2017**, *19*, 15160-15171.

(39) Szilagyi, I.; Sadeghpour, A.; Borkovec, M.: Destabilization of colloidal suspensions by multivalent ions and polyelectrolytes: From screening to overcharging. *Langmuir* **2012**, *28*, 6211-6215.

(40) Rouster, P.; Pavlovic, M.; Szilagyi, I.: Destabilization of titania nanosheet suspensions by inorganic salts: Hofmeister series and Schulze-Hardy rule. *The Journal of Physical Chemistry B* **2017**, *121*, 6749-6758.

(41) Ji, Y.-Q.; Black, L.; Weidler, P. G.; Janek, M.: Preparation of nanostructured materials by heterocoagulation interaction of montmorillonite with synthetic hematite particles. *Langmuir* **2004**, *20*, 9796-9806.

(42) Pavlovic, M.; Rouster, P.; Bourgeat-Lami, E.; Prevot, V.; Szilagyi, I.: Design of latex-layered double hydroxide composites by tuning the aggregation in suspensions. *Soft Matter* **2017**, *13*, 842-851.

(43) Uricanu, V.; Eastman, J. R.; Vincent, B.: Stability in colloidal mixtures containing particles with a large disparity in size. *J Colloid Interface Sci* **2001**, *233*, 1-11.

(44) Vincent, B.; Young, C. A.; Tadros, T. F.: Equilibrium aspects of heteroflocculation in mixed sterically-stabilised dispersions. *Faraday Discussions of the Chemical Society* **1978**, *65*, 296-305.

(45) Vincent, B.; Young, C. A.; Tadros, T. F.: Adsorption of small, positive particles onto large, negative particles in the presence of polymer. Part 1.—Adsorption isotherms. *Journal of the Chemical Society, Faraday Transactions 1: Physical Chemistry in Condensed Phases* **1980**, *76*, 665-673.

(46) Luckham, P.; Vincent, B.; Hart, C.; Tadros, T. F.: The controlled flocculation of particulate dispersions using small particles of opposite charge I. Sediment volumes and morphology. *Colloids and Surfaces* **1980**, *1*, 281-293.

(47) Hansen, F. K.; Matijević, E.: Heterocoagulation. Part 5.—Adsorption of a carboxylated polymer latex on monodispersed hydrated metal oxides. *Journal of the Chemical Society, Faraday Transactions 1: Physical Chemistry in Condensed Phases* **1980**, *76*, 1240-1262.

(48) Böhmer, M. R.; van der Zeeuw, E. A.; Koper, G. J.: Kinetics of particle adsorption in stagnation point flow studied by optical reflectometry. *J Colloid Interface Sci* **1998**, *197*, 242-250.

(49) Lüthi, Y.; Rička, J.; Borkovec, M.: Colloidal particles at water-glass interface: deposition kinetics and surface heterogeneity. *J Colloid Interface Sci* **1998**, *206*, 314-321.

(50) Grolimund, D.; Elimelech, M.; Borkovec, M.; Barmettler, K.; Kretzschmar, R.; Sticher, H.: Transport of in situ mobilized colloidal particles in packed soil columns. *Environ Sci Technol* **1998**, *32*, 3562-3569.

(51) Elimelech, M.: Kinetics of capture of colloidal particles in packed beds under attractive double layer interactions. *J Colloid Interface Sci* **1991**, *146*, 337-352.

(52) Dumont, F.; Ameryckx, G.; Watillon, A.: Heterocoagulation between small and large colloidal particles. Part I. Equilibrium aspects. *Colloids and Surfaces* **1990**, *51*, 171-188.

(53) Ottewill, R.; Schofield, A.; Waters, J.; Williams, N. S. J.: Preparation of core-shell polymer colloid particles by encapsulation. *Colloid and Polymer Science* **1997**, *275*, 274.

(54) Caruso, F.: Nanoengineering of particle surfaces. *Advanced Materials* **2001**, *13*, 11-22.

(55) Ryde, N.; Matijević, E.: Kinetics of heterocoagulation. Part 4.—Evaluation of absolute coagulation rate constants using a classical light scattering technique. *Journal of the Chemical Society, Faraday Transactions* **1994**, *90*, 167-171.

(56) Puertas, A.; Fernandez-Barbero, A.; De Las Nieves, F.: Charged colloidal heteroaggregation kinetics. *The Journal of Chemical Physics* **2001**, *114*, 591-595.

(57) Yu, W.; Matijević, E.; Borkovec, M.: Absolute heteroaggregation rate constants by multiangle static and dynamic light scattering. *Langmuir* **2002**, *18*, 7853-7860.

(58) Puertas, A. M.; Fernandez-Barbero, A.; De Las Nieves, F.: Induced asymmetries in the heteroaggregation of oppositely charged colloidal particles. *J Colloid Interface Sci* **2003**, *265*, 36-43.

(59) Kihira, H.; Matijevic, E.: Kinetics of heterocoagulation. 3. Analysis of effects causing the discrepancy between the theory and experiment. *Langmuir* **1992**, *8*, 2855-2862.

(60) Yu, W.; Borkovec, M.: Distinguishing heteroaggregation from homoaggregation in mixed binary particle suspensions by multiangle static and dynamic light scattering. *The Journal of Physical Chemistry B* **2002**, *106*, 13106-13110.

(61) Lin, W.; Kobayashi, M.; Skarba, M.; Mu, C.; Galletto, P.; Borkovec, M.: Heteroaggregation in binary mixtures of oppositely charged colloidal particles. *Langmuir* **2006**, *22*, 1038-1047.

(62) Mishchenko, M. I.; Mackowski, D. W.: Electromagnetic scattering by randomly oriented bispheres: comparison of theory and experiment and benchmark calculations. *Journal of Quantitative Spectroscopy and Radiative Transfer* **1996**, *55*, 683-694.

(63) Galletto, P.; Lin, W.; Mishchenko, M. I.; Borkovec, M.: Light-scattering form factors of asymmetric particle dimers from heteroaggregation experiments. *The Journal of Chemical Physics* **2005**, *123*, 064709.

(64) Gregory, J.: Monitoring particle aggregation processes. *Adv Colloid Interface Sci* **2009**, *147*, 109-123.

(65) Trefalt, G.; Szilagyi, I.; Oncsik, T.; Sadeghpour, A.; Borkovec, M.: Probing colloidal particle aggregation by light scattering. *CHIMIA International Journal for Chemistry* **2013**, *67*, 772-776.

(66) Holthoff, H.; Egelhaaf, S. U.; Borkovec, M.; Schurtenberger, P.; Sticher, H.: Coagulation rate measurements of colloidal particles by simultaneous static and dynamic light scattering. *Langmuir* **1996**, *12*, 5541-5549.

(67) Matsuoka, H.; Murai, H.; Ise, N.: ‘‘Ordered’’structure in colloidal silica particle suspensions as studied by small-angle x-ray scattering. *Physical Review B* **1988**, *37*, 1368.

(68) Bohren, C. F.; Huffman, D. R.: *Absorption and scattering of light by small particles*; John Wiley & Sons, 2008.

(69) Mackowski, D. W.; Mishchenko, M. I.: Calculation of the T matrix and the scattering matrix for ensembles of spheres. *JOSA A* **1996**, *13*, 2266-2278.

(70) Hassan, P. A.; Rana, S.; Verma, G.: Making sense of Brownian motion: colloid characterization by dynamic light scattering. *Langmuir* **2014**, *31*, 3-12.

(71) Pusey, P. N.: Dynamic light scattering. In *Neutrons, X-Rays and Light*; Lindner, P., Zemb, T., Eds.; Elsevier Science B.V.: Amsterdam, 2002.

(72) Russel, W. B.; Russel, W.; Saville, D. A.; Schowalter, W. R.: *Colloidal dispersions*; Cambridge university press, 1991.

(73) Carnie, S. L.; Chan, D. Y.: Interaction free energy between plates with charge regulation: a linearized model. *J Colloid Interface Sci* **1993**, *161*, 260-264.

(74) Behrens, S. H.; Borkovec, M.: Electrostatic interaction of colloidal surfaces with variable charge. *The Journal of Physical Chemistry B* **1999**, *103*, 2918-2928.

(75) Trefalt, G.; Szilagyi, I.; Borkovec, M.: Poisson–Boltzmann description of interaction forces and aggregation rates involving charged colloidal particles in asymmetric electrolytes. *J Colloid Interface Sci* **2013**, *406*, 111-120.

(76) Honig, E.; Roebersen, G.; Wiersema, P.: Effect of hydrodynamic interaction on the coagulation rate of hydrophobic colloids. *J Colloid Interface Sci* **1971**, *36*, 97-109.

(77) Sugimoto, T.; Cao, T.; Szilagyi, I.; Borkovec, M.; Trefalt, G.: Aggregation and charging of sulfate and amidine latex particles in the presence of oxyanions. *J Colloid Interface Sci* **2018**, *524*, 456-464.

(78) Popa, I.; Papastavrou, G.; Borkovec, M.: Charge regulation effects on electrostatic patch-charge attraction induced by adsorbed dendrimers. *Physical Chemistry Chemical Physics* **2010**, *12*, 4863-4871.

(79) Montes Ruiz-Cabello, F. J.; Trefalt, G.; Oncsik, T.; Szilagyi, I.; Maroni, P.; Borkovec, M.: Interaction forces and aggregation rates of colloidal latex particles in the presence of monovalent counterions. *The Journal of Physical Chemistry B* **2015**, *119*, 8184-8193.

(80) Cao, T.; Trefalt, G.; Borkovec, M.: Aggregation of Colloidal Particles in the Presence of Hydrophobic Anions: Importance of Attractive Non-DLVO Forces. *Langmuir* **2018**, *34*, 14368-14377.

(81) O'Brien, R. W.; White, L. R.: Electrophoretic mobility of a spherical colloidal particle. *Journal of the Chemical Society-Faraday Transactions II* **1978**, *74*, 1607-1626.

(82) Delgado, Á. V.; González-Caballero, F.; Hunter, R.; Koopal, L.; Lyklema, J.: Measurement and interpretation of electrokinetic phenomena. *J Colloid Interface Sci* **2007**, *309*, 194-224.

(83) Hunter, R. J.: *Zeta potential in colloid science: principles and applications*; Academic press, 2013; Vol. 2.

(84) Evans, D. F.; Wennerstrom, H.: *The Colloidal Domain*; John Wiley: New York, 1999.

CHAPTER 2

Aggregation of Colloidal Particles in the Presence of Multivalent Co-Ions: the Inverse Schulze–Hardy Rule

Cao, T.; Szilagyi, I.; Oncsik, T.; Borkovec, M.; Trefalt, G.

Langmuir **2015**, 31,6610–6614.

Langmuir

Letter

pubs.acs.org/Langmuir

Aggregation of Colloidal Particles in the Presence of Multivalent Co-Ions: The Inverse Schulze–Hardy Rule

Tianchi Cao, Istvan Szilagyi, Tamas Oncsik, Michal Borkovec,* and Gregor Trefalt*

Department of Inorganic and Analytical Chemistry, University of Geneva, Sciences II, 30 Quai Ernest-Ansermet, 1205 Geneva, Switzerland

Supporting Information

ABSTRACT: Shifts of the critical coagulation concentration (CCC) in particle suspensions in salt solutions containing multivalent co-ions and monovalent counterions are rationalized. One observes that the CCC is inversely proportional to the valence, and this behavior is referred to as the inverse Schulze–Hardy rule. This dependence is established by means of measurements of the stability ratio for positively and negatively charged latex particles with time-resolved light scattering. The same dependence is equally suggested by calculations of the CCC with the Derjaguin, Landau, Verwey, and Overbeek (DLVO) theory, whereby the full Poisson–Boltzmann equation for the asymmetric electrolytes has to be used. The latter aspect is essential, since in the case of multivalent co-ions the surface charge is principally neutralized by monovalent counterions. This rule complements the classical Schulze–Hardy rule, which applies in the case of multivalent counterions, and states that the CCC is inversely proportional to the sixth power of the valence.

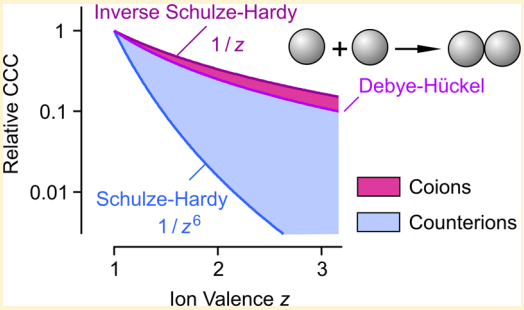

INTRODUCTION

More than a century ago, Schulze and Hardy discovered that multivalent ions destabilize colloidal suspensions much more effectively than monovalent ones.[1,2] Half a century later, Derjaguin, Landau, Verwey, and Overbeek (DLVO) explained this behavior by assuming that interactions between particles are governed by superposition of van der Waals forces and double layer forces.[3,4] Based on these assumptions, one finds—in agreement with experiment—that colloidal suspensions are stable at low salt concentrations, while they are unstable at higher ones. The abrupt transition between these two regimes is referred to as the critical coagulation concentration (CCC). For highly charged particles and symmetric z:z electrolytes, the DLVO theory predicts that[5−7]

$$\mathrm{CCC} \propto \frac{1}{z^6} \quad \text{(Schulze–Hardy)} \tag{1}$$

where z is the ionic valence. This dependence was suggested on experimental grounds earlier, and is nowadays referred to as the *Schulze–Hardy rule*.

Multivalent, symmetric z:z electrolytes are hardly soluble, and whenever this rule is compared to experiment, one uses soluble asymmetric z:1 or 1:z electrolytes. Curiously, researchers have always studied systems where the multivalent ions represent the *counterions*, meaning that negatively charged particles can be more effectively coagulated by multivalent cations, while positively charged particles with multivalent anions. The CCCs in such systems often follow the Schulze–Hardy rule.[8−15]

To the best of our knowledge, however, the situation where multivalent ions represent the *co-ions* was not investigated so far. We therefore focus on this situation here, and investigate effects of multivalent anions on the aggregation of negatively charged particles or multivalent cations on positively charged ones. We argue that an analogous *inverse Schulze–Hardy rule* can be formulated in this situation, namely

$$\mathrm{CCC} \propto \frac{1}{z} \quad \text{(inverse Schulze–Hardy)} \tag{2}$$

This dependence on the valence is weaker, but characteristic for the present situation of multivalent co-ions.

EXPERIMENTAL SECTION

Two batches of polystyrene latex particles with a diameter of about 300 nm were used. In one batch, the particle surface was functionalized with amidine groups, while for the second one with sulfate groups. The particles were suspended in various salt solutions at a concentration of 10 mg/L, and the rate constants of doublet formation were measured in the early stages of the aggregation by time-resolved dynamic light scattering.[10,16−19] The stability ratio W was obtained from the relative rate of increase of the hydrodynamic radius normalized to its value at high salt conditions. The stability ratio is defined as $W = k_{fast}/k$ where k_{fast} is the aggregation rate in the fast aggregation regime and k is the actual rate constant in question. The experiments were carried out at pH 4.0 and 25 °C. More details on the experimental procedures are

Received: May 5, 2015
Revised: June 1, 2015
Published: June 3, 2015

DOI: 10.1021/acs.langmuir.5b01649
Langmuir 2015, 31, 6610–6614

presented in the Supporting Information, and they are similar to the ones used previously.[10]

RESULTS

We have investigated colloidal stability of negatively charged sulfate latex particles suspended in solutions of KCl, K_2SO_4, and $K_3Fe(CN)_6$ electrolytes, and of positively charged amidine latex particles in solutions of KCl, $MgCl_2$, and $LaCl_3$. Figure 1 shows

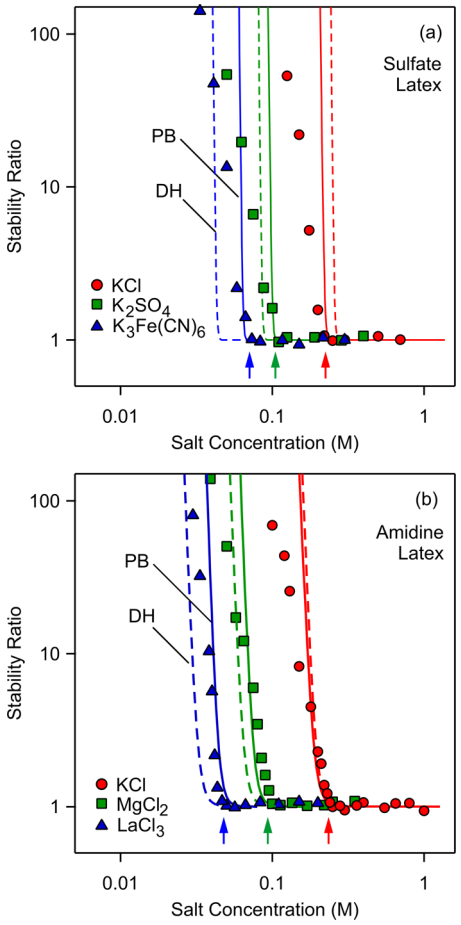

Figure 1. Comparison of experimental and calculated stability ratios in charged latex particle suspension versus the concentration of salts containing multivalent co-ions and monovalent counterions. The arrows indicate the experimental CCCs. DLVO calculations compare the Poisson–Boltzmann (PB) and Debye–Hückel (DH) models for double layer interactions. (a) Negatively charged sulfate latex particles in the presence of Cl^-, SO_4^{2-}, and $Fe(CN)_6^{3-}$ co-ions. (b) Positively charged amidine latex particles in the presence of K^+, Mg^{2+}, and La^{3+} co-ions.

the measured stability ratios plotted versus the electrolyte concentration. The CCC can be identified from the break point in the stability curve (arrows in Figure 1). One observes that the CCC shifts toward lower salt concentrations with increasing valence of the co-ion. The dependence on the valence of the co-ion can be seen more clearly in Figure 2a, where we plot the CCC normalized to its value in the monovalent electrolyte. Indeed, one observes characteristic decrease of the normalized CCC with the ionic valence for both types of particles, namely for positively as well as negatively charged ones. Especially the behavior of the SL particles closely follows the $1/z$ dependence given in eq 2. These shifts may seem surprising, since the

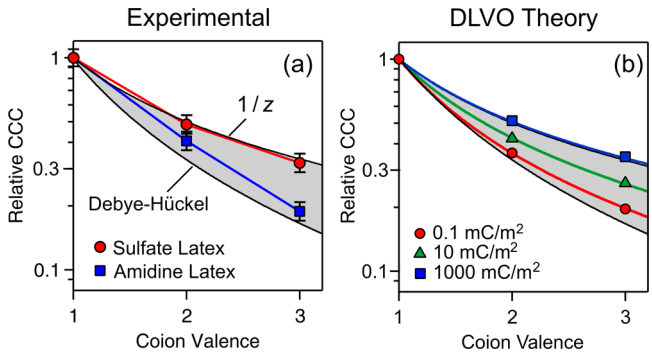

Figure 2. CCC normalized to its value in the monovalent electrolyte versus the valence of the co-ions in the salt solutions used. The shaded area lies between the Debye–Hückel result and the inverse Schulze–Hardy rule. (a) The present experimental data. (b) Calculations with DLVO theory with the surface charge densities indicated.

multivalent ions bear the *same* sign of charge as the particles, and therefore are hardly expected to adsorb to the particle surface.

To investigate this situation further, we have calculated the CCCs with DLVO theory. This theory surmises that the interaction energy potential between two particles $V(h)$, which is a function of the surface separation h, can be obtained as

$$V(h) = V_{\mathrm{vdW}}(h) + V_{\mathrm{dl}}(h) \tag{3}$$

where $V_{\mathrm{vdW}}(h)$ and $V_{\mathrm{dl}}(h)$ are contributions from van der Waals interactions and double layer overlap, respectively. By invoking the Derjaguin approximation and neglecting retardation effects, one has $V_{\mathrm{vdW}}(h) = -HR/(12h)$, where H is the Hamaker constant and R is the particle radius. To calculate the contribution of the double layer, it is essential to solve the full Poisson–Boltzmann (PB) equation between two charged plates in the asymmetric z:1 or 1:z electrolytes. The electric potential profile $\psi(x)$ can be obtained from[7]

$$\frac{\mathrm{d}^2\psi}{\mathrm{d}x^2} = -\frac{q}{\varepsilon_0\varepsilon}\sum_i z_i c_i \, \mathrm{e}^{-z_i q\psi/k_{\mathrm{B}}T} \tag{4}$$

where z_i is the ionic valence, c_i is the number concentration, and i runs over all ions in solution. The additional constants entering eq 4 include the elementary charge q, the dielectric permittivity of vacuum ε_0, the dielectric constant of water ε, the absolute temperature T, and the Boltzmann constant k_{B}. Once the electric potential profile $\psi(x)$ is known, the pressure between the plates can be calculated from its value at the midplane, and the energy profile $V_{\mathrm{dl}}(h)$ can be then obtained by integrating the pressure twice. When the full energy profile $V(h)$ is known, the aggregation rate coefficient k can be evaluated from the solution of the forced diffusion equation under steady-state conditions.[5,7] The stability ratio is then obtained by appropriate normalization of the rate coefficient. All these calculations are performed numerically. For weakly charged particles, the PB equation can be linearized, and the Debye–Hückel approximation can be used instead. In this case, the electrolyte composition enters through the Debye length, which depends on the ionic strength only. Further details on these calculations can be found in the Supporting Information, and they are similar to the ones presented elsewhere.[7]

Results of such DLVO calculations for asymmetric z:1 or 1:z electrolytes where the multivalent ions are co-ions for the charged particles are compared with the experimental data in

DOI: 10.1021/acs.langmuir.5b01649
Langmuir 2015, 31, 6610–6614

Figure 1. The corresponding results obtained with the Debye–Hückel theory are equally shown. A charge regulation parameter of 0.5 is chosen throughout. For sulfate latex, we use a surface charge density of −35 mC/m^2 and a Hamaker constant of 1.0 × 10^{-20} J. The latter value is close to the theoretical value for smooth polystyrene in water.[20,21] Once these parameters are fixed, the DLVO theory predicts the valence dependence without further parameter adjustment. For amidine latex particles, we use a surface charge density of +14 mC/m^2 and a Hamaker constant of 2.0 × 10^{-21} J. The resulting diffuse layer potentials at CCC are given in the Supporting Information (Table S1). These values are approximately independent of the valence, and they are are around −30 mV for the sulfate particles and about +10 mV for the amidine particles.

The smaller value of the fitted Hamaker constant for the amidine particles could be due to their larger surface roughness. Such reduction of the Hamaker constant by roughness was recently demonstrated for larger polystyrene latex particles by direct force measurements.[21] Another explanation of the discrepancy between the fitted Hamaker constants could be related to a larger hydrophobicity of the sulfate particles, which would result in stronger attraction, and would be in turn interpreted as a larger apparent Hamaker constant. Van der Waals and hydrophobic attraction have very similar effects on aggregation rates, and cannot be disentangled without direct force measurements. Possibly, the two types of particles may have different roughness as well as hydrophobicity.

One observes that the PB theory rationalizes the shape of the stability curve and the respective shift with the valence quite well. Not surprisingly, the results of PB and Debye–Hückel theories are similar for the more weakly charged amidine particles, while the differences between these two theories become substantial for the more highly charged sulfate particles. In both cases, however, the use of the PB theory is essential in order to accurately rationalize the trends with the valence.

Further insight can be obtained by analyzing the dependence of the CCC on the valence. For weakly charged particles, the Debye–Hückel theory predicts that[7]

$$\mathrm{CCC} \propto \frac{1}{z(z+1)} \quad \text{(Debye–Hückel)} \tag{5}$$

One obtains this dependence, since only the ionic strength enters this theory. For asymmetric z:1 or 1:z electrolytes, the ionic strength I can be expressed in terms of the salt concentration c as $I = z(z+1)c/2$. This dependence is similar to the frequently quoted[5,7] dependence on $1/z^2$, which applies for a symmetric z:z electrolyte, where $I = z^2c/2$. The derivation of these relations is given in the supplement.[3,9] The dependencies of the CCC on the valence predicted by eqs 2 and 5 are compared with the experimental data in Figure 2a. The amidine system follows more closely the Debye–Hückel dependence due to its weaker charge density, while the sulfate system follows the $1/z$ dependence rather well. We have also carried out DLVO calculations of the CCCs within the PB theory for different charge densities, whereby a particle diameter of 300 nm and a Hamaker constant of 1.0 × 10^{-20} J were used. These results are shown in Figure 2b. For low charge densities, the Debye–Hückel dependence is recovered. For high charge densities, one empirically finds an $1/z$ dependence. This dependence suggests that the monovalent ions, whose concentration for z:1 or 1:z electrolytes is proportional to the valence z, control the CCC by neutralization of the surface charge. This picture is consistent with the fact that for multivalent co-ions, the surface charge is largely neutralized by the monovalent counterions.[22] Currently, however, we have failed to derive the $1/z$ dependence analytically, since the double layer forces in the presence of multivalent co-ions cannot be approximated by a simple exponential.[22] While these forces can be described by the PB equation in the salt-free region at short distances, this dependence is inaccurate at larger distances, and does not reproduce the expected dependence of the CCC. For this reason, we rely on the numerical solution of the PB equation.

Let us now compare this situation with the commonly investigated case of multivalent counterions. A selection of experimental CCCs in the classical situation of multivalent counterions[10,19,23,24] is shown in Figure 3a. Similar dependencies were established experimentally in other systems and wider ranges of valence.[8−12] The results of analogous DLVO calculations are summarized in Figure 3b. The calculations show that the dependence of the CCC on the valence becomes more pronounced with increasing surface charge density. However, even for surface charge densities as high as 1000 mC/m^2, one does not yet reach the $1/z^6$ dependence, which is implied by the Schulze-Hardy rule. As shown in the supplement, this dependence is only obtained in the mathematical limit of $\psi_D \to \infty$ for symmetric z:z electrolytes. A similar dependence is obtained approximately for asymmetric electrolytes for multivalent counterions.[7,25] The experimental CCCs typically show a dependence on the valence, which situates between the Debye–Hückel and $1/z^6$ dependencies. While the magnitude of surface potential is generally low in these systems, its magnitude is further reduced by adsorption of multivalent counterions. For such low surface charge densities, the Debye–Hückel theory is applicable, and one rather expects the weaker $1/z^2$or $1/[z(z+1)]$ dependencies for the CCC. With increasing valence, however, the multivalent ions adsorb more strongly, and they progressively reduce the surface charge density. This reduction leads to a further decrease of the CCC with valence. When both effects are combined, one sometimes observes—accidentally—the $1/z^6$ dependence. While this mechanism was already advocated in the past,[8,9] the details

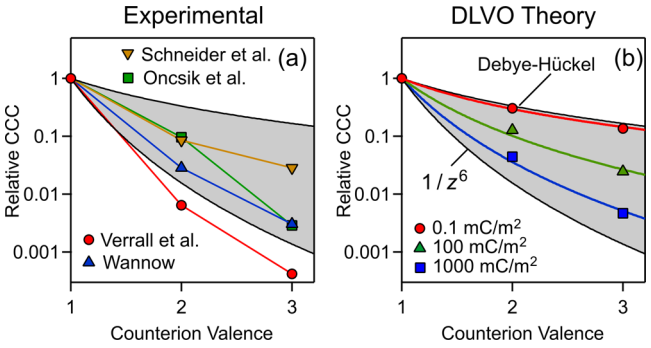

Figure 3. CCC normalized to its value in the monovalent electrolyte versus the valence of the counterions in the salt solutions used. The shaded area lies between the Debye–Hückel result and the Schulze–Hardy rule. (a) Experimental literature data refer to negatively charged sulfate latex by Oncsik et al.[10] and Schneider et al.,[19] positively charged hematite by Verrall et al.,[23] and negatively charged arsenic sulfide by Wannow.[24] (b) Calculations with DLVO theory with the surface charge densities indicated.

DOI: 10.1021/acs.langmuir.5b01649
Langmuir 2015, 31, 6610−6614

are far from being understood, especially quantitatively. The situation could be further complicated by the breakdown of the PB theory, which relies on a mean-field approximation, and neglects ion−ion correlations.[26] Such correlation effects have been shown to be relevant for multivalent counterions.

The present situation of multivalent co-ions is actually much simpler, since these highly charged ions will hardly adsorb on charged surfaces of the same sign.[22] In this case, the surface charge density remains independent of valence. Furthermore, the PB theory is expected to be valid, since this theory accurately captures experimental force curves.[22] While this fact may seem surprising, one must realize that the multivalent co-ions are strongly repelled from the charged surfaces, and that the surface charge is mainly neutralized by monovalent counterions. In this situation, the PB theory has been repeatedly shown to work correctly.[21,26] By the same token, effects of finite ionic size and of image charges are equally negligible.[26,27]

To understand why we refer to the $1/z$ dependence as the *inverse* Schulze−Hardy rule, one must convert the salt concentration to the ionic strength, and consider the dependence of the corresponding critical coagulation ionic strength (CCIS) on the valence. In the Debye−Hückel regime, the CCIS is independent of valence. In the classical case of multivalent counterions, as given by eq 1, the CCIS scales approximately as $1/z^4$, and therefore the CCIS decreases with increasing valence. In the present case of multivalent co-ions, as given in eq 2, the CCIS scales approximately with z, and therefore the CCIS increases with the valence. When comparing these two situations, the dependence of the CCIS for the co-ions is *inversed* with respect to the ones of the counterions.

CONCLUSION

We report on a characteristic dependence of the aggregation rates of charged colloidal particles with multivalent co-ions. The corresponding CCC decreases with valence, but the shift is much smaller than the one expected from the classical Schulze−Hardy rule, which is normally used in the opposite case of multivalent counterions. In the present case of multivalent co-ions, the CCC approximately scales as the inverse of the valence. We refer to this dependence as the *inverse Schulze−Hardy rule*.

ASSOCIATED CONTENT

Supporting Information

Details on materials, particle aggregation experiments, and DLVO calculations. The Supporting Information is available free of charge on the ACS Publications website at DOI: 10.1021/acs.langmuir.5b01649.

AUTHOR INFORMATION

Corresponding Authors

*E-mail: michal.borkovec@unige.ch.
*E-mail: gregor.trefalt@unige.ch.

Notes

The authors declare no competing financial interest.

ACKNOWLEDGMENTS

This research was supported by the Swiss National Science Foundation and the University of Geneva.

REFERENCES

(1) Schulze, H. Schwefelarsen in wässriger Lösung. *J. Prakt. Chem.* **1882**, *25*, 431−452.
(2) Hardy, W. B. A preliminary investigation of the conditions which determine the stability of irreversible hydrosols. *Proc. R. Soc. London* **1900**, *66*, 110−125.
(3) Derjaguin, B.; Landau, L. D. Theory of the stability of strongly charged lyophobic sols and of the adhesion of strongly charged particles in solutions of electrolytes. *Acta Phys. Chim.* **1941**, *14*, 633−662.
(4) Verwey, E. J. W.; Overbeek, J. T. G. *Theory of Stability of Lyophobic Colloids*; Elsevier: Amsterdam, 1948.
(5) Russel, W. B.; Saville, D. A.; Schowalter, W. R. *Colloidal Dispersions*; Cambridge University Press: Cambridge, 1989.
(6) Elimelech, M.; Gregory, J.; Jia, X.; Williams, R. A. *Particle Deposition and Aggregation: Measurement, Modeling, and Simulation*; Butterworth-Heinemann Ltd.: Oxford, 1995.
(7) Trefalt, G.; Szilagyi, I.; Borkovec, M. Poisson-Boltzmann description of interaction forces and aggregation rates involving charged colloidal particles in asymmetric electrolytes. *J. Colloid Interface Sci.* **2013**, *406*, 111−120.
(8) Frens, G.; Heuts, J. J. F. G. The double layer potential as a rate determining factor in the coagulation of electrocratic colloids. *Colloids Surf.* **1988**, *30*, 295−305.
(9) Overbeek, J. T. G. The rule of Schulze and Hardy. *Pure Appl. Chem.* **1980**, *52*, 1151−1161.
(10) Oncsik, T.; Trefalt, G.; Csendes, Z.; Szilagyi, I.; Borkovec, M. Aggregation of negatively charged colloidal particles in the presence of multivalent cations. *Langmuir* **2014**, *30*, 733−741.
(11) Matijevic, E.; Kerker, M. The charge of some heteropoly anions in aqueous solutions as determined by coagulation effects. *J. Phys. Chem.* **1958**, *62*, 1271−1276.
(12) Rubin, A. J.; Hayden, P. L.; Hanna, G. P. Coagulation of escherichia coli by neutral salts. *Water Res.* **1969**, *3*, 843−852.
(13) Tezak, B.; Matijevic, E.; Shulz, K.; Mirnik, M.; Herak, J.; Vouk, V. B.; Slunjski, M.; Babic, S.; Kratohvil, J.; Palmar, T. The mechanism of coagulation of lyophobic sols as revealed through investigations of silver halide sols in statu-nascendi. *J. Phys. Chem.* **1953**, *57*, 301−307.
(14) Sano, M.; Okamura, J.; Shinkai, S. Colloidal nature of single-walled carbon nanotubes in electrolyte solution: The Schulze-Hardy rule. *Langmuir* **2001**, *17*, 7172−7173.
(15) Petrov, Y. Y.; Avvakumova, S. Y.; Sidorova, M. P.; Ermakova, L. E.; Voitylov, V. V.; Voitylov, A. V. Stability of tungsten(VI) oxide dispersions in electrolyte solutions. *Colloid J.* **2011**, *73*, 834−840.
(16) Holthoff, H.; Egelhaaf, S. U.; Borkovec, M.; Schurtenberger, P.; Sticher, H. Coagulation rate measurements of colloidal particles by simultaneous static and dynamic light scattering. *Langmuir* **1996**, *12*, 5541−5549.
(17) Sandkuhler, P.; Lattuada, M.; Wu, H.; Sefcik, J.; Morbidelli, M. Further insights into the universality of colloidal aggregation. *Adv. Colloid Interface Sci.* **2005**, *113*, 65−83.
(18) Chen, K. L.; Mylon, S. E.; Elimelech, M. Enhanced aggregation of alginate-coated iron oxide (hematite) nanoparticles in the presence of, calcium, strontium and barium cations. *Langmuir* **2007**, *23*, 5920−5928.
(19) Schneider, C.; Hanisch, M.; Wedel, B.; Jusufi, A.; Ballauff, M. Experimental study of electrostatically stabilized colloidal particles: Colloidal stability and charge reversal. *J. Colloid Interface Sci.* **2011**, *358*, 62−67.
(20) Bevan, M. A.; Prieve, D. C. Direct measurement of retarded van der Waals attraction. *Langmuir* **1999**, *15*, 7925−7936.
(21) Elzbieciak-Wodka, M.; Popescu, M.; Montes Ruiz-Cabello, F. J.; Trefalt, G.; Maroni, P.; Borkovec, M. Measurements of dispersion forces between colloidal latex particles with the atomic force microscope and comparison with Lifshitz theory. *J. Chem. Phys.* **2014**, *140*, 104906.
(22) Montes Ruiz-Cabello, F. J.; Moazzami-Gudarzi, M.; Elzbieciak-Wodka, M.; Maroni, P.; Labbez, C.; Borkovec, M.; Trefalt, G. Long-

DOI: 10.1021/acs.langmuir.5b01649
Langmuir 2015, 31, 6610−6614

ranged and soft interactions between charged colloidal particles induced by multivalent coions. *Soft Matter* **2015**, *11*, 1562−1571.
(23) Verrall, K. E.; Warwick, P.; Fairhurst, A. J. Application of the Schulze-Hardy rule to haematite and haematite/humate colloid stability. *Colloids Surf., A* **1999**, *150*, 261−273.
(24) Wannow, H. A. Über eine neue Methode zur quantitativen Koagulationsmessung. *Kolloidchem. Beih.* **1939**, *50*, 367−472.
(25) Hsu, J. P.; Kuo, Y. C. An extension of the Schulze-Hardy rule to asymmetric electrolytes. *J. Colloid Interface Sci.* **1995**, *171*, 254−255.
(26) Naji, A.; Kanduc, M.; Forsman, J.; Podgornik, R. Perspective: Coulomb fluids - weak coupling, strong coupling, in between and beyond. *J. Chem. Phys.* **2013**, 139.
(27) Hatlo, M. M.; Lue, L. The role of image charges in the interactions between colloidal particles. *Soft Matter* **2008**, *4*, 1582−1596.

DOI: 10.1021/acs.langmuir.5b01649
Langmuir 2015, 31, 6610−6614

Supplementary Information

Aggregation of Colloidal Particles in the Presence of Multivalent Coions: The Inverse Schulze-Hardy Rule

Tianchi Cao, Istvan Szilagyi, Tamas Oncsik, Michal Borkovec*, Gregor Trefalt*
Department of Inorganic and Analytical Chemistry, University of Geneva, Sciences II, 30 Quai Ernest-Ansermet, 1205 Geneva, Switzerland

*Corresponding authors: Email. michal.borkovec@unige.ch, gregor.trefalt@unige.ch

---

Materials. The surface modified polystyrene latex particles were purchased from Invitrogen Corporation. Positively charged amidine functionalized particles as well as negatively charged sulfate functionalized particles were used. The manufacturer reported a radius (determined by transmission electron microscopy) of 150 nm (coefficient of variation is 5.7%) for the amidine and 145 nm (coefficient of variation is 5.1%) for the sulfate particles. Dynamic light scattering (DLS) measurements in stable dispersions yielded hydrodynamic radii of 166 nm and 160 nm for amidine and sulfate, respectively. The particles were dialyzed with cellulose ester membrane against Milli-Q water (Millipore) until the conductivity value became comparable to the value for pure water. The sign of the particle charge was verified with electrophoretic mobility measurements. The particle concentrations of the stock suspensions were determined by static light scattering after dialysis by calibration of the signal with the original suspensions of known concentrations. Analytical grade KCl, $MgCl_2 \cdot 6H_2O$ (Acros Organics), $LaCl_3 \cdot 7H_2O$, $K_3Fe(CN)_6$ (Sigma-Aldrich), and K_2SO_4 (Fluka) were dissolved in Milli-Q water and the pH was adjusted to 4.0 with HCl (Merck). All electrolytes used dissociate fully and the resulting ions undergo neither protonation nor hydrolysis reactions. The salt solutions were filtered with a 0.1 μm syringe filter (Millipore) to remove dust contamination. All experiments were performed at a temperature of 25.0±0.2 °C.

Particle Aggregation. Time-resolved DLS measurements were carried out with a light scattering goniometer (ALV/CGS-8F) with a solid-state laser of a wavelength of 532 nm at a scattering angle of 90°. The experiments were carried out in borosilicate cuvettes, which were first cleaned in piranha solution (mixture of concentrated H_2SO_4 and 30% H_2O_2 of a volume ratio of 3:1), then washed with pure water, and dried in a dust-free oven. The respective salt solutions were mixed with water, which was previously adjusted to pH 4.0, to obtain the desired salt concentrations in the cuvette, and the aggregation was initiated by adding the latex stock dispersion, which results in a final particle concentration of 10 mg/L. The latter concentration corresponds to 6.7×10^{14} m^{-3} and 7.4×10^{14} m^{-3} for amidine and sulfate latex, respectively. The apparent hydrodynamic radii were measured at different time intervals over 8–110 minutes. The translational diffusion coefficient was extracted from the correlation function with the second cumulant method, and the hydrodynamic radius was calculated by the Stokes-Einstein equation.[1] The apparent dynamic aggregation rates were obtained from the increase in the apparent hydrodynamic radii as[2]

$$\Delta = \frac{1}{r_{\mathrm{h}}(0)} \cdot \left. \frac{dr_{\mathrm{h}}(t)}{dt} \right|_{t\to 0} \qquad (1)$$

where $r_h(0)$ is the initial hydrodynamic radius, $r_h(t)$ is the apparent hydrodynamic radius, and t is the time. The stability ratio W was evaluated by means of the relation

$$W = \frac{\Delta_{\text{fast}}}{\Delta} \tag{2}$$

where Δ_{fast} was the apparent rate determined in 1.0 M KCl solution where the aggregation processes are diffusion controlled. The increase in the hydrodynamic radii was always below 30% during the experiments which allowed us to study the early stages of the particle aggregation where mainly dimers were formed.

DLVO Calculations. For the calculations of stability ratios the DLVO theory was used. This theory defines the total interaction energy potential between two charged particles V, as a sum of van der Waals V_{vdW}, and double layer interactions V_{dl}, namely

$$V(h) = V_{\text{vdW}}(h) + V_{\text{dl}}(h) \tag{3}$$

Van der Waals interactions between equally sized spheres are calculated with the Derjaguin approximation and neglecting the retardation effects

$$V_{\text{vdW}}(h) = -\frac{HR}{12h} \tag{4}$$

where *H* is the Hamaker constant and *R* is the particle radius. Double layer interactions are obtained by solving the Poisson-Boltzmann (PB) equation for equally charged parallel plates

$$\frac{d^2\psi}{dx^2} = -\frac{q}{\varepsilon_0 \varepsilon} \sum_i z_i c_i e^{-z_i \beta q \psi} \tag{5}$$

where $\psi(x)$ is the electrical potential profile, z_i is the ionic valence, c_i number concentration, and *i* runs over all ions in solution. The additional constants used in eq. (5) are the elementary charge *q*, the dielectric permittivity of vacuum ε_0, is the dielectric constant of water ε, and the inverse thermal energy $\beta = 1/k_{\text{B}}T$. The PB equation is solved numerically within the constant regulation boundary conditions

$$\pm\varepsilon_0 \varepsilon \left.\frac{d\psi}{dx}\right|_{x=\pm h/2} = \sigma^{(\pm)} - C_{\text{I}}\left[\psi\left(\pm h/2\right) - \psi_{\text{D}}\right] \tag{6}$$

where the right and left surfaces are located at $x = +h/2$ and $x = -h/2$, respectively, while σ denotes the surface charge density, C_{I} the inner capacitance, and ψ_{D} the diffuse layer potential of the isolated surface. We replace the interlayer capacitance with the regulation parameter

$$p = \frac{C_{\text{D}}}{C_{\text{D}} + C_{\text{I}}} \tag{7}$$

where C_{D} is the diffuse layer capacitance defined as

$$C_D = \frac{d\sigma}{d\psi_{\text{D}}} \tag{8}$$

The surface charge density and diffuse layer potential of isolated surface are connected with the following equation

$$\sigma = \pm\left[2k_{\mathrm{B}}T\varepsilon_0\varepsilon\sum_i c_i\left(e^{-z_i\beta q\psi_{\mathrm{D}}}-1\right)\right]^{1/2} \tag{9}$$

Numerical solution of the PB equation yields the electric potential profile. The value of the potential at the mid-plane $\psi_{\mathrm{M}} = \psi(x=0)$ enables the calculation of the disjoining pressure

$$\Pi = k_{\mathrm{B}}T\sum_i c_i\left(e^{-z_i\beta q\psi_{\mathrm{M}}}-1\right) \tag{10}$$

Once the pressure is known, double layer force between two equally charged spherical particles can be obtained by integration and use of the Derjaguin approximation

$$F_{\mathrm{dl}} = \pi R\int_{\infty}^{h}\Pi(h')dh' \tag{11}$$

Finally, the energy potential of the double layer interaction follows from an additional integration

$$V_{\mathrm{dl}} = \int_{\infty}^{h}F_{\mathrm{dl}}(h')dh'\,. \tag{12}$$

When the total energy profile is known, the aggregation rate coefficient can be found through steady state solution of the forced diffusion equation[1,3]

$$k = \frac{4k_{\mathrm{B}}T}{3\eta R}\left[\int_0^{\infty}\frac{B(h/R)}{(2R+h)^2}\exp\left(\frac{V(h)}{k_{\mathrm{B}}T}\right)dh\right]^{-1} \tag{13}$$

where η is the viscosity of the medium and B is the hydrodynamic resistance function that is approximated as[4]

$$B(y) = \frac{6y^2+13y+2}{6y^2+4y} \tag{14}$$

The stability ratio is then obtained analogously to the experimental stability ratio, see eq. (2)

$$W = \frac{k_{\mathrm{fast}}}{k} \tag{15}$$

where the fast rate k_{fast} is calculated only with the van der Waals interaction and setting the double layer interaction potential to zero.

Valence Dependence of the CCC. The CCC can be estimated by assuming that the energy barrier is equal to zero.[5-8] This condition can be described by following equations

$$V(h_{\max}) = 0 \quad \text{and} \quad \left.\frac{dV(h)}{dh}\right|_{h=h_{\max}} = 0 \tag{16}$$

where $h_{\max}$ is the separation distance at the energy barrier. Two cases can be distinguished, namely, the low potential and the high potential limit.

In the low potential limit, the double layer interaction is given by the Debye-Hückel theory[1]

$$V_{\mathrm{dl}} = 2\pi\varepsilon\varepsilon_0 R\psi_D^2 \, \mathrm{e}^{-\kappa h} \tag{17}$$

where κ is the inverse Debye length defined by

$$\kappa^2 = \frac{2\beta q^2 I}{\varepsilon_0 \varepsilon} \tag{18}$$

where I is the ionic strength given by

$$I = \frac{1}{2}\sum_i z_i^2 c_i \tag{19}$$

Combining eqns.(3), (4), and (16)-(17) one arrives at the following relation valid at CCC

$$\kappa = \frac{24\pi\varepsilon\varepsilon_0\psi_D^2}{eH} \tag{20}$$

where e is the basis of the natural logarithm. When one replaces in eq. (20) the diffuse layer potential by the surface charge density σ by means of the relation

$$\psi_D = \frac{\sigma}{\varepsilon\varepsilon_0\kappa} \tag{21}$$

one finds

$$\kappa^2 = \left(\frac{24\pi\sigma^2}{eH\varepsilon\varepsilon_0}\right)^{2/3} \tag{22}$$

Inserting relation (18) into eq. (22), one finds that the critical coagulation ionic strength (CCIS) is a constant,

$$\mathrm{CCIS} \propto \text{ const.} \tag{23}$$

namely it does not depend on ion valence z. For the symmetric z:z electrolyte, eq. (19) simplifies to

$$I = \frac{z^2}{2}c \tag{24}$$

where *c* is the salt concentration. The resulting CCC dependence becomes

$$\mathrm{CCC} \propto \frac{1}{z^2} \tag{25}$$

In the case of 1:*z* or *z*:1 electrolyte , eq. (19) leads to the following relation for the ionic strength

$$I = \frac{z(z+1)}{2} c \tag{26}$$

and one obtains an analogous expression for the CCC, namely

$$\mathrm{CCC} \propto \frac{1}{z(z+1)} \tag{27}$$

Note, however, that eq. (22) predicts that in this regime the CCC increases with the surface charge density, namely as $\mathrm{CCC} \propto \sigma^{4/3}$.

For the high potential limit and for symmetric *z*:*z* electrolytes, the double layer potential energy can be approximated at larger distances as[1]

$$V_{\mathrm{dl}} = 2\pi\varepsilon\varepsilon_0 R\psi_{\mathrm{eff}}^2 \, \mathrm{e}^{-\kappa h} \tag{28}$$

where the effective potential can be expressed as

$$\psi_{\mathrm{eff}} = \frac{4}{z\beta q} \tanh\left(\frac{z\beta q \psi_{\mathrm{D}}}{4} \right) \tag{29}$$

Based on the same arguments, one arrives at an expression that is analogous to eq. (20) for the inverse Debye length

$$\kappa = \frac{24\pi\varepsilon\varepsilon_0 \psi_{\mathrm{eff}}^2}{eH} \tag{30}$$

For large diffuse layer potentials ($\psi_{\mathrm{D}} \to \infty$), eq. (29) simplifies to

$$\psi_{\mathrm{eff}} = \frac{4}{z\beta q} \tag{31}$$

while eq. (30) reduces to

$$\kappa = \frac{386\pi\varepsilon\varepsilon_0}{eH\beta^2 q^2 z^2} \tag{32}$$

Combining with eq. (18) one obtains

$$\mathrm{CCIS} \propto \frac{1}{z^4} \tag{33}$$

With eq. (25) one obtains the classical Schulze-Hardy rule for symmetric *z*:*z* electrolyte

$$\mathrm{CCC} \propto \frac{1}{z^6} \tag{34}$$

In this saturation limit, the CCC is independent of the surface charge density.

Table S1. Diffuse layer potentials at the critical coagulation concentrations for amidine and sulfate latex particles.

Particle	Salt	ψ_D at CCC (mV)
Amidine Latex	KCl	+12
	$MgCl_2$	+11
	$LaCl_3$	+12
Sulfate Latex	KCl	–34
	K_2SO_4	–27
	$K_3Fe(CN)_6$	–24

The diffuse layer potentials were calculated from the fitted surface charge densities with the Poisson-Boltzmann theory.

References

1. Elimelech, M.; Gregory, J.; Jia, X.; Williams, R. A., *Particle Deposition and Aggregation: Measurement, Modeling, and Simulation*. Butterworth-Heinemann Ltd.: Oxford, 1995.
2. Holthoff, H.; Egelhaaf, S. U.; Borkovec, M.; Schurtenberger, P.; Sticher, H., Coagulation rate measurements of colloidal particles by simultaneous static and dynamic light scattering. *Langmuir* **1996,** 12, 5541-5549.
3. Russel, W. B.; Saville, D. A.; Schowalter, W. R., *Colloidal Dispersions*. Cambridge University Press: Cambridge, 1989.
4. Honig, E. P.; Roebersen, G. J.; Wiersema, P. H., Effect of hydrodynamic interaction on coagulation rate of hydrophobic colloids. *J. Colloid Interface Sci.* **1971,** 36, 97-102.
5. Derjaguin, B.; Landau, L. D., Theory of the stability of strongly charged lyophobic sols and of the adhesion of strongly charged particles in solutions of electrolytes. *Acta Phys. Chim.* **1941,** 14, 633-662.
6. Verwey, E. J. W.; Overbeek, J. T. G., *Theory of Stability of Lyophobic Colloids*. Elsevier: Amsterdam, 1948.
7. Reerink, H.; Overbeek, J. T. G., The rate of coagulation as a measure of the stability of silver iodide sols. *Discuss. Farad. Soc.* **1954**, 74-84.
8. Trefalt, G.; Szilagyi, I.; Borkovec, M., Poisson-Boltzmann description of interaction forces and aggregation rates involving charged colloidal particles in asymmetric electrolytes. *J. Colloid Interf. Sci.* **2013,** 406, 111-120.

CHAPTER 3

Aggregation of Colloidal Particles in the Presence of Hydrophobic Anions: Importance of Attractive Non-DLVO Forces

Cao, T.; Trefalt, G.; Borkovec, M.

Langmuir **2018**, 34, 14368–14377.

LANGMUIR Cite This: *Langmuir* 2018, 34, 14368−14377 Article pubs.acs.org/Langmuir

Aggregation of Colloidal Particles in the Presence of Hydrophobic Anions: Importance of Attractive Non-DLVO Forces

Tianchi Cao, Gregor Trefalt, and Michal Borkovec*

Department of Inorganic and Analytical Chemistry, University of Geneva, Sciences II, 30 Quai Ernest-Ansermet, 1205 Geneva, Switzerland

ABSTRACT: Aqueous suspensions of amidine latex (AL) and sulfate latex (SL) particles containing sodium tetraphenylborate and NaCl are studied with electrokinetic and time-resolved light-scattering techniques. In monovalent salt solutions, AL is positively charged, whereas SL is negatively charged. Electrophoretic mobility measurements demonstrate that adsorption of tetraphenylborate anions leads to a charge reversal of AL particles. At higher concentrations, both types of particles accumulate negative charge. For AL particles, the charge reversal leads to a narrow fast aggregation region and an intermediate regime of slow aggregation. For SL particles, the intermediate slow regime is also observed. These aspects can be explained with classical theory of Derjaguin, Landau, Verwey, and Overbeek (DLVO). Another regime of fast aggregation is observed at intermediate concentrations, and the existence of this regime can be rationalized by an additional attractive non-DLVO force. We suspect that this additional force is caused by surface charge heterogeneities.

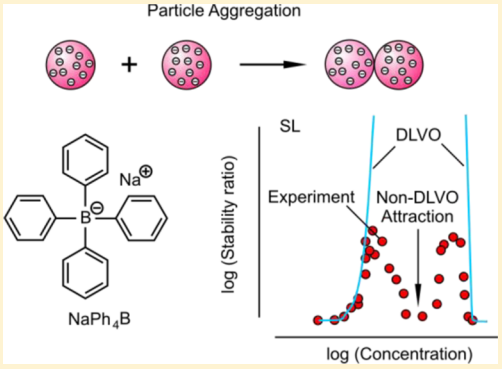

INTRODUCTION

Particle aggregation is one of the key pathways for the destabilization of colloidal particle suspensions.[1,2] Because this process is relevant in many industrial phenomena, including water treatment or papermaking, it has been studied in substantial detail in the past.[3,4] The time scale of the aggregation process is set by the formation rate of particle doublets in a dilute suspension. When the interaction between the colloidal particles is attractive, particle aggregation is fast and controlled by diffusional approach. When the interactions are repulsive, the particles must overcome an activation barrier, and therefore, the particle aggregation is slow. As the transition region between the fast regimes is relatively narrow, it is normally characterized by the so-called critical coagulation concentration (CCC).

The famous theory of Derjaguin, Landau, Verwey, and Overbeek (DLVO) suggests that the interactions between the particles are governed by two main contributions, namely, van der Waals and double-layer forces.[1,2,5,6] For weakly charged particles and high salt levels, double-layer forces are negligible and interactions are governed by attractive van der Waals forces. Under these conditions, fast aggregation is expected. For highly charged particles and lower salt levels, repulsive double-layer forces become important, which induces a slowdown of the aggregation process.

This theory further stipulates that a key parameter determining the rate of colloidal aggregation is the electric diffuse layer potential, because this potential dictates the strength of the double-layer forces. For small colloidal particles, the diffuse layer potential cannot be easily measured experimentally, but one can instead use the electrokinetic potential, which is also referred to as the ζ-potential. This potential can be extracted from experimentally accessible electrophoretic mobility, and such potentials have been shown to approximate diffuse layer potentials rather well.[7,8] Researchers have exploited the relation between the electrokinetic potential and colloidal aggregation rate most successfully. In many systems, the aggregation rate is governed by the electrokinetic potential, which includes effects of salt concentration as well as of charge reversal. Examples include solutions of various additives, such as salts containing monovalent and multivalent ions, polyelectrolytes, and ionic surfactants.[9−18] Indeed, for sufficiently high salt conditions, the magnitude of the electrokinetic potential is low, and particles in colloidal suspensions aggregate rapidly. For low salt conditions, the magnitude of the potential becomes high, and slow aggregation is observed. When an additive induces a charge reversal, the electrokinetic potential goes through zero, and at this point the aggregation becomes rapid too.

Here we demonstrate that this picture is only partially valid in the case of polystyrene latex particles with different surface functionalities in the presence of tetraphenylborate (Ph_4B^-) anions. Polystyrene latex particles represent a well-studied monodisperse and spherical colloids, whose aggregation behavior can be well described by DLVO theory, definitely in the case of simple monovalent and multivalent ions.[11−13] However, the charging behavior of the particles must be known and included through measured electrokinetic potentials.

Received: September 19, 2018
Revised: October 31, 2018
Published: November 1, 2018

DOI: 10.1021/acs.langmuir.8b03191
Langmuir 2018, 34, 14368−14377

Table 1. Selected Properties of the Latex Particles Used

	radius (nm)			polydispersity (CV, %)				
particles	TEM[a]	SLS[b]	DLS[c]	TEM[a]	SLS[b]	ζ-potential[d] (mV)	CCC[e] (mM)	fast rate[f] k_{fast} ($\times 10^{-18}$ m^3/s)
amidine latex (AL)	150	149 ± 2	153 ± 3	5.7	6.5 ± 0.9	+48 ± 2	152 ± 9	3.1 ± 0.2
sulfate latex (SL)	125	117 ± 2	123 ± 2	3.1	7.2 ± 0.7	−50 ± 1	149 ± 2	2.9 ± 0.2

[a]Measured by TEM by the manufacturer. [b]Measured by SLS. [c]Measured by DLS. [d]Electrokinetic potential measured by electrophoresis without added salt at pH 4.0. [e]CCC in NaCl solutions at pH 4.0. [f]Measured absolute fast aggregation rate coefficients in 600 mM NaCl solutions of pH 4.0.

Ph_4B^- anions and analogous tetraphenylphosphonium (Ph_4P^+) or tetraphenylarsonium (Ph_4As^+) cations are hydrophobic monovalent ions, whose salts readily dissolve in water. Such ions should be positioned on the extremes of the Hofmeister series, which classifies ions according to their hydrophobicity.[19] Similar to ionic surfactants, they strongly adsorb to hydrophobic substrates, and may induce a charge reversal.[20−22] In contrast to ionic surfactants, which comprise a hydrophilic charged head group and a hydrophobic tail, tetraphenyl ions bear hydrophobic phenyl groups, which are bound to the central charged ion. To our knowledge, these ions do not form micelles in aqueous solutions. For this reason, they represent an interesting class of monovalent ions that are highly suitable to study effects of hydrophobic interactions on adsorption processes, electrophoretic mobility, or colloidal aggregation. Although few studies are available concerning the influence of these ions on electrokinetic and diffuse layer potentials,[20−23] there is basically no information concerning their effects on particle aggregation.

The present study explores the aggregation of colloidal particles in the presence of Ph_4B^- ions experimentally. We demonstrate that DLVO theory, which relies on electrokinetic data, is insufficient even to qualitatively rationalize the aggregation behavior in such systems. We thus argue that additional attractive non-DLVO forces, which appear similar to the ones recently reported in direct force measurements,[7,23−25] are the cause for the presence of an additional fast aggregation region.

EXPERIMENTAL AND METHODS

Materials. Two types of functionalized, surfactant-free polystyrene particles (Invitrogen Corporation) were used, namely, amidine latex (AL) and sulfate latex (SL). The average particle radius and their polydispersity as determined by the manufacturer with transmission electron microscopy (TEM) are given in Table 1. The particle suspensions were purified by dialysis in Milli-Q water (Millipore) for about a week, until the conductivity of water was below 80 mS/m. Polyvinylidene fluoride and cellulose ester membranes were used to dialyze the AL and SL suspensions, respectively. The same AL particles were already used in previous studies.[26,27]

Analytical-grade sodium tetraphenylborate, $NaPh_4B$, and sodium chloride, NaCl, both from Sigma-Aldrich, were dissolved with Milli-Q water and the pH was adjusted to 4.0 with HCl. Prior to use, the $NaPh_4B$ stock solution with a concentration of 1.2 M was left to stand overnight, centrifuged at 18 000*g* during 30 min, and then filtered with a 0.1 μm syringe filter (Millipore). The latter steps were needed to free the salt solution from particulate impurities.

Electrophoresis. Zetasizer Nano ZS (Malvern Instruments) was used to measure the electrophoretic mobility of the particles in aqueous suspensions containing different salt concentrations. Suspensions used in the experiments were prepared by first mixing stock solutions of NaCl and $NaPh_4B$ stock solution with Milli-Q water to obtain the desired concentrations. Immediately prior to the measurement, a stock suspension of the latex particles was added and the suspension was mixed. The final particle concentrations used were 5 mg/L for both particles. This mass concentration corresponds to a number concentration of 3.4×10^{14} m^{-3} for AL and 7.1×10^{14} m^{-3} for SL. The measured electrophoretic mobility was converted to electrokinetic potentials (ζ-potential) by means of the O'Brien and White model.[28]

Light Scattering. Particle aggregation was measured with a light-scattering goniometer equipped with eight fiberoptic detectors (ALV/CGS-8F) and a solid-state laser with a wavelength of 532 nm. The experiments were performed in borosilicate cuvettes. The cuvettes were cleaned in hot piranha solution, which is a mixture of 96% H_2SO_4 and 30% H_2O_2 in a volume ratio of 3:1, then thoroughly washed with Milli-Q water, and dried in a dust-free oven at 60 °C. The signal was accumulated for 20 s and correlation functions were analyzed with a second-order cumulant fit. The experiments were carried out in the early stages of the aggregation process, and this condition was ensured by verifying that the apparent hydrodynamic radius did not increase more than 30% during the experiment.

Absolute aggregation rates were determined in particle suspensions by time-resolved simultaneous static and dynamic light scattering (SSDLS). The suspensions were adjusted to pH 4.0 and contained NaCl at a concentration of 600 mM. The particle concentrations were 0.62 mg/L (4.2×10^{13} m^{-3}) for AL and 0.69 mg/L (9.8×10^{13} m^{-3}) for SL. The apparent static $\Sigma = I(0)^{-1}\, dI/dt|_{t\to 0}$ and dynamic $\Delta = R(0)^{-1}\, dR/dt|_{t\to 0}$ aggregation rates were extracted from the initial dependence of the scattering intensity I and the apparent hydrodynamic radius R on time t. The absolute rates were then obtained by fitting the linear relation between these two quantities[29,30]

$$\Sigma = \left(1 - \frac{1}{\alpha}\right)\Delta - kN_0 \qquad (1)$$

where N_0 is the initial particle number density and α is the hydrodynamic factor. The experimental results are shown in Figure 1

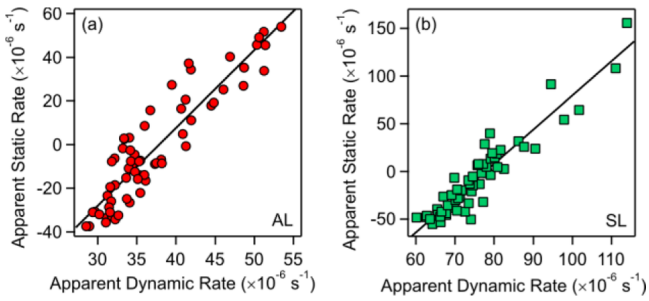

Figure 1. Scatter plots of apparent static rates vs the apparent dynamic rates measured by time-resolved SSDLS in 600 mM NaCl and pH 4.0 to extract fast aggregation rate coefficients, which are given in Table 1. (a) AL, (b) SL.

and the resulting rate coefficients are given in Table 1. The fitted hydrodynamic factors agree within experimental error with the theoretical value of 1.38 reported earlier.[29] For the AL particles, the measured rate coefficient is the same as the one published earlier within experimental error.[26,27] For other conditions, the apparent dynamic rate was measured at a scattering angle of 90°, from which the stability ratio was extracted. The suspensions used in the latter experiments were prepared in the same way as for the electrophoresis.

Static light scattering (SLS) was used to extract accurate particle radii and polydispersities. Scattering intensity was measured as a

DOI: 10.1021/acs.langmuir.8b03191
Langmuir 2018, 34, 14368−14377

function of the scattering angle in particle suspensions adjusted to pH 4.0 and without added NaCl at particle concentrations of 1.4 mg/L (9.5×10^{14} m^{-3}) for AL and 2.7 mg/L (3.8×10^{14} m^{-3}) for SL. The scattering profile was fitted to Mie theory, including particle polydispersity and back reflection, as described earlier.[26,27] SLS was also used to determine the particle concentrations of the dialyzed suspensions. These concentrations were determined by comparing the scattering intensities of dialyzed suspensions with the ones of the original suspensions, where the concentrations were known. Particle radius was also measured by dynamic light scattering (DLS) at a scattering angle of 90° in particle suspensions without added NaCl adjusted to pH 4.0 at particle concentration of 5.0 mg/L for both types of particles. The measured radii and polydispersities are summarized in Table 1, and they agree well with the ones reported by the manufacturer. The slightly larger radii measured by DLS are likely caused by polydispersity effects.

Model Calculations. The aggregation rate coefficient, k, of doublet formation of monodisperse spherical particles can be calculated by finding the steady-state solution of the forced diffusion equation. This resulting expression involves the interaction potential, $V(h)$, acting between the particles, where h is the smallest surface separation and can be written as[1,2]

$$k = \frac{4}{3\eta R\beta}\left[\int_0^\infty \frac{B(h)}{(2R+h)^2}\exp[\beta V(h)]\,dh\right]^{-1} \tag{2}$$

where η is the shear viscosity, R the particle radius, $\beta = 1/(k_B T)$ is the inverse thermal energy, and $B(h)$ is the hydrodynamic resistance function. We use $\eta = 8.90 \times 10^{-4}$ Pas as appropriate for water at 25 °C. We further denote by T the absolute temperature, by k_B the Boltzmann constant, and the hydrodynamic function is approximated as[1,2]

$$B(h) = \frac{6h^2 + 13hR + 2R^2}{6h^2 + 4hR} \tag{3}$$

Instead of the rate coefficient, we normally report the stability ratio defined as

$$W = \frac{k_{fast}}{k} \tag{4}$$

where k_{fast} is the rate coefficient under fast aggregation conditions as realized at high salt concentration.

The interaction potential profile, $V(h)$, between two particles is obtained by integrating the interaction energy, $W(h)$, in the plate–plate geometry within the Derjaguin approximation[1,2]

$$V(h) = \pi R\int_h^\infty W(h')\,dh' \tag{5}$$

We assume that this interaction has three additive contributions, namely,

$$W = \overbrace{W_{vdW} + W_{dl}}^{DLVO} + W_{att} \tag{6}$$

where W_{vdW} denotes the contribution because of van der Waals interaction and W_{dl} because of the double layer, and W_{att} is an additional attractive interaction.

The two DLVO contributions, W_{vdW} and W_{dl}, are calculated as follows. van der Waals interactions are obtained from the non-retarded expression[1,2]

$$W_{vdW} = -\frac{H}{12\pi h^2} \tag{7}$$

where H is the Hamaker constant. The double-layer interaction is inferred from the Poisson–Boltzmann (PB) equation for a monovalent electrolyte between two identical and homogeneously charged plates. The electric potential profile, $\psi(x)$, is a function of the position x and satisfies the equation

$$\frac{d^2\psi}{dx^2} = \frac{2ec}{\varepsilon_0\varepsilon}\sinh(\beta e\psi) \tag{8}$$

where e is the elementary charge, ε_0 is the permittivity of vacuum, and ε is the dielectric constant of water. The latter parameter is taken as ε = 80 throughout, as applicable for water at 25 °C. The PB equation is solved numerically between the two charged plates located at $x = \pm h/2$ subject to the constant charge (CC) and constant potential (CP) boundary conditions. In either case, the charge of the isolated surface is characterized by its electric potential, ψ_D, referred to as the diffuse layer potential. The swelling pressure, Π, is then evaluated from the value of the electric potential at the midplane $\psi_m = \psi(0)$ as

$$\Pi = 2k_B T[\cosh(\beta e\psi_m) - 1] \tag{9}$$

Finally, the interaction potential between the plates is found by integrating the pressure profile, namely,

$$W_{dl}(h) = \int_h^\infty \Pi(h')\,dh' \tag{10}$$

Further details on similar PB calculations can be found in the literature.[1,2,27]

Although DLVO theory stipulates that interactions can be approximated with the first two terms, an additional attractive non-DLVO force will be considered here. This additional contribution is modeled by an exponential function, namely,

$$W_{att} = -A\,e^{-qh} \tag{11}$$

where $A > 0$ is the amplitude of the interaction and q^{-1} its decay length. Such exponential attractive forces were proposed theoretically to originate from patch–charge heterogeneities or hydrophobic interactions.[31,32] In system containing multivalent or hydrophobic ions, direct force measurements equally reveal the existence of exponential non-DLVO forces with a decay length around 1 nm.[7,23,24] Patch–charge interactions were also invoked to interpret forces acting between charged surfaces with adsorbed polyelectrolytes of opposite charge.[33−35] However, the respective length scales are substantially larger in the latter systems.

RESULTS AND DISCUSSION

This article presents measurements of particle aggregation rates and of electrophoretic mobilities for submicron AL and SL particles in aqueous solutions containing sodium tetraphenylborate ($NaPh_4B$) and NaCl. All experiments were carried out in aqueous solutions adjusted to pH 4.0 and at a temperature of 25 °C. In monovalent salt solutions, the AL particles are positively charged, whereas the SL particles are negatively charged. Further properties of these particles are summarized in Table 1. As the Ph_4B^- anion is hydrophobic, it strongly adsorbs on the latex particle surfaces. This adsorption process induces an accumulation of negative charge on the particles, and the accumulated charge modifies the aggregation behavior substantially. Further analysis of these results and comparison with model calculations based on DLVO theory reveals that additional attractive non-DLVO forces are active and modify the aggregation behavior further.

Charging Behavior. Electrophoresis measurements were performed to study the influence of Ph_4B^- ions on the charging behavior of the AL and SL particles. The electrophoretic mobilities were converted to electrokinetic potentials (ζ-potentials) and their dependence on the Ph_4B^- concentration is shown in Figure 2. The effect of adding NaCl was equally studied.

Figure 2a shows the measured electrokinetic potentials for AL particles. At very low concentrations of Ph_4B^-, the potentials are positive and they reflect the positive charge caused by the cationic amidine groups at the AL particle

DOI: 10.1021/acs.langmuir.8b03191
Langmuir 2018, 34, 14368−14377

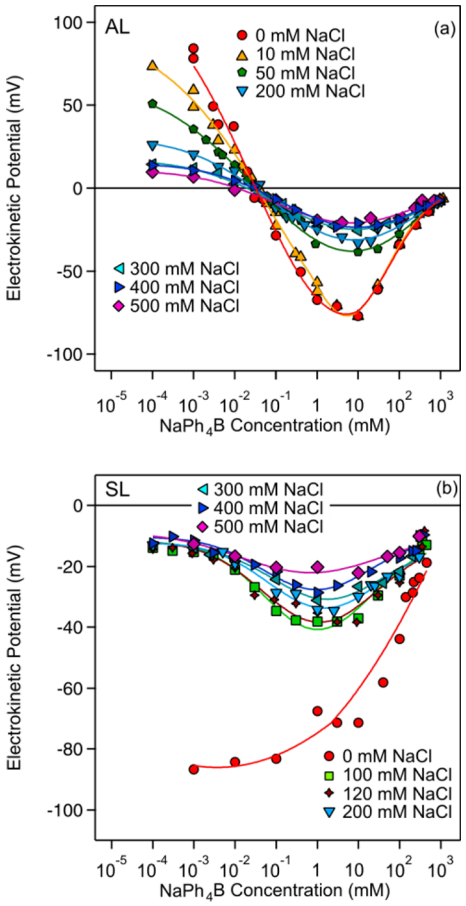

Figure 2. Electrokinetic potentials (ζ-potentials) measured by electrophoresis vs the concentration of $NaPh_4B$ and different concentrations of added NaCl at pH 4.0. Solid lines are empirical interpolating functions used in the model calculations. (a) AL, (b) SL.

surface. As the concentration is increased, Ph_4B^- anions adsorb to the positively charged AL particles and cause an accumulation of negative charge. This accumulation first leads to charge neutralization at a concentration of 0.030 ± 0.005 mM and subsequently to a pronounced charge reversal. The electrokinetic potential reaches a minimum around a concentration of 10 mM, and then the potential increases because of screening. Addition of the indifferent NaCl electrolyte reduces the magnitude of the potentials, but otherwise leaves the features unchanged. However, when one calculates the respective electrokinetic charge by means of the Grahame equation, one observes that the magnitude of the charge density slightly increases with increasing NaCl concentration. This trend suggest that the presence of salt promotes the adsorption of Ph_4B^- anions. However, the position of the charge neutralization point remains the same, indicating that this effect is relatively weak.

These observations concerning the charge reversal are in line with recent electrophoresis experiments with negatively charged latex particles in the presence of Ph_4P^+ cations.[21,22] These authors also observe a charge neutralization point at Ph_4P^+ concentrations in the range 0.5−3 mM, and they do not report any shifts of this point upon addition of KCl. Direct force measurements between sulfate particles in the presence of Ph_4As^+ at pH 4.0 without added salt reveal that the charge neutralization point is located at somewhat lower concentration, near 0.2 mM. These publications and our findings all suggest that monovalent tetraphenyl ions systematically induce a charge reversal of oppositely charged latex particles and that this reversal occurs in the mM concentration range or below.

Similar charge reversal phenomena were also observed with colloidal particles in the presence of other strongly adsorbing species. These systems include oxide particle suspensions containing oppositely charged surfactants[15,36−40] or when subject to pH variations,[11,17,18] and latex particle suspensions in the presence of oppositely charged polyelectrolytes or highly charged multivalent ions.[14,16,26,41,42]

Figure 2b shows the respective electrokinetic potentials for SL particles. At very low concentrations of Ph_4B^-, the potentials are negative, as they reflect the negative charge of the anionic sulfate groups at the SL particle surface. Without added NaCl, the electrokinetic potentials increase with increasing Ph_4B^- concentration. However, as soon NaCl is added, one observes an intermediate minimum in the electrokinetic potential, which indicates that the Ph_4B^- anions also adsorb to the negatively charged SL particles. The potentials go again through a minimum near 10 mM and they increase at higher concentrations. The latter increase is caused by screening. The electrokinetic charge shows a similar trend as for the AL particles.

The occurrence of adsorption in this like-charged situation strongly suggests that other forces than electrostatic ones are responsible for this adsorption process. These forces are probably of hydrophobic nature. The presence of the phenyl rings makes the Ph_4B^- anion hydrophobic, and the same applies to the polystyrene latex particles, and in this situation strong hydrophobic and $\pi-\pi$ stacking interactions are likely present. Nevertheless, a similar accumulation of negative charge was observed for clay minerals and carbon nanotubes in the presence of sodium dodecyl sulfate by similar electrophoresis experiments.[43,44]

The adsorption of Ph_4B^- to SL particles in the like-charged situation further indicates that the same forces are responsible for the adsorption of Ph_4B^- to the AL particles in the oppositely charged case. The fact that the main features of the electrokinetic potential do not depend on the addition of an indifferent electrolyte for both types of particles further supports the fact that effects of electrostatic forces on the adsorption process are minor. Thus, we conclude that hydrophobic forces are responsible for the strong adsorption of Ph_4B^- to both types of latex particles, irrespective of the sign of their charge.

Aggregation Rates. In solutions of indifferent NaCl electrolyte, which are free of the Ph_4B^- ions, the investigated latex particles show the classical aggregation behavior. At high concentrations of indifferent salt, NaCl, the particles aggregate rapidly, and their absolute aggregation rate coefficients are summarized in Table 1. These values are typical for fast aggregation controlled by diffusion. When the NaCl concentration is decreased, the aggregation starts to slow down, which happens below the CCC of around 150 mM. This concentration marks the onset of double-layer repulsion. Model calculations based on DLVO theory reveal very similar patterns. This observed behavior is typical for highly charged colloidal particles and has been reported in numerous studies earlier.[26,45−47]

The presence of Ph_4B^- in solution profoundly modifies the aggregation rates of the AL and SL particles investigated. Figure 3 summarizes the experimentally measured stability ratios, which were calculated from the aggregation rates using

DOI: 10.1021/acs.langmuir.8b03191
Langmuir 2018, 34, 14368−14377

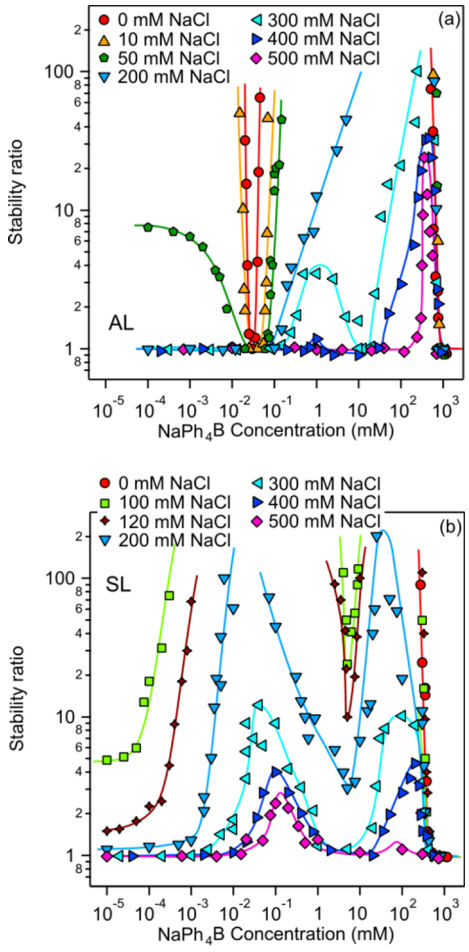

Figure 3. Stability ratios measured by time-resolved light scattering vs the concentration of $NaPh_4B$ and different concentrations of added NaCl at pH 4.0. The solid lines serve to guide the eyes. (a) AL, (b) SL.

eq 4. The fast aggregation rate, k_{fast}, in this relation is the one in the concentrated NaCl solution. The effect of different concentrations of NaCl on the aggregation behavior in the presence of Ph_4B^- was equally investigated.

The dependence of the stability ratios of the AL particles on the Ph_4B^- concentration is shown in Figure 3a. At very low Ph_4B^- concentrations, the particles are stable, but as the NaCl concentration is increased, the stability ratio decreases to unity, where the fast aggregation conditions are reached. As the Ph_4B^- concentration is being increased, the stability ratio decreases, and near 0.03 mM the ratio becomes unity even in the absence of NaCl. As evidenced by electrophoresis experiments, this point marks the charge neutralization point. At this point, double-layer repulsion between the particles is absent, and therefore, the stability ratio becomes unity. As the Ph_4B^- concentration is increased further, the stability ratio again increases strongly, mainly because of double-layer repulsion. The minimum in the stability ratio widens with increasing NaCl concentration, which suggests the onset of screening effects and the importance of double forces. This minimum in the stability ratio leads to the presence of two CCCs, which are located below and above the charge neutralization point. Similar minima in the stability ratios that widen with increasing concentration of an indifferent salt were reported for many other colloidal systems undergoing a charge reversal. These systems include oxide particle suspensions containing oppositely charged surfactants[15,36,37,39] or when subject to pH variations[11,18] and latex particle suspensions in the presence of oppositely charged polyelectrolytes or highly charged multivalent ions.[14,16,26,41,42]

At very high concentrations of Ph_4B^-, the stability ratio decreases rapidly with the concentration and becomes unity for Ph_4B^- concentrations above 790 ± 20 mM. This concentration marks the CCC because of screening, and is comparable to, but higher than, the one observed in NaCl solutions (Table 1). In between the charge neutralization point and this CCC, the stability ratios become very high for lower concentrations of NaCl. At high NaCl concentrations, on the other hand, the stability ratio is basically unity.

However, we observe an unexpected effect at intermediate NaCl and Ph_4B^- concentrations. This effect is especially prominent in solutions containing 300 mM NaCl, where an intermediate minimum in the stability ratio can be observed around 10 mM $NaPh_4B$. Moreover, for NaCl concentrations of 400 and 500 mM, a sharp maximum in the stability ratio in the $NaPh_4B$ concentration range of 300−400 mM is present. These features point toward the importance of an additional attractive force.

Before discussing this unexpected effect further, let us address the dependence of the stability ratios for the SL particles on the Ph_4B^- concentration as shown in Figure 3b. Without added NaCl, the particles aggregate extremely slowly, and fast aggregation is observed only at very high Ph_4B^- concentrations. When NaCl is added, the aggregation behavior becomes more complicated. At very low Ph_4B^- concentrations, the stability ratios again reflect the behavior in pure NaCl solutions. The particles are stable at low NaCl concentrations, and with increasing NaCl concentration, the stability ratio decreases again to unity. As the concentration of $NaPh_4B$ is increased, the stability ratio increases, most strongly at low NaCl concentration, but even at the highest NaCl concentration of 500 mM investigated, an onset of this increase can be observed. This effect induces a CCC at low Ph_4B^- concentrations. We interpret this stabilization by the accumulation of additional negative charge on the negatively charged particles. This accumulation is caused by the adsorption of Ph_4B^- ions, and this effect could also be evidenced by electrophoresis. At very high concentrations of Ph_4B^-, near 500 ± 10 mM, the stability ratio becomes unity again. This concentration again marks another CCC, above which one enters the fast aggregation region, where double-layer forces are screened. The fast aggregation rates attained at high salt conditions are identical for NaCl and $NaPh_4B$ and for both types of particles within experimental error.

At intermediate concentrations of $NaPh_4B$ and NaCl, a similar unexpected effect as already mentioned for the AL particles occurs. This effect is more pronounced for SL than for AL, and now manifests itself most clearly as an intermediate minimum in the stability ratio around 10 mM. This minimum is measurable already at NaCl concentrations of 100 mM, but it becomes more prominent with increasing NaCl concentration. A stability ratio of unity is reached for NaCl concentrations above 300 mM, which leads to two additional CCCs. Furthermore, the existence of these CCCs leads to two intermediate maxima, and even at NaCl concentrations of 500 mM, one maximum is still present.

The four CCCs observed in our system can be rationalized as follows. The lowest CCC originates from the accumulation

DOI: 10.1021/acs.langmuir.8b03191
Langmuir 2018, 34, 14368−14377

of negative charge on the SL particle through the adsorption of the Ph_4B^- anion. The highest CCC is because of screening of the double-layer forces by salt. The two intermediate CCCs are caused by the presence of a further destabilization region, which must be caused by additional attractive non-DLVO interactions. A similar intermediate destabilization region can also be observed for AL particles.

A maximum similar to the ones shown in Figure 3b was also reported in a like-charged systems, namely, an anionic copolymeric latex in the presence of anionic surfactant, potassium stearate.[48] However, that study reports the maximum to occur at rather low concentrations of 0.3 mM extending only over a narrow concentration region. The authors interpret this maximum in terms of structural transition within the adsorbed surfactant film. Whether this maximum has the same origin than the ones reported here is currently unclear to us.

The stability maps shown in Figure 4 clarify the effects of $NaPh_4B$ and NaCl on the aggregation of the AL and SL

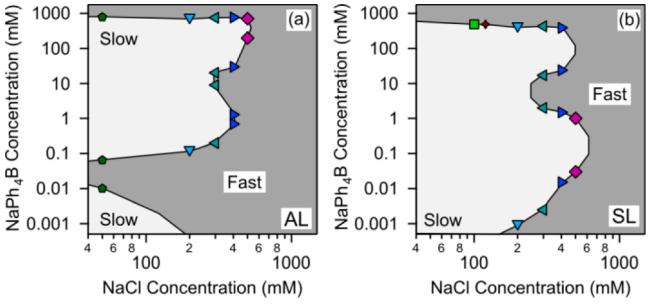

Figure 4. Stability maps of the $NaPh_4B$ concentration vs the NaCl concentration where the regions of slow and fast aggregation are separated by the CCC at pH 4.0. (a) AL, (b) SL.

particles further. The maps show regions of slow and fast aggregation by plotting $NaPh_4B$ concentration versus NaCl concentration, whereby the separating lines represent the CCCs.

Consider first the situation for AL particles shown in Figure 4a. At low $NaPh_4B$ and NaCl concentrations, one observes a fast aggregation channel, which reflects the charge reversal. At high NaCl and $NaPh_4B$ concentrations, the aggregation is fast throughout because of screening. These effects generate the coastlines of the slow regions in the bottom of the map and the peninsula. The unexpected intermediate fast regime manifests itself as an indentation on the right-hand side of the peninsula. Inspecting vertical cross sections of this map, one finds three CCCs at low NaCl concentrations, but four CCCs around 300 mM NaCl.

The stability map for the SL particles shown in Figure 4b is similar. Because the particles do not undergo a charge reversal, the fast channel is missing. Similar to the AL particles after their charge reversal, the SL particles also increase the magnitude of their charge through the adsorption of the Ph_4B^- ions, which also results in a slow peninsula in the SL system. The indentation of the right-hand side of the peninsula is again present, but is now more pronounced, and therefore, the intermediate fast regime is larger. At low $NaPh_4B$ concentrations, one observes two CCCs, but again four CCCs in the regime of 300−400 mM NaCl.

DLVO Calculations. We have first attempted to interpret the observed stability ratios with DLVO theory. Thereby, the interaction energies between charged interfaces were estimated by adding van der Waals and double-layer contributions, and subsequently the interaction energy between the particles was estimated with the Derjaguin approximation. From these interaction energies, the aggregation rates were calculated by considering the diffusional motion of the particles. These rates were subsequently normalized to obtain the stability ratio. The strength of van der Waals interaction was estimated with the Hamaker constant of 3.1×10^{-21} J, which was earlier used in similar calculations.[27] This value is very close to the ones extracted from direct force measurements between latex particles.[7,23]

The double-layer force was obtained from the known concentration of monovalent salt and by approximating the diffuse layer potential by the electrokinetic potential (ζ-potential) as measured by electrophoresis. Thereby, the experimental values were interpolated by empirical fitting functions, as shown in Figure 2. Therefore, these calculations contain no adjustable parameters. Computational details can be found in the Experimental and Methods section.

The stability ratios calculated with DLVO theory are shown in Figure 5. For AL particles, the calculations qualitatively reflect the observed stability patterns; see Figure 5a. The minimum in the stability ratio near the neutralization point is

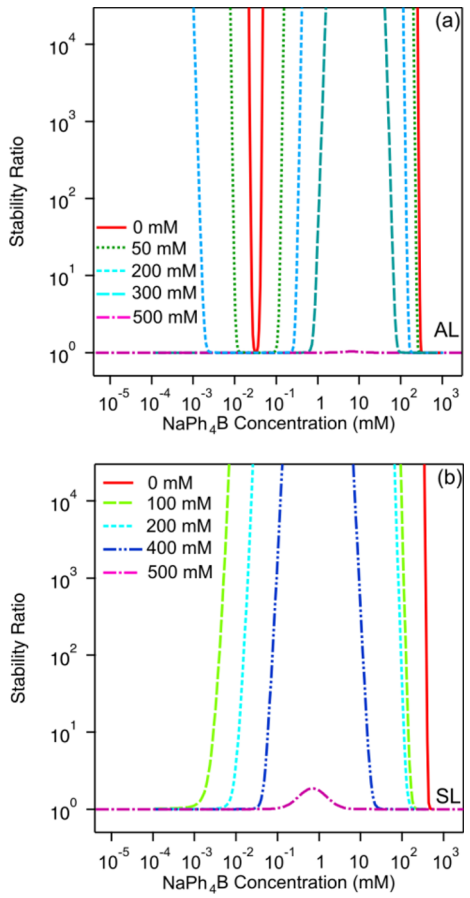

Figure 5. Stability ratios calculated with DLVO theory with CP boundary conditions vs the concentration of $NaPh_4B$ and different concentrations of added NaCl at pH 4.0. The diffuse layer potentials were approximated with the empirical fits of the electrokinetic potentials shown in Figure 2. The Hamaker constant used was 3.1×10^{-21} J. (a) AL, (b) SL.

DOI: 10.1021/acs.langmuir.8b03191
Langmuir 2018, 34, 14368−14377

reproduced rather well, as well as the sharp decrease in the stability ratio at high concentrations. DLVO theory correctly captures the upward shift of the highest CCC to 500−800 mM in $NaPh_4B$ solutions with respect to 150 mM in NaCl solutions (Table 1). Otherwise, however, the predictions lack accuracy. Especially, the DLVO theory fails to predict the experimentally observed intermediate minimum of the stability ratio around 10 mM. Moreover, the calculations predict a too strong dependence on the concentration, as evident from the too steep slopes of the calculated stability curves. Overall, DLVO theory suggests that the particles should be more stable than they actually are.

For SL particles, the predictions of the DLVO theory reproduce the behavior of the stability ratios only at low and high Ph_4B^- concentrations; see Figure 5b. These calculations demonstrate clearly that the increase in the stability ratio at low concentration is indeed because of the accumulation of negative charge on the particle surface because of adsorption of Ph_4B^-. The decrease in the stability ratio at high concentrations is also predicted, but this aspect is not surprising because double-layer interactions will always be screened at sufficiently high salt concentrations.

The stability maps calculated with DLVO theory shown in Figure 6 clarify the situation further. These maps were

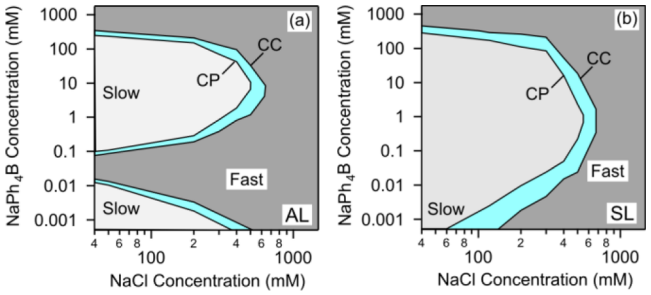

Figure 6. Stability maps of the $NaPh_4B$ concentration vs the NaCl concentration calculated with DLVO theory with CP and CC boundary conditions. Same parameters as in Figure 5 were used. (a) AL, (b) SL.

obtained by extracting the respective CCCs from the calculated stability profiles and by plotting the respective $NaPh_4B$ concentration versus the NaCl concentration. The calculated stability maps reflect the measured ones reasonably well, especially for the AL particles. In this case, one finds the fast channel near the neutralization point as well the slow peninsula at higher $NaPh_4B$ concentrations. For the SL particles, the calculations correctly predict the existence of the slow peninsula. For both systems, however, the DLVO calculations fail to account for the fast indentations at the tip of the peninsula.

In the DLVO calculations discussed so far, CP boundary conditions were assumed. These boundary conditions correspond to substantial regulation of the surface charge approach, and this regulation would be caused by desorption of the Ph_4B^- anions. The other important boundary condition is the one with CC. This condition assumes that the surface charge remains constant and that no desorption upon approach takes place. We have thus compared the results of the calculations with these two boundary conditions. Because double-layer forces with CC conditions are more repulsive than with CP conditions, the calculated stability ratios are higher. However, the generic features remain the same. This effect is particularly evident in the stability maps, where results obtained with CP and CC boundary conditions are compared. One should further note that more appropriate boundary conditions would lie in between CP and CC, but the consideration of more realistic boundary conditions will not influence these results substantially. Therefore, the origin of the intermediate destabilization region cannot be explained by different boundary conditions and must lie beyond DLVO theory.

Calculations Including Non-DLVO Interactions. Various experiments based on direct force measurements have revealed that systems containing strongly adsorbing ions feature additional attractive non-DLVO forces.[7,23−25] In particular, such forces were also observed to act between SL and silica particles in the presence of Ph_4As^+ ions.[23] These forces can be fitted with the exponential law given in eq 11 with a decay length around q^{-1} = 3 nm. The amplitude, A, of this force goes through a maximum versus the Ph_4As^+ concentration. Moreover, theoretical analysis suggests that additional attractive interactions between surfaces with a patch−charge distribution may occur and that such interactions decay exponentially.[31]

We suspect that similar non-DLVO forces are acting in the systems containing Ph_4B^- anions studied here. We thus use the decay length of 3 nm, and we empirically adjust the magnitude of the amplitude together with the position and the width of the maximum on the concentration axis, as shown in Figure 7.

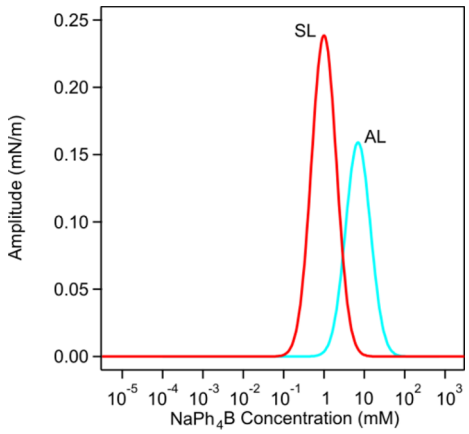

Figure 7. Dependence of the amplitude, A, used in eq 11 on the concentration of $NaPh_4B$ for the two types of latex particles.

The dependence of the amplitude, A, in eq 11 on the concentration, c, of Ph_4B^- is thus modeled by the empirical expression

$$A = A_0 \exp\left[-\frac{\ln^2(c/c_0)}{2w}\right] \quad (12)$$

where we use w = 0.5 for both types of particles. The maximum amplitude, A_0, and the concentration, c_0, at the peak are taken to be 0.16 mN/m and 7 mM for AL and 0.24 mN/m and 1 mM for SL. As illustrated in eq 6, the additional interaction is added to the DLVO potential used previously, and the respective stability ratios are calculated in the same fashion again. The parameters were chosen such that the experimental stability data could be reproduced best. The width of the peak is similar to the one reported by Smith et

DOI: 10.1021/acs.langmuir.8b03191
Langmuir 2018, 34, 14368−14377

al.[23] for Ph_4As^+, but the maximum amplitude chosen here is about 2−3 times larger. The latter study reported that this peak is positioned at charge neutralization point, but a similar peak was positioned way above this point in a system containing multivalent amine cations.[7] Note that this interaction is assumed not depending on the concentration of added NaCl.

The calculated stability ratios by including the non-DLVO interaction are shown in Figure 8. The additional attractive

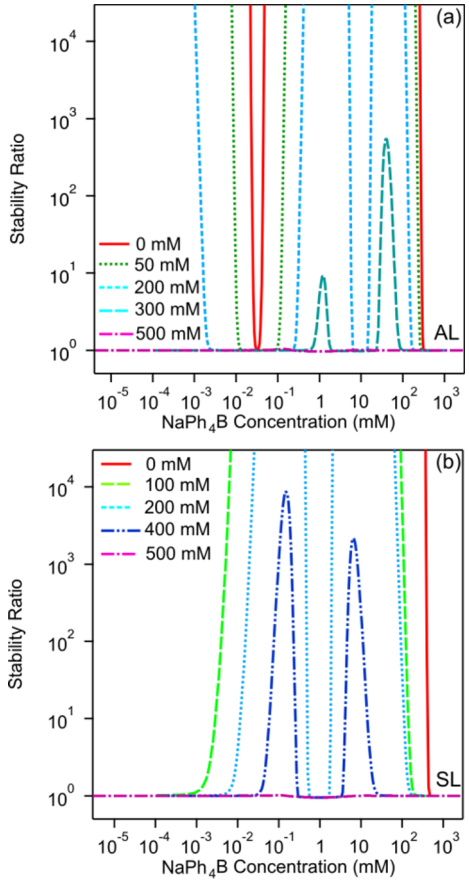

Figure 8. Stability ratios calculated by including the attractive non-DLVO interactions vs the concentration of $NaPh_4B$ and different concentrations of added NaCl at pH 4.0. The DLVO part of the calculations was the same as used in Figure 5. (a) AL, (b) SL.

non-DLVO force indeed induces an additional destabilization regime, which resembles the experimentally observed one. For both types of latex particles, the calculated stability ratios now feature four CCCs at certain NaCl levels, which is in accordance with the experimental observations.

Clearly, the agreement is hardly quantitative. The predicted dependencies on the concentration are again too strong, which manifest in the large slopes in the calculated stability plots. Nevertheless, the asymmetries between the two intermediate maxima in the stability plots are reproduced by the calculations reasonably well.

The calculated stability maps including the non-DLVO interactions are shown in Figure 9 and they reproduce the experimental maps surprisingly well. In particular, these maps now also show the characteristic fast indentations in the peninsulas, which is in full agreement with experiment. Therefore, we think that the calculations including the non-

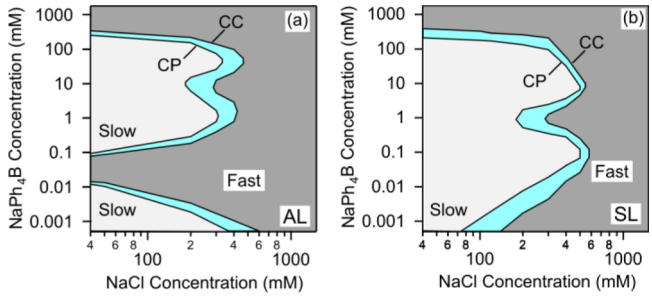

Figure 9. Stability maps of the $NaPh_4B$ concentration vs the NaCl concentration calculated by including the attractive non-DLVO interactions vs the concentration of $NaPh_4B$ and different concentrations of added NaCl at pH 4.0. The DLVO part of the calculations is the same used in Figure 6. (a) AL, (b) SL.

DLVO force, albeit not fully quantitative, reflect the essential features observed experimentally and thus capture the mechanism of the aggregation process induced by the presence of Ph_4B^- anions for AL as well as SL particles.

We thus strongly suspect that additional attractive non-DLVO interactions are responsible for the destabilization behavior observed at intermediate $NaPh_4B$ and NaCl concentrations. The strength of the non-DLVO interactions goes through a maximum as a function of the $NaPh_4B$ concentration, and these interactions appear similar to the ones that were recently observed in direct force measurements between negatively charged surfaces in the presence of Ph_4As^+.[23] For this reason, we also suspect that their origin is similar. From the direct force measurements, it was concluded that these forces are induced by surface charge heterogeneities, which are generated by the adsorption of the hydrophobic ions. These heterogeneities are expected to occur in both AL and SL systems because in the relevant region the adsorbed films will be rather dense, but defects in these films would induce the charge heterogeneities in question. These heterogeneities are expected to occur on small length scales, probably on the order of 1 nm, as one can estimate from the Debye length at the respective salt levels. However, charge fluctuations or hydrophobic interactions may contribute to these interactions as well.

Our parameterization of the additional non-DLVO interaction is admittedly crude. In particular, we assume that this force has no dependence on the presence of added NaCl, which is probably incorrect.[24] For the calculations of the stability ratios, however, this force is relevant only in a relatively narrow window of NaCl concentrations, and within this window the parameters used might indeed remain approximately constant. Nevertheless, more detailed studies would be necessary to characterize this additional force more fully. Our calculations of the stability ratios further suffer from a too strong concentration dependence, which overestimates the magnitudes of the slopes in the stability graphs. This shortcoming of the DLVO theory has been remarked already quite some time ago.[11,12,47,49] Although surface charge heterogeneities have been proposed to be the origin of these discrepancies, it remains unclear how to include this effect into the stability calculations in a quantitative manner.

CONCLUSIONS

Electrophoretic mobility and aggregation rates are studied in aqueous suspensions of AL and SL particles containing

DOI: 10.1021/acs.langmuir.8b03191
Langmuir 2018, 34, 14368−14377

$NaPh_4B$ and NaCl. The hydrophobic Ph_4B^- anion is found to adsorb strongly, which leads to an accumulation of negative charge on both types of particles. This accumulation induces a region of slow aggregation, which is consistent with the classical DLVO theory. However, we observe an additional region of fast aggregation at intermediate concentrations. We argue that this fast aggregation region is caused by attractive non-DLVO forces, which are probably caused by surface charge heterogeneities within the adsorbed layer. Although similar attractive forces were recently observed with direct force measurements,[7,23,24] the present data are the first ones that demonstrate the importance of such attractive non-DLVO forces in particle aggregation. Further studies have to be carried out to find out to what extent the observed effects also occur for other types of hydrophobic ions, especially for short-chain surfactants.

AUTHOR INFORMATION

Corresponding Author

*E-mail: michal.borkovec@unige.ch.

ORCID

Michal Borkovec: 0000-0002-1114-4865

Notes

The authors declare no competing financial interest.

ACKNOWLEDGMENTS

This research was supported by the Swiss National Science Foundation through projects nos. 159874 and 178759 and the University of Geneva.

REFERENCES

(1) Russel, W. B.; Saville, D. A.; Schowalter, W. R. *Colloidal Dispersions*; Cambridge University Press: Cambridge, 1989.

(2) Elimelech, M.; Gregory, J.; Jia, X.; Williams, R. A. *Particle Deposition and Aggregation: Measurement, Modeling, and Simulation*; Butterworth-Heinemann Ltd.: Oxford, 1995.

(3) Bolto, B.; Gregory, J. Organic Polyelectrolytes in Water Treatment. *Water Res.* **2007**, *41*, 2301−2324.

(4) Horn, D.; Linhart, F. *Retention Aids*, 2nd ed.; Blackie Academic and Professional: London, 1996.

(5) Derjaguin, B.; Landau, L. D. Theory of the Stability of Strongly Charged Lyophobic Sols and of the Adhesion of Strongly Charged Particles in Solutions of Electrolytes. *Acta Phys. Chim.* **1941**, *14*, 633−662.

(6) Verwey, E. J. W.; Overbeek, J. T. G. *Theory of Stability of Lyophobic Colloids*; Elsevier: Amsterdam, 1948.

(7) Moazzami Gudarzi, M.; Trefalt, G.; Szilagyi, I.; Maroni, P.; Borkovec, M. Forces between Negatively Charged Interfaces in the Presence of Cationic Multivalent Oligoamines Measured with the Atomic Force Microscope. *J. Phys. Chem. C* **2015**, *119*, 15482−15490.

(8) Hartley, P. G.; Larson, I.; Scales, P. J. Electrokinetic and Direct Force Measurements between Silica and Mica Surfaces in Dilute Electrolyte Solutions. *Langmuir* **1997**, *13*, 2207−2214.

(9) Wiese, G. R.; Healy, T. W. Coagulation and Electrokinetic Behavior of TiO_2 and Al_2O_3 Colloidal Dispersions. *J. Colloid Interface Sci.* **1975**, *51*, 427−433.

(10) Frens, G.; Heuts, J. J. F. G. The double layer potential Øδ as a rate determining factor in the coagulation of electrocratic colloids. *Colloids Surf.* **1988**, *30*, 295−305.

(11) Schudel, M.; Behrens, S. H.; Holthoff, H.; Kretzschmar, R.; Borkovec, M. Absolute Aggregation Rate Constants of Hematite Particles in Aqueous Suspensions: A Comparison of Two Different Surface Morphologies. *J. Colloid Interface Sci.* **1997**, *196*, 241−253.

(12) Behrens, S. H.; Christl, D. I.; Emmerzael, R.; Schurtenberger, P.; Borkovec, M. Charging and Aggregation Properties of Carboxyl Latex Particles: Experiments versus DLVO Theory. *Langmuir* **2000**, *16*, 2566−2575.

(13) Szilagyi, I.; Polomska, A.; Citherlet, D.; Sadeghpour, A.; Borkovec, M. Charging and aggregation of negatively charged colloidal latex particles in the presence of multivalent oligoamine cations. *J. Colloid Interface Sci.* **2013**, *392*, 34−41.

(14) Pavlovic, M.; Huber, R.; Adok-Sipiczki, M.; Nardin, C.; Szilagyi, I. Ion Specific Effects on the Stability of Layered Double Hydroxide Colloids. *Soft Matter* **2016**, *12*, 4024−4033.

(15) Kobayashi, M.; Yuki, S.; Adachi, Y. Effect of Anionic Surfactants on the Stability Ratio and Electrophoretic Mobility of Colloidal Hematite Particles. *Colloids Surf., A* **2016**, *510*, 190−197.

(16) Szabó, T.; Tóth, V.; Horváth, E.; Forró, L.; Szilagyi, I. Tuning the Aggregation of Titanate Nanowires in Aqueous Dispersions. *Langmuir* **2015**, *31*, 42−49.

(17) Barringer, E. A.; Bowen, H. K. High-Purity, Monodisperse TiO_2 Powders by Hydrolysis of Titanium Tetraethoxide 1. Synthesis and Physical Properties. *Langmuir* **1985**, *1*, 414−420.

(18) Barringer, E. A.; Bowen, H. K. High-purity, Monodisperse TiO_2 Powders by Hydrolysis of Titanium Tetraethoxide 2. Aqueous Interfacial Electrochemistry and Dispersion Stability. *Langmuir* **1985**, *1*, 420−428.

(19) Schwierz, N.; Horinek, D.; Netz, R. R. Reversed Anionic Hofmeister Series: The Interplay of Surface Charge and Surface Polarity. *Langmuir* **2010**, *26*, 7370−7379.

(20) Calero, C.; Faraudo, J.; Bastos-González, D. Interaction of Monovalent Ions with Hydrophobic and Hydrophilic Colloids: Charge Inversion and Ionic Specificity. *J. Am. Chem. Soc.* **2011**, *133*, 15025−15035.

(21) Sugimoto, T.; Nishiya, M.; Kobayashi, M. Electrophoretic Mobility of Carboxyl Latex Particles: Effects of Hydrophobic Monovalent Counter-Ions. *Colloid Polym. Sci.* **2017**, *295*, 2405−2411.

(22) Hakim, A.; Nishiya, M.; Kobayashi, M. Charge Reversal of Sulfate Latex Induced by Hydrophobic Counterion: Effects of Surface Charge Density. *Colloid Polym. Sci.* **2016**, *294*, 1671−1678.

(23) Smith, A. M.; Maroni, P.; Borkovec, M. Attractive Non-DLVO Forces Induced by Adsorption of Monovalent Organic Ions. *Phys. Chem. Chem. Phys.* **2018**, *20*, 158−164.

(24) Zohar, O.; Leizerson, I.; Sivan, U. Short Range Attraction between Two Similarly Charged Silica Surfaces. *Phys. Rev. Lett.* **2006**, *96*, 177802.

(25) Dishon, M.; Zohar, O.; Sivan, U. Effect of Cation Size and Charge on the Interaction between Silica Surfaces in 1:1, 2:1, and 3:1 Aqueous Electrolytes. *Langmuir* **2011**, *27*, 12977−12984.

(26) Cao, T.; Sugimoto, T.; Szilagyi, I.; Trefalt, G.; Borkovec, M. Heteroaggregation of Oppositely Charged Particles in the Presence of Multivalent Ions. *Phys. Chem. Chem. Phys.* **2017**, *19*, 15160−15171.

(27) Sugimoto, T.; Cao, T.; Szilagyi, I.; Borkovec, M.; Trefalt, G. Aggregation and Charging of Sulfate and Amidine Latex Particles in the Presence of Oxyanions. *J. Colloid Interface Sci.* **2018**, *524*, 456−464.

(28) O'Brien, R. W.; White, L. R. Electrophoretic Mobility of a Spherical Colloidal Particle. *J. Chem. Soc., Faraday Trans. 2* **1978**, *74*, 1607−1626.

(29) Holthoff, H.; Schmitt, A.; Fernández-Barbero, A.; Borkovec, M.; Cabrerízo-Vílchez, M. á.; Schurtenberger, P.; Hidalgo-álvarez, R. Measurement of Absolute Coagulation Rate Constants for Colloidal Particles: Comparison of Single and Multiparticle Light Scattering Techniques. *J. Colloid Interface Sci.* **1997**, *192*, 463−470.

(30) Xu, S.; Sun, Z. Progress in Coagulation Rate Measurements of Colloidal Dispersions. *Soft Matter* **2011**, *7*, 11298−11308.

(31) Miklavic, S. J.; Chan, D. Y. C.; White, L. R.; Healy, T. W. Double Layer Forces between Heterogeneous Charged Surfaces. *J. Phys. Chem.* **1994**, *98*, 9022−9032.

(32) Donaldson, S. H.; Røyne, A.; Kristiansen, K.; Rapp, M. V.; Das, S.; Gebbie, M. A.; Lee, D. W.; Stock, P.; Valtiner, M.; Israelachvili, J. Developing a General Interaction Potential for Hydrophobic and Hydrophilic Interactions. *Langmuir* **2015**, *31*, 2051−2064.

DOI: 10.1021/acs.langmuir.8b03191
Langmuir 2018, 34, 14368−14377

(33) Adamczyk, Z.; Jaszczółt, K.; Michna, A.; Siwek, B.; Szyk-Warszyńska, L.; Zembala, M. Irreversible Adsorption of Particles on Heterogeneous Surfaces. *Adv. Colloid Interface Sci.* **2005**, *118*, 25−42.
(34) Popa, I.; Papastavrou, G.; Borkovec, M. Charge Regulation Effects on Electrostatic Patch-Charge Attraction Induced by Adsorbed Dendrimers. *Phys. Chem. Chem. Phys.* **2010**, *12*, 4863−4871.
(35) Santore, M. M.; Kozlova, N. Micrometer Scale Adhesion on Nanometer-scale Patchy Surfaces: Adhesion Rates, Adhesion Thresholds, and Curvature-Based Selectivity. *Langmuir* **2007**, *23*, 4782−4791.
(36) Watanabe, A. Physico-Chemical Studies on Surface Active Agents. 2. The Coagulation of Positive Silver Iodide Sols by Anionic Surface Active Agents. *Bull. Inst. Chem. Res., Kyoto Univ.* **1960**, *38*, 179−215.
(37) Ottewill, R. H.; Rastogi, M. C. The stability of hydrophobic sols in the presence of surface-active agents. Part 2.-The stability of silver iodide sols in the presence of cationic surface-active agents. *Trans. Faraday Soc.* **1960**, *56*, 866−879.
(38) Somasundaran, P.; Healy, T. W.; Fuerstenau, D. W. Surfactant Adsorption at the Solid-Liquid Interface-Dependence of Mechanism on Chain Length. *J. Phys. Chem.* **1964**, *68*, 3562−3566.
(39) Liang, L.; Morgan, J. J. Chemical aspects of iron oxide coagulation in water: Laboratory studies and implications for natural systems. *Aquat. Sci.* **1990**, *52*, 32−55.
(40) Goloub, T. P.; Koopal, L. K. Adsorption of Cationic Surfactants on Silica. Comparison of Experiment and Theory. *Langmuir* **1997**, *13*, 673−681.
(41) Szilagyi, I.; Sadeghpour, A.; Borkovec, M. Destabilization of Colloidal Suspensions by Multivalent Ions and Polyelectrolytes: From Screening to Overcharging. *Langmuir* **2012**, *28*, 6211−6215.
(42) Gregory, J. Rates of Flocculation of Latex Particles by Cationic Polymers. *J. Colloid Interface Sci.* **1973**, *42*, 448−456.
(43) Kaya, A.; Yukselen, Y. Zeta Potential of Soils with Surfactants and its Relevance to Electrokinetic Remediation. *J. Hazard. Mater.* **2005**, *120*, 119−126.
(44) White, B.; Banerjee, S.; O'Brien, S.; Turro, N. J.; Herman, I. P. Zeta-Potential Measurements of Surfactant-Wrapped Individual Single-Walled Carbon Nanotubes. *J. Phys. Chem. C* **2007**, *111*, 13684−13690.
(45) Lin, W.; Kobayashi, M.; Skarba, M.; Mu, C.; Galletto, P.; Borkovec, M. Heteroaggregation in Binary Mixtures of Oppositely Charged Colloidal Particles. *Langmuir* **2006**, *22*, 1038−1047.
(46) Ortega-Vinuesa, J. L.; Martín-Rodríguez, A.; Hidalgo-Álvarez, R. Colloidal Stability of Polymer Colloids with Different Interfacial Properties: Mechanisms. *J. Colloid Interface Sci.* **1996**, *184*, 259−267.
(47) Kihira, H.; Ryde, N.; Matijević, E. Kinetics of heterocoagulation. Part.2-The effect of the discreteness of surface charge. *J. Chem. Soc., Faraday Trans.* **1992**, *88*, 2379−2386.
(48) Zaccone, A.; Wu, H.; Lattuada, M.; Morbidelli, M. Correlation between Colloidal Stability and Surfactant Adsorption/Association Phenomena Studied by Light Scattering. *J. Phys. Chem. B* **2008**, *112*, 1976−1986.
(49) Shulepov, S. Y.; Frens, G. Surface Roughness and Particle Size Effect on the Rate of Perikinetic Coagulation: Experimental. *J. Colloid Interface Sci.* **1996**, *182*, 388−394.

DOI: 10.1021/acs.langmuir.8b03191
Langmuir 2018, 34, 14368−14377

CHAPTER 4

Heteroaggregation of Oppositely Charged Particles in the Presence of Multivalent Ions

Cao, T.; Sugimoto, T.; Szilagyi, I.; Trefalt G.; Borkovec, M.

Phys. Chem. Chem. Phys. **2017**, 19, 15160–15171.

PCCP

PAPER

View Article Online
View Journal | View Issue

Cite this: *Phys. Chem. Chem. Phys.*, 2017, **19**, 15160

Heteroaggregation of oppositely charged particles in the presence of multivalent ions†

Tianchi Cao,[a] Takuya Sugimoto,[ab] Istvan Szilagyi,[a] Gregor Trefalt[a] and Michal Borkovec*[a]

Received 27th March 2017,
Accepted 12th May 2017

DOI: 10.1039/c7cp01955f

rsc.li/pccp

Time-resolved dynamic light scattering is used to measure absolute heteroaggregation rate coefficients and the corresponding stability ratios for heteroaggregation between amidine and sulfate latex particles. These measurements are complemented by the respective quantities for the homoaggregation of the two systems and electrophoresis. Based on the latter measurements, the stability ratios are calculated using Derjaguin–Landau–Verwey–Overbeek (DLVO) theory. In monovalent salt solutions, the two types of particles investigated are oppositely charged. In the presence of multivalent ions, however, one particle type reverses its charge, while the charge of the other particle type is hardly affected. In this region, the heteroaggregation stability ratio goes through a pronounced maximum when plotted *versus* concentration. This region of slow aggregation is wider than the one observed in the corresponding homoaggregation process. One also finds that the onset of this region sensitively depends on the boundary conditions used to calculate the double layer force. The present results are more in line with constant potential boundary conditions.

Introduction

The stability of colloidal suspensions can be strongly influenced by the presence of multivalent ions, as already pointed out in the landmark studies by Schulze[1] and Hardy.[2] Colloidal suspensions are destabilized by the formation of particle aggregates, whereby the early aggregation regime is governed by the formation of particle doublets. Derjaguin, Landau, Verwey, and Overbeek (DLVO)[3,4] have shown that the formation of particle doublets is governed by one of the following mechanisms, namely fast and slow aggregation. The fast aggregation process is controlled by the diffusional approach of a pair of attractive colloidal particles, and typically occurs at high salt concentrations. Slow aggregation is controlled by an activated crossing of an energy barrier within an initially repulsive potential, and occurs at low salt concentrations. The transition between these two regimes takes place at a rather well-defined concentration, referred to as the critical coagulation concentration (CCC). The Schulze–Hardy rule states that the CCC strongly decreases with increasing valence of the counterions.[5,6] These trends have been confirmed experimentally in various aqueous particle suspensions in the presence of different types of counterions.[7–13] Time-resolved light scattering techniques have proven to be particularly useful for such studies.[14–17] Since multivalent counterions adsorb on oppositely charged particles strongly, this mechanism does not only destabilize the particle suspension, but also induces a charge reversal of the particles in question. As a consequence, one also observes an additional re-stabilization region at intermediate salt concentrations.[10,18] Similarly, multivalent co-ions also lead to a decrease of the CCC.[13,19] However, the resulting dependence on valence is much weaker, and has been referred to as the inverse Schulze–Hardy rule. For spherical particles, DLVO theory can be sometimes used to successfully predict such phenomena, including their dependence on the particle size in the slow regime.[12,16,20] Thereby, the interaction potential is modeled by a superposition of van der Waals and double layer forces and hydrodynamic interaction must be considered as well. While these predictions are not always accurate, we think that a reasonably good understanding of the aggregation processes of aqueous colloidal particle suspensions has been achieved today.

However, this conclusion only holds for homoaggregation, meaning that aggregates are being formed out of identical (or very similar) particles. Heteroaggregation, meaning that aggregates are being formed out of different particles, is understood to a much lesser extent. The most important reason for this situation is that the measurement of heteroaggregation rates is more difficult than for homoaggregation. The main obstacle is that in a binary mixture of colloidal particles, the heteroaggregation processes may occur simultaneously with two different

[a] *Department of Inorganic and Analytical Chemistry, University of Geneva, Sciences II, 30 Quai Ernest-Ansermet, 1205 Geneva, Switzerland. E-mail: michal.borkovec@unige.ch*
[b] *Faculty of Life and Environmental Sciences, University of Tsukuba, 1-1-1 Tennoudai, Tsukuba, Ibaraki 305-8572, Japan*

† Electronic supplementary information (ESI) available: Fig. S1–S3 and Tables S1–S3. See DOI: 10.1039/c7cp01955f

homoaggregation processes, and these three processes must be properly separated in order to extract the heteroaggregation rate. One possibility to overcome this problem is to carry out experiments with two types of particles that feature different surface functionalities, but otherwise have the same (or similar) size and bulk composition. One may then study such a system using any of the established methods to study homoaggregation, and measure the apparent aggregation rate as a function of the ratio of the two types of particles. In the early aggregation regime, the heteroaggregation rate can be extracted from the dependence of the apparent aggregation rate on that ratio.[21–24] While such experiments are simply analyzed, this technique is extremely laborious, and strongly limits the choice of particles to be investigated. In spite of these reservations, a similar approach was also used to study particles of widely different shapes and sizes.[25–28] While useful conclusions could be drawn from these measurements too, the analysis remains qualitative, as the situation is often further complicated by the fact that the aggregation conditions often extend beyond early stages.

More recently, some of us have proposed an alternative technique, which can be applied to study heteroaggregation in any kind of mixtures of pairs of differently sized colloidal particles.[29] This technique is based on time-resolved multi-angle light scattering, and exploits the specific angular dependence of the form factors of the different particle doublets to distinguish the contributions from heteroaggregation and homoaggregation. While this technique offers a wider freedom in the choice of particles, its drawback is that the data analysis is more complex, and requires the form factors of the asymmetric dimers in question. For spherical and monodisperse particles, however, these form factors can be accurately calculated using the T-matrix technique.[30,31]

In spite of these complications, heteroaggregation processes were addressed by these techniques to some extent. A key finding was that the heteroaggregation rate of oppositely charged colloidal particles is comparable to the ones in the case of heteroaggregation at high salt levels, but becomes faster when the salt level is decreased.[24,29,32–35] This trend can be quantified through the strengthening of attractive double layer forces acting between oppositely charged particles at low salt levels. A similar trend could be also established for the deposition of colloidal particles onto oppositely charged collector beads.[36] Another important observation was made concerning the dependence of the heteroaggregation between two types of oxide particles upon pH. This rate is fast between the two points of zero charge, but is rapidly slowed down below and above these points.[21] This finding confirms the importance of double layer forces in these processes. However, these measurements reported the apparent stability ratio of binary colloidal suspensions, and extracting the heteroaggregation rate was not attempted. For this reason, the interpretation of these experiments remained difficult.[37]

Heteroaggregation processes in the presence of multivalent ions have not been studied so far. For this reason, we investigate here binary suspensions of amidine and sulfate latex particles. These particles are oppositely charged in the presence of a monovalent salt. In the presence of multivalent ions, however, the charge of one particle type becomes neutralized, while the other particle type remains highly charged. No experimental studies in such situations are available, and the present study reports the measurements of such heteroaggregation rates for the first time.

Theory

Heteroaggregation rates by light scattering

During the early stages of aggregation in a binary colloidal suspension containing two different types of particles A and B, three types of dimers may form, namely symmetric AA and BB dimers, and the asymmetric AB dimer. For the two homoaggregation processes, the formation of the symmetric dimers follows the kinetic equations

$$\frac{dN_{AA}(t)}{dt} = \frac{1}{2}k_{AA}N_A^2(t) \quad (1)$$

$$\frac{dN_{BB}(t)}{dt} = \frac{1}{2}k_{BB}N_B^2(t) \quad (2)$$

where $N_A(t)$ and $N_B(t)$ refer to the number concentrations of the particle monomers A and B, which depend on time t, and $N_{AA}(t)$ and $N_{BB}(t)$ to the ones of the particle dimers AA and BB, which form with homoaggregation rate coefficients k_{AA} and k_{BB}. For the heteroaggregation processes, the formation of the asymmetric dimers follows

$$\frac{dN_{AB}(t)}{dt} = k_{AB}N_A(t)N_B(t) \quad (3)$$

where $N_{AB}(t)$ is the number concentration of the dimer AB, which forms with the heteroaggregation rate coefficient k_{AB}.

These rate coefficients can be determined by time-resolved multi-angle static or dynamic light scattering. To obtain such results from static light scattering, one has to measure the apparent initial rate of change of scattering intensity $I(\theta,t)$, where θ is the scattering angle and t is the time, namely

$$\Sigma(\theta) = \frac{1}{I(\theta,0)} \cdot \left.\frac{dI(\theta,t)}{dt}\right|_{t\to 0} \quad (4)$$

where $t = 0$ refers to the initial time, when no aggregates have yet occurred. This apparent static rate turns out to be a linear superposition of the contributions from the three aggregation processes, and can be written as[29]

$$\Sigma(\theta) = k_{AA}F_{AA}(\theta) + 2k_{AB}F_{AB}(\theta) + k_{BB}F_{BB}(\theta) \quad (5)$$

The weighting functions are given by

$$F_{ij}(\theta) = \frac{N_0 x_i x_j}{2} \cdot \frac{I_{ij}(\theta) - I_i(\theta) - I_j(\theta)}{x_A I_A(\theta) + x_B I_B(\theta)} \quad (6)$$

where $I_{ij}(\theta)$ is the scattering intensity for a single dimer ij and $I_i(\theta)$ the one for a single particle monomer i. The subscripts i and j refer to particles A or B. The initial particle number concentration is given by $N_0 = N_A(0) + N_B(0)$ and the particle number fractions are denoted by $x_i = N_i(0)/N_0$. The scattering intensities for spherical particles and the corresponding dimers

can be accurately calculated by Mie theory or T-matrix techniques, whereby corrections for sample polydispersity and reflection from the cuvette wall must be considered. Details of these calculations are described elsewhere.[29,31] Homoaggregation rate coefficients k_{AA} and k_{BB} can be determined from experiments on suspensions containing only one type of particles. The heteroaggregation rate coefficient k_{AB} can be then determined by fitting the angle-dependent apparent static rate measured in a binary suspension. The contrast is sensitive to the number fraction of the particles, and for a given system its value must be properly adjusted.

The analysis of time-resolved dynamic light scattering proceeds similarly. Now one measures the apparent initial rate of change of the apparent hydrodynamic radius $R(\theta,t)$, which is obtained from the measured diffusion coefficient by means of the Stokes–Einstein relation. The apparent dynamic rate is defined as

$$\Delta(\theta) = \frac{1}{R(\theta,0)} \cdot \left.\frac{\mathrm{d}R(\theta,t)}{\mathrm{d}t}\right|_{t\to 0} \tag{7}$$

This quantity can be similarly decomposed in the contributions of the three aggregation processes, namely[29]

$$\Delta(\theta) = k_{AA}H_{AA}(\theta) + 2k_{AB}H_{AB}(\theta) + k_{BB}H_{BB}(\theta) \tag{8}$$

where $H_{ij}(\theta) = F_{ij}(\theta) - G_{ij}(\theta)$. Thereby, the function $F_{ij}(\theta)$ is defined in eqn (6) and the function $G_{ij}(\theta)$ is given by

$$G_{ij}(\theta) = \frac{N_0 x_i x_j}{2} \cdot \frac{I_{ij}(\theta)/R_{ij} - I_i(\theta)/R_i - I_j(\theta)/R_j}{x_A I_A(\theta)/R_A + x_B I_B(\theta)/R_B} \tag{9}$$

where R_{ij} are the hydrodynamic radii of the dimers and R_i the ones of the monomers, which coincide with the actual particle radii. The relative hydrodynamic radii of the dimers are given by the expression

$$\alpha_{ij} = \frac{2R_{ij}}{R_i + R_j} = 1.392 + 0.608\left(\frac{R_i - R_j}{R_i + R_j}\right)^2 \tag{10}$$

This empirical relation approximates well the exact results obtained from the analysis of the hydrodynamics of a pair of unequal spheres at low Reynolds numbers.[29,38]

The analysis of the apparent dynamic rate proceeds similarly to the static one. The homoaggregation rate coefficients k_{AA} and k_{BB} are determined from suspensions containing only one type of particles. The angle-dependent apparent dynamic rate measured in a binary suspension is then fitted to eqn (8), from which the heteroaggregation rate coefficient k_{AB} can be extracted. Thereby, the known values of the homoaggregation rate coefficients k_{AA} and k_{BB} are used in the analysis. We find that the dynamic data are more easily analyzed, especially since the measured time-dependence of $R(t)$ is linear over longer time periods, and can be extrapolated to the initial time more easily. This extrapolation assures that only early stages of aggregation are being considered, and the effects of higher order aggregates remain negligible. This analysis further assumes sufficiently dilute suspensions, where the effects of interactions between the isolated particles and/or between the aggregates are negligible.[6] These conditions are largely satisfied in the systems that are studied here.

Calculation of aggregation rate coefficients by DLVO theory

In order to obtain quantitative estimates of the aggregation rate coefficient, the interaction energy profile of a pair of particles must be known. This profile can be calculated from the pressure acting between two planar walls by assuming that this pressure is dominated by two contributions from van der Waals and double layer forces, namely[39,40]

$$\Pi = \Pi_{vdW} + \Pi_{dl} \tag{11}$$

The contribution from van der Waals forces is calculated from the non-retarded expression[6]

$$\Pi_{vdW} = -\frac{H}{6\pi} \cdot \frac{1}{h^3} \tag{12}$$

where h is the distance between the plates and $H = 9.0 \times 10^{-21}$ J is the Hamaker constant, which is assumed to be the same for the two types of latex particles investigated.[41] The pressure originating from the overlapping double layers is obtained by numerically solving the Poisson–Boltzmann (PB) equation for the electrostatic potential profile ψ between two charged plates immersed in an electrolyte solution containing ions of type μ with number concentrations c_μ and valence z_μ, and is given by[39,40]

$$\frac{\mathrm{d}^2\psi}{\mathrm{d}x^2} = -\frac{q}{\varepsilon_0\varepsilon}\sum_\mu z_\mu c_\mu \mathrm{e}^{-z_\mu\beta q\psi} \tag{13}$$

where q is the elementary charge, ε_0 is the permittivity of vacuum, ε is the dielectric constant of water, and β is the inverse thermal energy given by $\beta^{-1} = k_B T$, where k_B is the Boltzmann constant and T the absolute temperature. We use the experimental temperature of 25 °C and the corresponding value of $\varepsilon = 80$. Eqn (13) is solved subject to the constant regulation (CR) boundary conditions at the walls situated $x = \pm h/2$

$$\pm\varepsilon_0\varepsilon\left.\frac{\mathrm{d}\psi}{\mathrm{d}x}\right|_{x=\pm h/2} = \sigma_\pm - C_{in}^{(\pm)}[\psi(\pm h/2) - \psi_\pm] \tag{14}$$

where $\sigma_\pm$ refers to the surface charge density, $\psi_\pm$ to the diffuse layer potential, and $C_{in}^{(\pm)}$ to the inner capacitance of the two isolated surfaces. The regulation properties of each surface can be parameterized more easily using the regulation parameter

$$p_\pm = \frac{C_{dl}^{(\pm)}}{C_{dl}^{(\pm)} + C_{in}^{(\pm)}} \tag{15}$$

where $C_{dl}^{(\pm)} = \partial\sigma_\pm/\partial\psi_\pm$ is the diffuse layer capacitance of the isolated surface. The regulation parameter assumes simple values for the classical boundary conditions of constant charge (CC, $p_\pm = 1$) and constant potential (CP, $p_\pm = 0$). When the electrostatic potential is known, the pressure originating from the double layer overlap can then be obtained from the relation

$$\Pi_{dl} = k_B T\sum_\mu c_\mu\left(\mathrm{e}^{-z_\mu\beta q\psi} - 1\right) - \frac{\varepsilon_0\varepsilon}{2}\left(\frac{\mathrm{d}\psi}{\mathrm{d}x}\right)^2 \tag{16}$$

In spite of the inherent mean-field approximation and the neglect of ion–ion correlations, PB theory is a good approximation to calculate interaction forces at larger separations, typically beyond

a few nm.[42,43] The aggregation rate coefficients can be calculated from the steady-state solution of the forced diffusion equation[40]

$$k_{ij} = \frac{4}{3\beta\eta\sigma_{ij}}\left[\int_0^\infty \frac{B_{ij}(h)e^{\beta V_{ij}(h)}}{(R_i + R_j + h)^2}dh\right]^{-1} \quad (17)$$

where η is the shear viscosity of water, $B_{ij}(h)$ is the hydrodynamic resistance function, and $V_{ij}(h)$ is the interaction energy involving particles of types i and j, and σ_{ij} is defined by $2\sigma_{ij}^{-1} = R_i^{-1} + R_j^{-1}$. We use $\eta = 8.9 \times 10^{-4}$ Pa s as appropriate for water at 25 °C. The resistance function can be approximated by

$$B_{ij}(h) = \frac{6h^2 + 13\sigma_{ij}h + 2\sigma_{ij}^2}{6h^2 + 4\sigma_{ij}h} \quad (18)$$

The interaction energy V_{ij} is obtained by integration of the force profile f_{ij}, which in turn is obtained from the Derjaguin approximation

$$f_{ij} = \pi\sigma_{ij}\int_h^\infty \Pi(h')dh' \quad (19)$$

where the Π is the overall pressure between the plates, which have the same surface and bulk properties as the particles involved, see eqn (11).

The rate coefficients were calculated by fixing the regulation parameters to the same value for both surfaces and by assuming that the diffuse layer potentials $\psi_\pm$ can be approximated by the electrokinetic potential obtained from electrophoresis (ζ-potentials). Instead of the aggregation rate coefficients, we always report the stability ratio defined as

$$W_{ij} = \frac{k_{ij}^{(\mathrm{fast})}}{k_{ij}} \quad (20)$$

where $k_{ij}^{(\mathrm{fast})}$ is the aggregation rate obtained under fast aggregation conditions in suspensions containing 0.5 M KCl.

Experimental

Materials

Two types of spherical, surfactant-free polystyrene latex particles were purchased from Invitrogen Corporation, namely positively charged amidine latex (AL) particles and negatively charged sulfate latex (SL) particles. Before use, the particle suspensions were dialyzed about one week in pure water until the conductivity of the surrounding solution dropped below 80 μS m^{-1}. Milli-Q water (Millipore) was used throughout. For the AL particles, polyvinylidene difluoride membranes were used, while for the SL particles, cellulose ester membranes were used. The particle concentrations of the final dialyzed suspensions were determined by comparing the light scattering intensities of dialyzed suspensions with the ones of the original suspensions of known concentrations.

Static and dynamic light scattering experiments were carried out with stable suspensions in order to determine the accurate radii of the particles and their polydispersities. For these experiments, the particles were suspended in water adjusted to pH 4.0 at a concentration of 0.6 mg L^{-1} (4.0×10^{13} m^{-3}) for the AL particles and 1.7 mg L^{-1} (1.4×10^{13} m^{-3}) for the SL particles. The angular dependence of the scattering intensity was measured using a multi-angle goniometer equipped with eight fiber optic detectors (ALV/CGS-8F) and a solid-state laser with a wavelength of 532 nm. The intensity profile was fitted with a superposition of Mie functions to incorporate polydispersity effects including a reflectivity correction (Fig. S1, ESI†). The analysis further relies on the refractive indices of 1.337 for water and 1.596 for polystyrene.[44] The reflection coefficient is found to be 0.042. Details of this procedure were presented earlier.[31] Dynamic light scattering was carried out at a scattering angle of 90°.

Table 1 Radii and polydispersities of the particles investigated

	Radius (nm)			CV (%)	
Particles	TEM[a]	SLS[b]	DLS[c]	TEM[a]	SLS[b]
Amidine latex (AL)	150	149 ± 2	153 ± 3	5.7	6.5 ± 0.9
Sulfate latex (SL)	300	297 ± 3	310 ± 7	2.2	3.0 ± 0.7

[a] Obtained by the manufacturer by transmission electron microscopy (TEM). [b] Obtained by static light scattering (SLS) and analysis using Mie functions. [c] Obtained by dynamic light scattering (DLS).

Table 1 compares these results with the number weighted average particle radii reported by the manufacturer. The average particle radii are in excellent agreement with the ones obtained by static light scattering. The hydrodynamic radii obtained by dynamic light scattering (Table 1) are slightly larger than the ones obtained by static light scattering, probably due to the effects of polydispersity and hydration. The polydispersities, which were expressed as the coefficient of variation (CV) of the number weighted distribution, measured by static light scattering were somewhat larger than the values determined by the manufacturer. In further analysis, we have used the results obtained from static light scattering given in Table 1 as well as the refractive indices and reflection coefficient quoted above.

Analytical grade KCl (Acros Organics), K_2SO_4 (Fluka), $K_3Fe(CN)_6$ and $K_4Fe(CN)_6$ (Sigma-Aldrich) were dissolved in water and the pH was adjusted to 4.0 with HCl. In these solutions, all ions are fully ionized, with the exception of $Fe(CN)_6^{4-}$. In the latter case, a minor fraction of the complex $Fe(CN)_5(HCN)^{3-}$ is expected to form.[45] Pentaethylenehexamine (N6) with the chemical formula $H_2N(CH_2CH_2NH)_4CH_2CH_2NH_2$ was obtained from Sigma-Aldrich. A stock solution of N6 with a concentration of 39.6 g L^{-1} was prepared in water and its pH was adjusted to 4.0 with HCl. The concentration of the monovalent electrolyte was adjusted by adding KCl solution adjusted to pH 4.0. Under these conditions, the N6 molecule is partially ionized. Based on the tabulated ionization constants at infinite dilution, the amount of the different ionic species in the N6 solution was calculated, which was 1% of the species with +3 charge, 88% with +4 charge, and 11% with +5 charge.[10]

Electrophoresis

The electrophoretic mobility of the particles was measured using a ZetaSizer Nano ZS (Malvern Instruments). Suspensions were prepared in an appropriate electrolyte solution of pH 4.0

at given particle concentrations. Two sets of particle concentrations were used. For the experiments in solutions of different types of multivalent salts, the particle concentration was 0.66 mg L^{-1} (4.4×10^{13} m^{-3}) for the AL and 7.4 mg L^{-1} (6.2×10^{13} m^{-3}) for SL. For the experiments in the presence of N6 with different monovalent electrolyte backgrounds, the particle concentration was 0.6 mg L^{-1} (4.0×10^{13} m^{-3}) for AL and 1.7 mg L^{-1} (1.4×10^{13} m^{-3}) for SL. The electrophoretic mobility was converted to the electrokinetic potential (ζ-potential) using the standard electrokinetic model by O'Brien and White.[6,46] Fitting the Grahame equation to the electrokinetic potentials in KCl solutions for concentrations above 5×10^{-3} M leads to surface charge densities of 18 mC m^{-2} for the AL particles and −40 mC m^{-2} for the SL particles. The surface charge densities reported by the manufacturer are somewhat higher in magnitude.

Multi-angle time-resolved light scattering

Particle aggregation was monitored by time-resolved static and dynamic light scattering using the multi-angle goniometer described above. Borosilicate cuvettes were used to carry out the experiments. Hot piranha solution, which is a mixture of 96% H_2SO_4 and 30% H_2O_2 with a volume ratio of 3 : 1, was used to clean the cuvettes. They were subsequently washed with water and dried in a dust-free oven at 60 °C. The samples were prepared by adding the electrolyte solution into the cuvette, and particle suspensions were injected, mixed rapidly, and inserted into the sample holder. Correlation functions were accumulated for 20 s with an angular resolution of 2°, and analyzed using a second-order cumulant fit. To ensure that only early stages of aggregation were probed, the measured hydrodynamic radii had to extrapolate to the correct radius of the particle monomers and the relative increase of the radius should be not more than 30%.

Fig. 1 (top row) shows such experimental data for homoaggregation for both types of particles in 0.5 M KCl solution. The angular dependence of the apparent dynamic rate was fitted with the form factors calculated using T-matrix theory and the respective hydrodynamic factor $\alpha_{AA} = \alpha_{BB} = 1.392$. The absolute fast aggregation rate coefficient is then the only adjustable parameter, and the resulting values are given in Table 2 and Table S1 (ESI†). The stability ratios for homoaggregation were then determined by time resolved dynamic light scattering at a scattering angle of 90°, as described in earlier studies.[10,29]

In the case of heteroaggregation experiments, mixtures of AL and SL particles were used. For experiments in the presence of different types of salts, the particle concentration was 0.66 mg L^{-1} (4.4×10^{13} m^{-3}) for AL and 7.4 mg L^{-1} (6.2×10^{13} m^{-3}) for SL leading to a total particle concentration of 1.1×10^{14} m^{-3} and an AL number fraction of 0.42. For the experiments in the presence of N6 with different salt backgrounds, the particle concentration was 0.6 mg L^{-1} (4.0×10^{13} m^{-3}) for AL, and 1.7 mg L^{-1} (1.4×10^{13} m^{-3}) for SL, which corresponds to a total particle concentration of 5.4×10^{13} m^{-3} and an AL number fraction of 0.74. These different fractions were chosen in order to achieve a better contrast between the symmetric and asymmetric dimers formed.

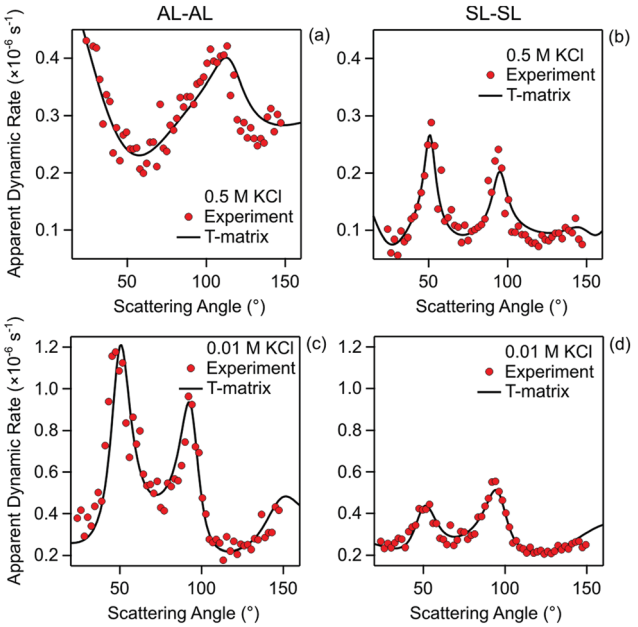

Fig. 1 Apparent aggregation rates obtained from time-resolved dynamic light scattering as a function of the scattering angle in suspensions with one type of aggregation process. The solid line is the best fit obtained by T-matrix theory. Homoaggregation in 0.5 M KCl solutions for (a) AL at total particle concentrations of 4.0×10^{13} m^{-3} and (b) SL of 1.4×10^{13} m^{-3}. Pure heteroaggregation between AL and SL particles in 0.01 M KCl solution with (c) a total particle concentration of 1.1×10^{14} m^{-3} and an AL number fraction of 0.42 and with (d) a total particle concentration of 5.4×10^{13} m^{-3} and an AL number fraction of 0.74. All suspensions have pH 4.0.

Table 2 Absolute aggregation rate coefficients in the fast regime induced by 0.5 M KCl

System	Experiment ($\times 10^{-18}$ m^3 s^{-1})	DLVO theory ($\times 10^{-18}$ m^3 s^{-1})
AL–AL	2.8 ± 0.2	8.61
SL–SL	3.1 ± 0.3	8.62
AL–SL	3.9 ± 0.4	9.79

To test the correctness of the optical model, heteroaggregation at low concentrations of the monovalent salt was investigated. Under these conditions, only heteroaggregation occurs. As shown in Fig. 1 (bottom row), the resulting apparent dynamic rates can be well fitted with optical factors obtained from T-matrix theory and the hydrodynamic factor of $\alpha_{AB} = 1.460$. This hydrodynamic factor expresses the ratio between the hydrodynamic radii of the particle dimer and the average radius of the two individual particles. Both particle number fractions yield consistent results (Table S1, ESI†).

Similar angle-resolved measurements are used to obtain the absolute heteroaggregation rate coefficients at high concentrations of the monovalent salt. In this case, however, heteroaggregation occurs simultaneously with the two homoaggregation processes. Since the respective homoaggregation rate coefficients are known from separate measurements, the heteroaggregation rate coefficient can be determined by a least-squares fit. Such data

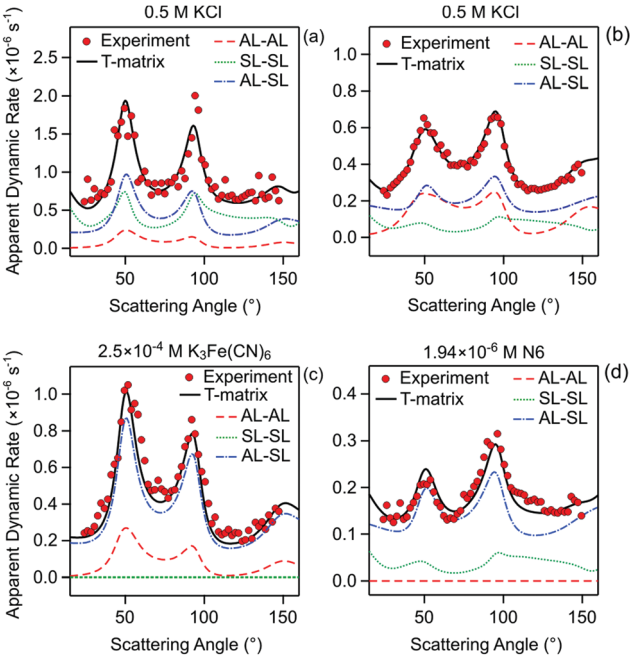

Fig. 2 Apparent aggregation rates obtained from dynamic light scattering as a function of the scattering angle in suspension containing AL and SL particles. The solid thick line is the best fit obtained by T-matrix theory and the dashed thin lines indicate the contributions of the individual aggregation processes. (a and b) Heteroaggregation and both homoaggregation processes occurring in suspensions containing 0.5 M KCl. Heteroaggregation and homoaggregation processes occurring in (c) 2.5×10^{-4} M $K_3Fe(CN)_6$ solution and (d) a solution of an aliphatic amine N6 at a concentration of 1.9×10^{-6} M. All suspensions have pH 4.0. For (a and c) the total particle concentration is 1.1×10^{14} m^{-3} and the AL number fraction is 0.42, and for (b and d) the total particle concentration is 5.4×10^{13} m^{-3} and the AL number fraction is 0.74.

are shown in Fig. 2 (top row) for two different particle number fractions. The individual contributions from heteroaggregation and homoaggregation are also shown. One should note that these contributions are at least comparable in magnitude, and therefore the heteroaggregation rate coefficient can be extracted with confidence. The resulting heteroaggregation rate coefficient is given in Table 2 and Table S1 (ESI†). Again, the two particle number fractions yield the same results within experimental error.

Under other experimental conditions, heteroaggregation rate coefficients can be determined in a similar way by fitting the apparent dynamic rate coefficients. Thereby, one can also use the known homoaggregation rate coefficients, which were determined in the experiments with the respective particle suspensions containing only one type of particles. Again, the heteroaggregation rate coefficient is the only adjustable parameter. Typical results are shown in Fig. 2 (bottom row). The analysis is simplified by the fact that under most conditions investigated, heteroaggregation occurs simultaneously only with one type of homoaggregation process. Both contributions must be at least comparable in magnitude such that one can extract the heteroaggregation rate coefficient reliably. The resulting rate coefficients are summarized in Table S1 (ESI†).

The measurements carried out by time-resolved dynamic light scattering were also compared with those performed by time-resolved static light scattering. The corresponding results are presented in the ESI† (Fig. S2 and S3). The resulting rate coefficients were in good agreement with the ones obtained by dynamic light scattering (Table S1, ESI†). This agreement confirms independently the validity of the data obtained from time-resolved dynamic light scattering. However, the latter technique provides more reliable estimates of the heteroaggregation rate coefficients and for this reason it was used to obtain the rate coefficients presented here.

Results and discussion

Time-resolved multi-angle dynamic light scattering was used to measure stability ratios and rate coefficients for heteroaggregation between amidine latex (AL) and sulfate latex (SL) particles in electrolytes containing multivalent ions. These results were completed with measurements of stability ratios and rate coefficients for homoaggregation and the determination of electrokinetic potentials (ζ-potentials). The latter results show that in monovalent KCl solutions the AL particles are positively charged, while the SL particles are negatively charged. In the presence of multivalent ions of higher valence, however, one type of particle undergoes a charge reversal. Comparison with calculations using DLVO theory suggests that near the charge reversal point the heteroaggregation stability ratios are very sensitive to the boundary conditions used to solve the PB equation. Comparison between theory and experiment in this region thus allows us to make conclusions concerning these boundary conditions.

Effects of simple salts containing multivalent anions

The dependence of electrokinetic potentials on the concentration of different salts is summarized in Fig. 3. The results for the AL particles are shown on the left, while those for the SL particles on the right. In the presence of monovalent K^+ cations, we have investigated the effect of SO_4^{2-}, $Fe(CN)_6^{3-}$, $Fe(CN)_6^{4-}$, and monovalent Cl^- for comparison. Fig. 3a illustrates that the

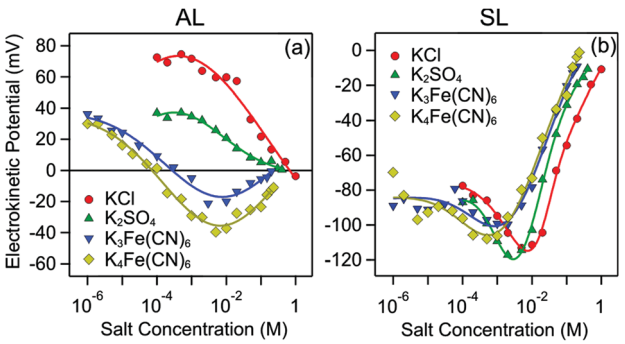

Fig. 3 Electrokinetic potentials (ζ-potentials) of the particles investigated *versus* the concentration of different salts indicated. The pH value was adjusted to 4.0. Solid lines are empirical functions used for approximate data interpolation. (a) AL and (b) SL particles.

AL particles have the highest positive potential in the presence of Cl^-. This potential also remains positive in the presence of SO_4^{2-}, but it is lowered due to adsorption of these anions. The more highly charged anions adsorb very strongly, and both ions induce a charge reversal, which is more pronounced for $Fe(CN)_6^{4-}$ than for $Fe(CN)_6^{3-}$. Fig. 3b shows that the negatively charged SL particles behave similarly irrespective of the type of anion, since these ions do not adsorb on a like-charged particle surface.

The stability ratios *versus* the concentration of different salts containing different multivalent ions are shown in Fig. 4. The top two rows reflect the data for homoaggregation, while the bottom row for heteroaggregation. The data points represent experimental data, while the solid lines are calculations based on DLVO theory. The theoretical lines indicate three different boundary conditions that were used to calculate the double layer forces, namely constant charge (CC, p = 1), constant potential (CP, p = 0), and constant regulation (CR) with a regulation parameter of p = 0.5. The diffuse layer potentials entering these calculations were estimated by empirical functions that were used for approximate interpolation of the electrokinetic potentials (solid lines, Fig. 3).

Consider first the known situation of monovalent KCl. The stability ratios for homoaggregation reflect the classical pattern of slow and fast aggregation. At high salt concentrations, aggregation is fast and the stability ratio is unity by definition. In this regime, the aggregation process is driven by diffusion. With decreasing salt concentration, the stability ratio increases strongly due to the onset of slow aggregation, which is caused by double layer repulsion. The transition between the two regimes marks the critical coagulation concentration (CCC). DLVO theory predicts the observed stability ratios reasonably

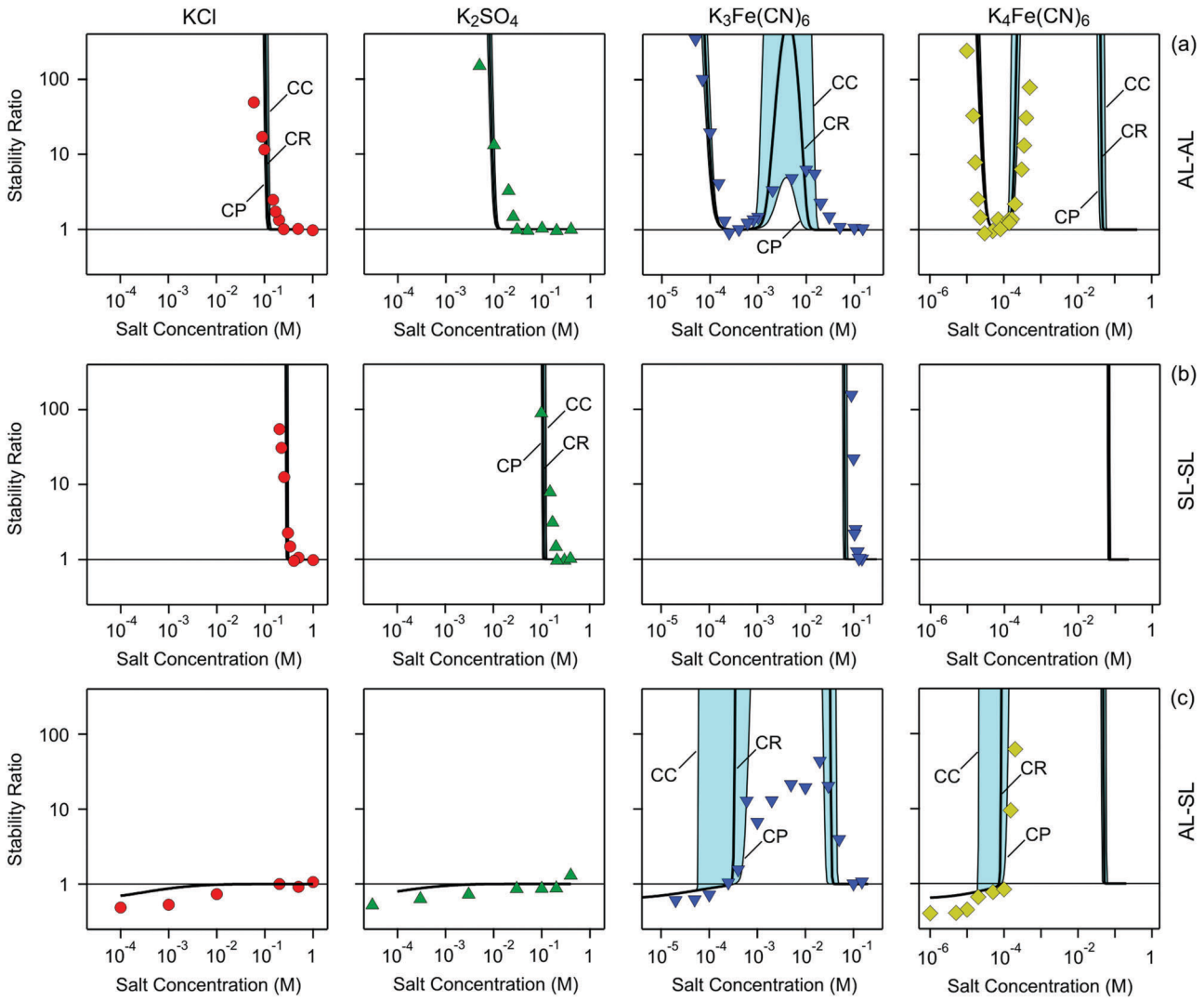

Fig. 4 Stability ratios for heteroaggregation between AL and SL particles *versus* the concentration of different types of salts containing monovalent and multivalent ions (columns). All suspensions have pH 4.0. Solid lines are calculations based on DLVO theory with constant regulation (CR) boundary conditions with a regulation parameter p = 0.5. The blue-shaded regions are bounded by the corresponding results for CC and CP boundary conditions. Homoaggregation for (a) AL particles and (b) SL particles. (c) Heteroaggregation between AL and SL particles.

well, including the lower CCC for the AL particles. This shift is caused by the lower magnitude of the charge density for AL than for SL. This scenario is well documented in the literature.[10,29] The experimentally observed increase in the slow regime is weaker than predicted theoretically, and these discrepancies are probably related to the presence of surface charge heterogeneities.[47–49]

The stability ratio for heteroaggregation decreases with decreasing concentration slowly, and attains a value of about 0.5 at 1.0×10^{-4} M. This trend is predicted by DLVO theory reasonably well. The reason for this behavior is that double layer forces acting between the oppositely charged particles are attractive and lead to a decrease in the stability ratio. Similar trends were reported in the literature earlier.[24,29,32,33]

The situation in the presence of K_2SO_4 reminds of the one in the presence of the monovalent salt. The observed trends are again well predicted by DLVO theory. One should note that the substantially lower CCC for the AL particles is caused by the adsorption of SO_4^{2-} to the oppositely charged surface of the AL particles, which leads to a lowering of their diffuse layer potential. The stability ratio for heteroaggregation again decreases weakly with decreasing salt concentration.

The qualitative behavior of the homoaggregation stability ratio changes for $K_3Fe(CN)_6$. While the stability ratio for the SL particles remains very similar to the other salts, the behavior of AL particles is now different. At low concentrations, the stability ratio decreases strongly and goes through a minimum near the charge reversal point. This quantity increases again at higher concentrations, and goes through an intermediate maximum. At very high concentrations, one again attains a stability ratio of unity. This characteristic behavior is related to the charge reversal induced by the adsorption of the $Fe(CN)_6^{3-}$ ions to the AL particles. At low concentrations, the surface is positive, but reverses its charge with increasing concentration. At higher concentrations, the charge becomes screened and fast aggregation is induced. Similar patterns for homoaggregation in the presence of multivalent counterions have been reported earlier.[10,50] The DLVO theory predicts this behavior semi-quantitatively provided the CP boundary conditions are being used. CR or CC boundary conditions overestimate the height of the maximum substantially. The remaining discrepancies between experiment and DLVO theory are probably related to additional non-DLVO forces due to the ion–ion correlation or to the presence of surface charge heterogeneities.[43,47,48,51]

The dependence of the CCC on valence is shown in the stability maps (Fig. 5). The two columns compare the experimental (left) and calculated (right) CCCs and they agree for homoaggregation rather well. For the AL particles, the CCC at low salt concentration decreases strongly with the valence of the counterions. The classical Schulze–Hardy rule suggests a dependence z^{-6} where z is the valence of the counterion.[6] The present data follow this rule quite well, similarly to other systems as described earlier.[13] For the SL particles, a smaller shift of the CCC towards lower concentrations is caused with increasing valence z of the multivalent co-ions. In this case, the CCC scales rather accurately as z^{-1}. This dependence was

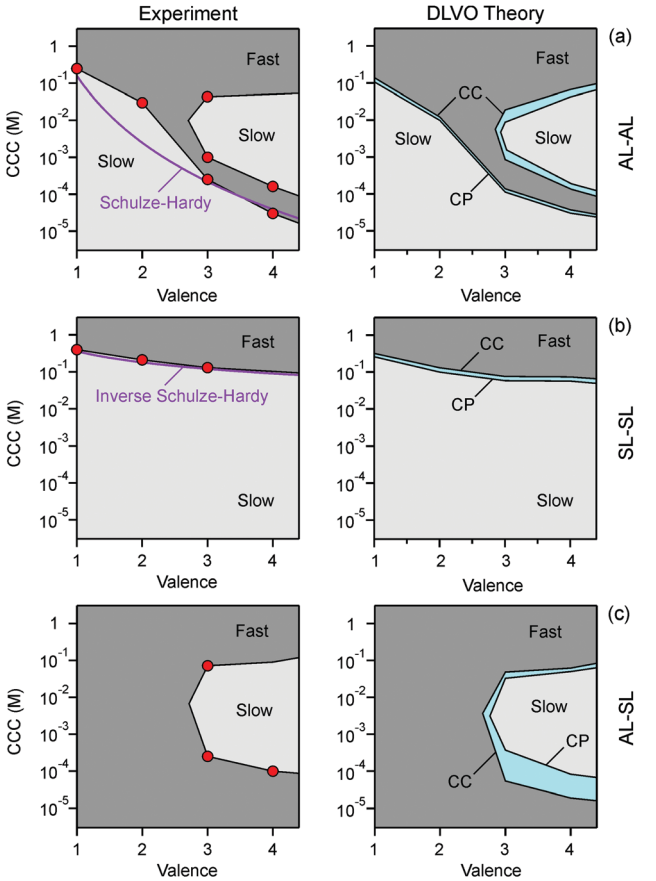

Fig. 5 Stability maps featuring the dependence of the critical coagulation concentration (CCC) *versus* the valence of the multivalent anions originating from KCl, K_2SO_4, $K_3Fe(CN)_6$, and $K_4Fe(CN)_6$. Experimental data (left column) and DLVO calculations indicating the results obtained with CC and CP boundary conditions (right column). Schulze–Hardy and the inverse Schulze–Hardy rules are indicated in purple (left column). Homoaggregation for (a) AL particles and (b) SL particles. (c) Heteroaggregation between AL and SL particles. The data are also given in Table S2 (ESI†).

referred to as the inverse Schulze–Hardy rule and can also be derived from DLVO theory.[13]

The heteroaggregation stability ratio features a novel pattern (Fig. 4c). At low concentrations, the stability ratio lies below unity, indicating the presence of attractive double layer forces. With increasing concentration, the stability ratio increases strongly and goes through a maximum at intermediate concentrations. This maximum is caused by the charge reversal of the AL particle, which induces repulsive double layer forces between the equally charged AL and SL particles. At higher concentrations, the double layer forces become progressively screened until the fast aggregation regime is attained. DLVO theory predicts the width of the slow aggregation regime reasonably well, provided CP boundary conditions are being used. The regime of slow heteroaggregation is wider than the one for homoaggregation and DLVO theory predicts this trend correctly as well. This difference can also be clearly seen in Fig. 5, as the peninsula of slow aggregation for the AL–SL system is larger than for the AL–AL system. This difference is related to the different magnitudes of surface charge densities near the charge

reversal point. For heteroaggregation, the magnitude of the surface charge of the AL particle is small, while the respective magnitude of the SL particle remains high. For homoaggregation, the magnitude of the surface charge of the two AL particles involved is low. Therefore, the repulsive double layer forces are weaker for homoaggregation than for heteroaggregation, which leads to a wider region of slow aggregation for the latter. One should further note the substantial sensitivity of the heteroaggregation stability ratio on the boundary conditions in the low concentration regime. This sensitivity is clearly visible in Fig. 5. The lower coastline of the peninsula shifts upwards by about one order of magnitude when the boundary conditions are changed from CC to CP. This sensitivity originates from the fact that near the charge reversal point the nature of the regulation influences the double layer forces very strongly.[40] This situation is in contrast to homoaggregation, where boundary conditions influence the CCCs weakly.

The data for $K_4Fe(CN)_6$ follow similar patterns, but the tetravalent anion involved induces a stronger charge reversal. In this case, we were unable to estimate the stability ratios at higher salt concentrations, probably due to the limited solubility of this salt and the formation of surface precipitates, which are possibly related to the traces of Prussian blue, $Fe_4[Fe(CN)_6]_3$.

The fast absolute aggregation rate coefficients in monovalent salt solutions are compared with the theoretical values obtained from DLVO theory in Table 2. These coefficients are comparable for all three different particle pairs, as they are all determined by their diffusional approach. The DLVO calculations were carried out by assuming that the interaction between the particles is governed by van der Waals forces only. While the calculation correctly predicts the fact that the rate of heteroaggregation is about 20% larger than that of homoaggregation, the values calculated systematically are about a factor 2–3 smaller than the experimental ones. This discrepancy does not disappear when the measured Hamaker constant is used in the calculation.[50] We suspect that discrepancies between experiment and DLVO theory are related to inaccuracies in the model used to describe the hydrodynamic friction at small surface separations.

Effects of an aliphatic polyamine and monovalent salt

The dependence of the electrokinetic potential on the concentration of an aliphatic polyamine, referred to as N6, is shown in Fig. 6 at different levels of the added monovalent salt. The lowest concentration of 1.0×10^{-4} M originates from the added HCl to adjust the pH to 4.0 and higher concentrations result from further additions of KCl. This polyamine is not fully ionized, and the valence of the principal species is +4. One observes that the electrokinetic potential of the AL particles remains positive in the presence of the like-charged N6 cation (Fig. 6a). On the other hand, this ion induces a pronounced charge reversal of the oppositely charged SL particles (Fig. 6b). With increasing concentration of the monovalent salt, however, the charge reversal point shifts to higher concentrations due to the competition between N6 and K^+ ions.[10,52]

The charge reversal is also clearly evident in the homoaggregation stability ratio for the SL particles, which goes through a pronounced minimum near the charge reversal

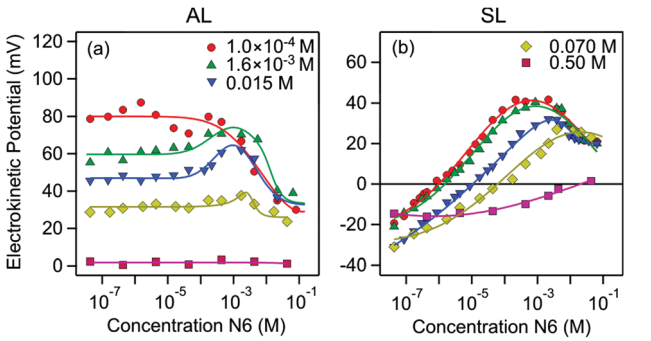

Fig. 6 Electrokinetic potentials (ζ-potentials) of the particles investigated *versus* the concentration of aliphatic polyamine N6 at different concentrations of the added monovalent salt at pH 4.0. Solid lines are empirical functions used for approximate data interpolation. (a) AL and (b) SL particles.

point, see Fig. 7. The stability ratio increases upon increasing the N6 concentration to very high values, which cannot be measured experimentally. At high concentrations, this ratio decreases again and attains unity as characteristic of the fast aggregation regime. The homoaggregation stability ratio for AL particles follows the simple pattern observed for the monovalent salt. This behavior confirms that the N6 cations interact with the AL particles only weakly. We have further verified that the stability ratio is unity within experimental error in solutions containing 0.5 M KCl within the whole concentration range of N6 investigated. The stability pattern of AL particles follows the classical behavior of slow aggregation at small N6 concentrations, and fast aggregation at higher ones.

Fig. 8 summarizes the dependence of the CCCs on the monovalent salt concentration. The two columns compare the experimental (left) and calculated (right) CCCs. The CCC in the AL–AL system, where N6 is the co-ion, remains approximately constant. The CCC for the SL–SL system, where N6 is the counterion, shows a coastline at low concentrations and a peninsula at intermediate concentrations. DLVO theory predicts this behavior reasonably well. This behavior was reported for a similar system earlier.[10] The tips of the peninsulas were located by performing experiments in solutions containing 0.1 M KCl. The corresponding calculation was based on interpolations of the electrophoretic data at a fixed N6 concentrations of 4.0×10^{-3} M and 0.01 M.

The heteroaggregation stability ratios shown in Fig. 7 again feature a novel pattern, which resembles the one for different salts discussed above. The stability ratio for heteroaggregation is below unity at low concentrations, which indicates the presence of attractive double layer forces acting between oppositely charged particles. After the charge reversal point, the heteroaggregation stability ratio increases rapidly. Only at high concentrations, the stability ratio decreases again to unity. The charge reversal is weakened upon addition of KCl and shifts towards higher N6 concentrations. One observes a subsequent narrowing of the regions of slow aggregation for homoaggregation and heteroaggregation, which leads to an intermediate maximum at 0.07 M KCl. Again, the width of the intermediate

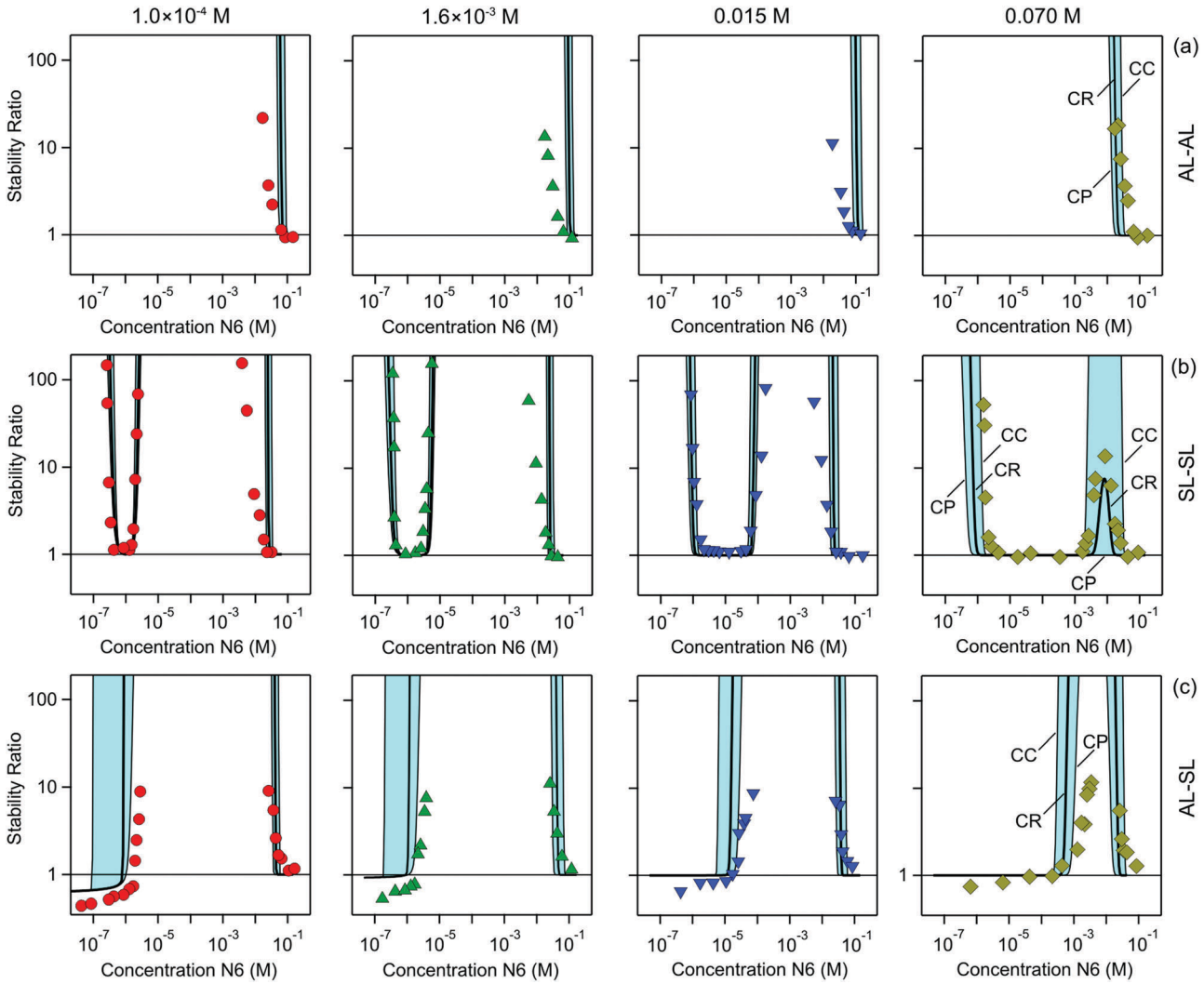

Fig. 7 Stability ratios for heteroaggregation between AL and SL particles *versus* the concentration of an aliphatic polyamine N6 at different concentrations of the added monovalent salt indicated (columns). All suspensions have pH 4.0. Solid lines are calculations based on DLVO theory with constant regulation (CR) boundary conditions with a regulation parameter $p = 0.5$. The blue-shaded regions are bounded by the corresponding results for CC and CP boundary conditions. Homoaggregation for (a) AL particles and (b) SL particles. (c) Heteroaggregation between AL and SL particles.

regime of slow aggregation is wider for heteroaggregation than for homoaggregation. This trend can be seen more clearly in Fig. 8.

As in the previous system, the experimental stability ratios are rather well predicted by DLVO theory. The intermediate region for slow heteroaggregation is again wider than the one for homoaggregation, and this difference is also related to the different surface charge densities of the particles involved. The calculated stability ratios for heteroaggregation are sensitive to the nature of the boundary conditions, as illustrated in the lower coastline of the peninsula shown in Fig. 8. When going from CC to CP conditions, their position increases by about an order of magnitude. Comparison with experimental data suggests that CP boundary conditions are the more appropriate ones. This finding is in line with earlier direct force measurements in a similar system.[52] That study also suggests that similar SL particles regulate close to CP boundary conditions in the presence of N6. At low N6 concentrations, the experimental stability ratios are systematically lower than the ones calculated by DLVO theory. This trend indicates an additional attractive non-DLVO force, which could originate from attraction due to the ion–ion correlation or the presence of surface charge heterogeneities.[43,47,48,51]

Conclusion

This study reports for the first time, the measurements of absolute heteroaggregation rates and corresponding stability ratios for heteroaggregation between amidine and sulfate latex particles in the presence of multivalent ions. These results are complemented by the respective measurements of stability ratios of the two systems containing the same type of particles and the corresponding electrokinetic potentials. Based on the latter measurements, the stability ratios can be calculated by

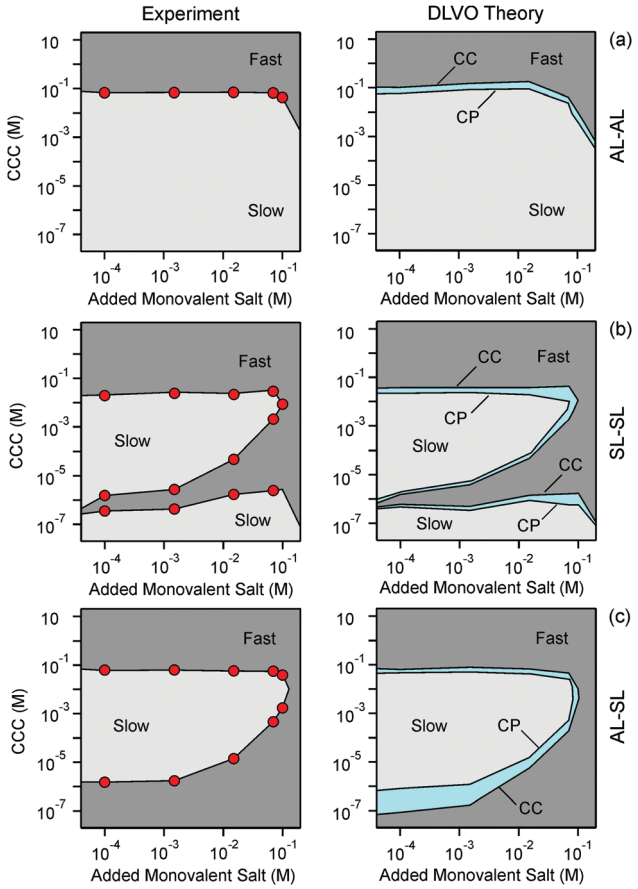

Fig. 8 Stability maps featuring the dependence of the critical coagulation concentrations (CCCs) of the aliphatic amine N6 on the concentration of the added monovalent salt. Experimental data (left column) and DLVO calculations indicating the results obtained with CC and CP boundary conditions (right column). Homoaggregation for (a) AL particles and (b) SL particles. (c) Heteroaggregation between AL and SL particles. The data are also given in Table S3 (ESI†).

DLVO theory, and they show a reasonably good agreement with the experimental results. In monovalent salt solutions, these two types of particles are oppositely charged. In the presence of multivalent ions, however, one particle type reverses its charge, while the charge of the other particle type remains approximately unaffected. With such data now available, we can draw two novel conclusions concerning heteroaggregation processes.

First, we identify two patterns for heteroaggregation between two types of oppositely charged particles. The classical pattern features fast aggregation under all conditions. This pattern is characteristic of oppositely charged particles, and in the present system occurs in solutions containing ions of low valence. The novel pattern shows an intermediate region of slow heteroaggregation. This region occurs, when one of the particles undergoes a charge reversal, which can be induced by addition of multivalent ions of higher valence. While these intermediate regions of slow heteroaggregation resemble the ones observed for homoaggregation, which are systematically wider for heteroaggregation than for homoaggregation. This difference is related to the fact that double layer forces are more repulsive in the asymmetric system, which involves one highly charged and another weakly charged surface. The symmetric system, on the other hand, features two weakly charged surfaces, which induce a weaker repulsion.

Second, stability ratios and CCCs for heteroaggregation are very sensitive to the boundary conditions entering the calculations of double layer forces, especially where one of the particles is close to the charge reversal point. This sensitivity is related to the fact that double layer forces acting between a charged and a neutral particle strongly depend on the charge regulation characteristics of the more weakly charged surface. When this surface is neutral, the charge regulation conditions in fact determine the sign of the interaction force.[40] Comparison of the present experimental data with DLVO calculation thus allows drawing conclusions concerning the charge regulation properties of the surfaces involved. The presently investigated systems are found to closely follow CP boundary conditions.

Acknowledgements

This work was supported by the Swiss National Science Foundation through awards 140327 and 159874 and the University of Geneva. TS acknowledges support from Japan Society of Promotion of Science through grant number 15J00805.

References

1 H. Schulze, *J. Prakt. Chem.*, 1882, **25**, 431–452.
2 W. B. Hardy, *Proc. R. Soc. London*, 1900, **66**, 110–125.
3 B. Derjaguin and L. D. Landau, *Acta Physicochim. URSS*, 1941, **14**, 633–662.
4 E. J. W. Verwey and J. T. G. Overbeek, *Theory of Stability of Lyophobic Colloids*, Elsevier, Amsterdam, 1948.
5 J. T. G. Overbeek, *Pure Appl. Chem.*, 1980, **52**, 1151–1161.
6 W. B. Russel, D. A. Saville and W. R. Schowalter, *Colloidal Dispersions*, Cambridge University Press, Cambridge, 1989.
7 B. Tezak, E. Matijevic and K. F. Schulz, *J. Phys. Chem.*, 1955, **59**, 769–773.
8 G. Frens and J. J. F. G. Heuts, *Colloids Surf.*, 1988, **30**, 295–305.
9 C. Schneider, M. Hanisch, B. Wedel, A. Jusufi and M. Ballauff, *J. Colloid Interface Sci.*, 2011, **358**, 62–67.
10 I. Szilagyi, A. Polomska, D. Citherlet, A. Sadeghpour and M. Borkovec, *J. Colloid Interface Sci.*, 2013, **392**, 34–41.
11 N. O. McHedlov-Petrossyan, V. K. Klochkov and G. V. Andrievsky, *J. Chem. Soc., Faraday Trans.*, 1997, **93**, 4343–4346.
12 M. Kobayashi, M. Skarba, P. Galletto, D. Cakara and M. Borkovec, *J. Colloid Interface Sci.*, 2005, **292**, 139–147.
13 G. Trefalt, I. Szilagyi, G. Tellez and M. Borkovec, *Langmuir*, 2017, **33**, 1695–1704.
14 J. H. van Zanten and M. Elimelech, *J. Colloid Interface Sci.*, 1992, **154**, 1–7.
15 K. L. Chen and M. Elimelech, *Langmuir*, 2006, **22**, 10994–11001.

16 S. H. Behrens, D. I. Christl, R. Emmerzael, P. Schurtenberger and M. Borkovec, *Langmuir*, 2000, **16**, 2566–2575.
17 S. H. Xu and Z. W. Sun, *Soft Matter*, 2011, **7**, 11298–11308.
18 M. Pavlovic, R. Huber, M. Adok-Sipiczki, C. Nardin and I. Szilagyi, *Soft Matter*, 2016, **12**, 4024–4033.
19 J. B. Rosenholm, J. Nylund and B. Stenlund, *Colloids Surf.*, 1999, **159**, 209–218.
20 L. Ehrl, Z. Jia, H. Wu, M. Lattuada, M. Soos and M. Morbidelli, *Langmuir*, 2009, **25**, 2696–2702.
21 R. O. James, A. Homola and T. W. Healy, *J. Chem. Soc., Faraday Trans. 1*, 1977, **73**, 1436–1445.
22 H. Kihira and E. Matijevic, *Langmuir*, 1992, **8**, 2855–2862.
23 A. Y. Kim and J. C. Berg, *J. Colloid Interface Sci.*, 2000, **229**, 607–614.
24 A. M. Puertas, A. Fernandez-Barbero and F. J. de las Nieves, *J. Colloid Interface Sci.*, 2003, **265**, 36–43.
25 J. Labille, C. Harns, J. Y. Bottero and J. Brant, *Environ. Sci. Technol.*, 2015, **49**, 6608–6616.
26 K. A. Huynh, J. M. McCaffery and K. L. Chen, *Environ. Sci. Technol.*, 2012, **46**, 5912–5920.
27 B. M. Smith, D. J. Pike, M. O. Kelly and J. A. Nason, *Environ. Sci. Technol.*, 2015, **49**, 12789–12797.
28 P. Dusak, A. Mertelj, S. Kralj and D. Makovec, *J. Colloid Interface Sci.*, 2015, **438**, 235–243.
29 W. Lin, M. Kobayashi, M. Skarba, C. Mu, P. Galletto and M. Borkovec, *Langmuir*, 2006, **22**, 1038–1047.
30 M. I. Mishchenko and D. W. Mackowski, *J. Quant. Spectrosc. Radiat. Transfer*, 1996, **55**, 683–694.
31 P. Galletto, W. Lin, M. I. Mishchenko and M. Borkovec, *J. Chem. Phys.*, 2005, **292**, 139–147.
32 J. M. Lopez-Lopez, A. Schmitt, A. Moncho-Jorda and R. Hidalgo-Alvarez, *Adv. Colloid Interface Sci.*, 2009, **147**, 186–204.
33 N. Ryde and E. Matijevic, *J. Chem. Soc., Faraday Trans.*, 1994, **90**, 167–171.
34 T. Sugimoto, Y. Watanabe and M. Kobayashi, *Theor. Appl. Mech., Proc. Jpn.*, 2015, **63**, 133–145.
35 J. M. Lopez-Lopez, A. Schmitt, A. Moncho-Jorda and R. Hidalgo-Alvarez, *Soft Matter*, 2006, **2**, 1025–1042.
36 M. Elimelech, *J. Colloid Interface Sci.*, 1994, **164**, 190–199.
37 R. Hogg, T. W. Healy and D. W. Fuerstenau, *Trans. Faraday Soc.*, 1966, **62**, 1638–1649.
38 W. L. Yu, E. Matijevic and M. Borkovec, *Langmuir*, 2002, **18**, 7853–7860.
39 G. Trefalt, I. Szilagyi and M. Borkovec, *J. Colloid Interface Sci.*, 2013, **406**, 111–120.
40 G. Trefalt, F. J. Montes Ruiz-Cabello and M. Borkovec, *J. Phys. Chem. B*, 2014, **118**, 6346–6355.
41 M. A. Bevan and D. C. Prieve, *Langmuir*, 1999, **15**, 7925–7936.
42 M. M. Hatlo and L. Lue, *Soft Matter*, 2009, **5**, 125–133.
43 A. Naji, M. Kanduc, J. Forsman and R. Podgornik, *J. Chem. Phys.*, 2013, **139**, 150901.
44 X. Y. Ma, J. Q. Lu, R. S. Brock, K. M. Jacobs, P. Yang and X. H. Hu, *Phys. Med. Biol.*, 2003, **48**, 4165–4172.
45 J. Jordan and G. J. Ewing, *Inorg. Chem.*, 1962, **1**, 587–591.
46 R. W. O'Brien and L. R. White, *J. Chem. Soc., Faraday Trans. 2*, 1978, **74**, 1607–1626.
47 H. Kihira, N. Ryde and E. Matijevic, *J. Chem. Soc., Faraday Trans.*, 1992, **88**, 2379–2386.
48 T. Hiemstra and W. H. van Riemsdijk, *Langmuir*, 1999, **15**, 8045–8051.
49 P. Sinha, I. Szilagyi, F. J. Montes Ruiz-Cabello, P. Maroni and M. Borkovec, *J. Phys. Chem. Lett.*, 2013, **4**, 648–652.
50 F. J. Montes Ruiz-Cabello, G. Trefalt, Z. Csendes, P. Sinha, T. Oncsik, I. Szilagyi, P. Maroni and M. Borkovec, *J. Phys. Chem. B*, 2013, **117**, 11853–11862.
51 L. Guldbrand, B. Jonsson, H. Wennerstrom and P. Linse, *J. Chem. Phys.*, 1984, **80**, 2221–2228.
52 M. Moazzami-Gudarzi, G. Trefalt, I. Szilagyi, P. Maroni and M. Borkovec, *Phys. Chem. Chem. Phys.*, 2016, **18**, 8739–8751.

Electronic Supplementary Material (ESI) for Physical Chemistry Chemical Physics.

Supplementary Information

Heteroaggregation of Oppositely Charged Particles in the Presence of Multivalent Ions

Tianchi Cao[1], Takuya Sugimoto[1,2], Istvan Szilagyi[1], Gregor Trefalt[1], Michal Borkovec[1,*]

[1]Department of Inorganic and Analytical Chemistry, University of Geneva, Sciences II, 30 Quai Ernest-Ansermet, 1205 Geneva, Switzerland

[2]Faculty of Life and Environmental Sciences, University of Tsukuba, 1-1-1 Tennoudai, Tsukuba, Ibaraki 305-8572, Japan

*Corresponding author. Email: michal.borkovec@unige.ch

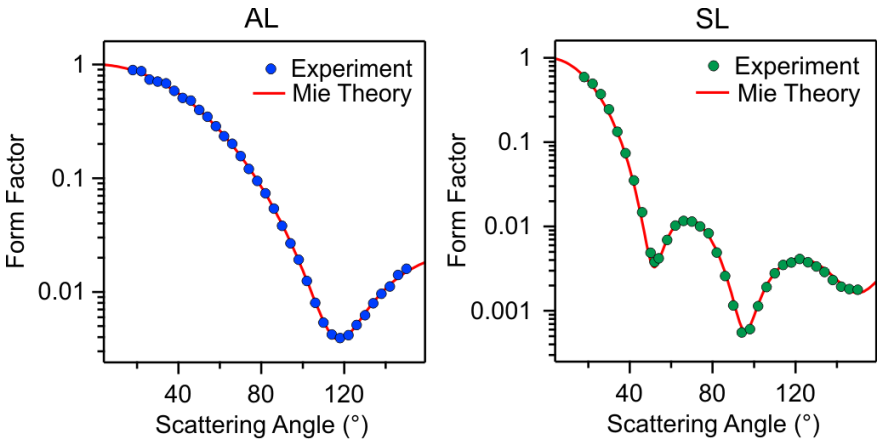

Figure S1. Static light scattering on suspensions of latex particles used in pure water adjusted to pH 4.0. Solid lines are best fits with Mie theory including polydispersity and a correction due to reflection. (a) AL and (b) SL particles.

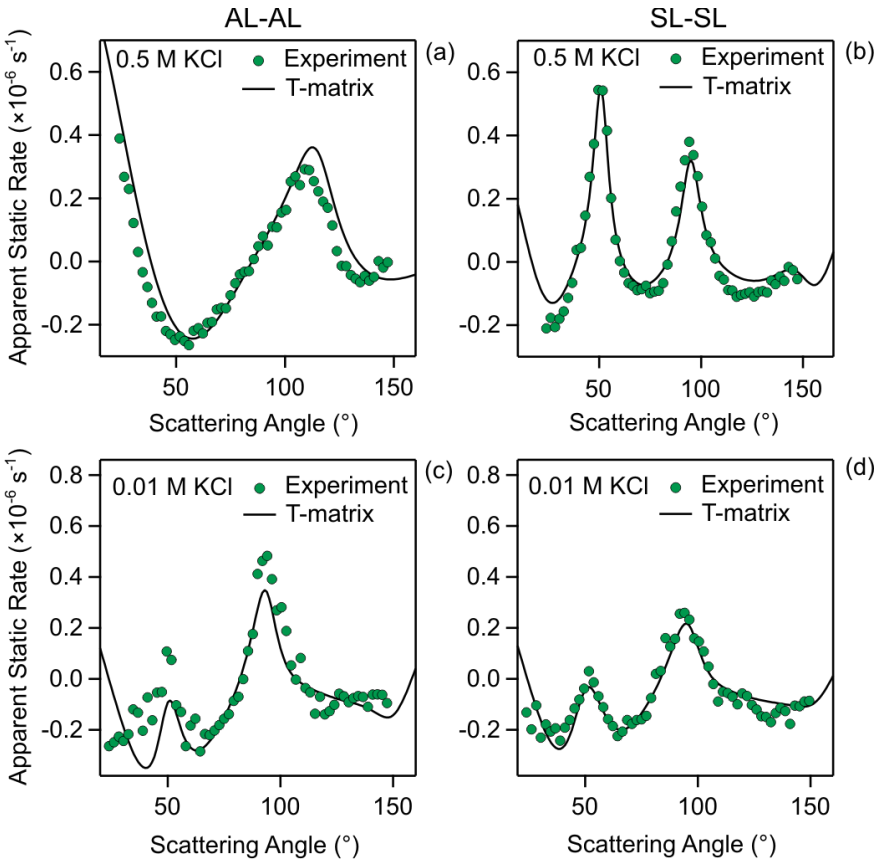

Figure S2. Apparent aggregation rates obtained from time-resolved static light scattering as a function of the scattering angle in suspensions with one type of aggregation process. Solid line is the best fit with T-matrix theory. Homoaggregation in 0.5 M KCl solutions for (a) AL at total particle concentrations of 4.0×10^{13} m^{-3} and (b) SL of 1.4×10^{13} m^{-3}. Pure heteroaggregation between AL and SL particles in 0.01 M KCl solution with (c) total particle concentration of 1.1×10^{14} m^{-3} and an AL number fraction of 0.42 and with (d) total particle concentration of 5.4×10^{13} m^{-3} and an AL number fraction of 0.74. All suspensions have pH 4.0.

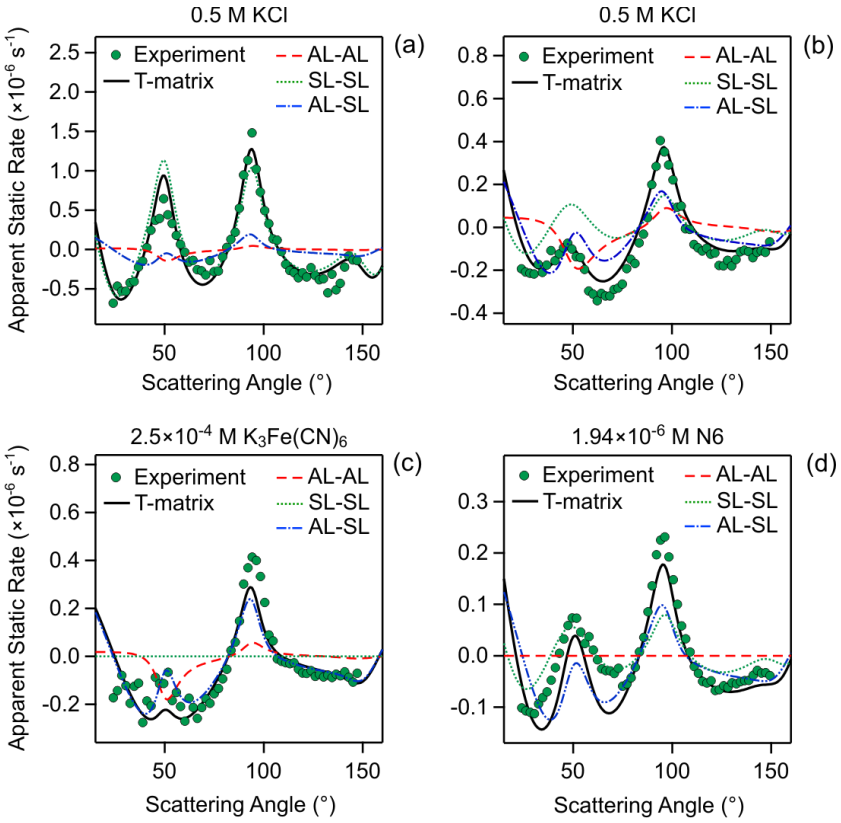

Figure S3. Apparent aggregation rates obtained from static light scattering as a function of the scattering angle in suspension containing AL and SL particles. Solid thick line is the best fit with T-matrix theory and the dashed thin lines indicate the contributions of the individual aggregation processes. (a,b) Heteroaggregation and both homoaggregation processes occurring in suspensions containing 0.5 M KCl. Heteroaggregation and one homoaggregation process occurring in suspension in (c) 2.5×10^{-4} M $K_3Fe(CN)_6$ solution and (d) a solution of an aliphatic amine N6 at a concentration of 1.9×10^{-6} M. All suspensions have pH 4.0. For (a,c) the total particle concentration is 1.1×10^{14} m^{-3} and AL number fraction 0.42, and for (b,d) the total particle concentration of 5.4×10^{13} m^{-3} and an AL number fraction of 0.74.

Table S1. Comparison of absolute aggregation rate coefficients obtained by dynamic light scattering (DLS) and static light scattering (SLS).

System	Figures[a]	DLS ($\times 10^{-18}$ m^3/s)	SLS ($\times 10^{-18}$ m^3/s)
AL-AL, 0.5 M KCl	1a, S2a	2.8±0.2	2.9±0.3
SL-SL, 0.5 M KCl	1b, S2b	3.1±0.3	3.3±0.3
AL-SL, 0.01 M KCl	1c, S2c	5.0±0.4	4.6±0.4
AL-SL, 0.01 M KCl	1d, S2d	5.7±0.4	5.4±0.4
AL-SL, 0.5 M KCl	2a, S3a	3.9±0.4	3.0±0.5
AL-SL, 0.5 M KCl	2b, S3b	3.9±0.4	3.6±0.4
AL-SL, 2.5×10^{-4} M $K_3Fe(CN)_6$	2c, S3c	3.6±0.4	3.4±0.4
AL-SL, 1.9×10^{-6} M N6	2d, S3d	3.2±0.3	2.9±0.3

[a]Data presented in respective figures.

Table S2. Comparison of experimental and calculated CCCs (M) for homoaggregation and heteroaggregation in systems containing different types of salt. The different boundary conditions are indicated.

Particle pair	Salt	Experiment	CP (p = 0)	CR (p = 0.5)	CC (p = 1)
AL-AL	KCl	2.5×10^{-1}	1.2×10^{-1}	1.3×10^{-1}	1.4×10^{-1}
	K_2SO_4	3.0×10^{-2}	1.1×10^{-2}	1.2×10^{-2}	1.2×10^{-2}
	$K_3Fe(CN)_6$	2.5×10^{-4}, 1.0×10^{-3}, 4.0×10^{-2}	1.2×10^{-4},1.6×10^{-3}, 8.8×10^{-3}	1.3×10^{-4}, 1.3×10^{-3},1.2×10^{-2}	1.4×10^{-4}, 8.5×10^{-4}, 1.8×10^{-2}
	$K_4Fe(CN)_6$	3.0×10^{-5}, 1.6×10^{-4}, –[a]	3.2×10^{-5}, 1.9×10^{-4}, 4.2×10^{-2}	3.4×10^{-5}, 1.7×10^{-4}, 5.0×10^{-2}	3.7×10^{-5}, 1.4×10^{-4}, 6.2×10^{-2}
SL-SL	KCl	4.0×10^{-1}	2.8×10^{-1}	3.0×10^{-1}	3.2×10^{-1}
	K_2SO_4	2.1×10^{-1}	1.1×10^{-1}	1.2×10^{-1}	1.3×10^{-1}
	$K_3Fe(CN)_6$	1.3×10^{-1}	6.3×10^{-2}	6.9×10^{-2}	7.6×10^{-2}
	$K_4Fe(CN)_6$	–[a]	6.1×10^{-2}	6.5×10^{-2}	7.4×10^{-2}
AL-SL	KCl				
	K_2SO_4				
	$K_3Fe(CN)_6$	2.5×10^{-4}, 7.1×10^{-2}	4×10^{-4}, 2.9×10^{-2}	2.8×10^{-4}, 3.8×10^{-2}	5.4×10^{-5}, 4.9×10^{-2}
	$K_4Fe(CN)_6$	1.0×10^{-4}, –[a]	8.9×10^{-5}, 4.6×10^{-2}	6.9×10^{-5}, 5.2×10^{-2}	1.9×10^{-5}, 6.2×10^{-2}

[a]The respective CCC could not be measured.

Table S3. Comparison of experimental and calculated CCCs (M) of N6 for homoaggregation and heteroaggregation in systems containing different concentration of monovalent salt. The different boundary conditions are indicated.

Particle pair	Monovalent Salt (M)	Experiment	CP (p = 0)	CR (p = 0.5)	CC (p = 1)
AL-AL	1.0×10^{-4}	6.8×10^{-2}	6.4×10^{-2}	7.7×10^{-2}	1.0×10^{-1}
	1.6×10^{-3}	7.0×10^{-2}	9.3×10^{-2}	1.1×10^{-1}	1.5×10^{-1}
	1.5×10^{-2}	6.6×10^{-2}	1.0×10^{-1}	1.3×10^{-1}	1.8×10^{-1}
	7.0×10^{-2}	6.7×10^{-2}	2.7×10^{-2}	3.1×10^{-2}	4.1×10^{-2}
	8.0×10^{-2}		1.0×10^{-2}		
	1.0×10^{-1}	4.3×10^{-2}			1.0×10^{-2}
	1.1×10^{-1}		4.0×10^{-3}		
	1.3×10^{-1}				4.0×10^{-3}
SL-SL	1.0×10^{-4}	3.5×10^{-7}, 1.5×10^{-6}, 1.9×10^{-2}	5.2×10^{-7}, 1.7×10^{-6}, 2.2×10^{-2}	5.3×10^{-7}, 1.8×10^{-6}, 2.7×10^{-2}	6.1×10^{-7}, 1.5×10^{-6}, 3.4×10^{-2}
	1.6×10^{-3}	4.3×10^{-7}, 2.7×10^{-6}, 2.4×10^{-2}	3.8×10^{-7}, 4.8×10^{-6}, 2.4×10^{-2}	4.2×10^{-7}, 4.3×10^{-6}, 2.7×10^{-2}	5.0×10^{-7}, 3.9×10^{-6}, 3.4×10^{-2}
	1.5×10^{-2}	1.7×10^{-6}, 4.7×10^{-5}, 2.1×10^{-2}	1.0×10^{-6}, 6.9×10^{-5}, 1.9×10^{-2}	1.2×10^{-6}, 6.0×10^{-5}, 2.5×10^{-2}	1.4×10^{-6}, 4.7×10^{-5}, 3.4×10^{-2}
	6.2×10^{-2}		4.0×10^{-3}		
	7.0×10^{-2}	2.5×10^{-6}, 2.1×10^{-3}, 2.9×10^{-2}	6.5×10^{-7}	9.6×10^{-7}, 3.8×10^{-3}, 1.7×10^{-2}	1.7×10^{-6}, 1.9×10^{-6}, 3.8×10^{-2}
	7.1×10^{-2}		1.0×10^{-2}		
	8.4×10^{-2}				4.0×10^{-3}
	1.0×10^{-1}	8.6×10^{-3}			1.0×10^{-2}
AL-SL	1.0×10^{-4}	1.5×10^{-6}, 6.3×10^{-2}	9.1×10^{-7}, 4.0×10^{-2}	7.5×10^{-7}, 4.8×10^{-2}	8.5×10^{-8}, 6.4×10^{-2}
	1.6×10^{-3}	1.7×10^{-6}, 6.4×10^{-2}	1.3×10^{-6}, 4.3×10^{-2}	9.1×10^{-7}, 5.4×10^{-2}	1.7×10^{-7}, 7.9×10^{-2}
	1.5×10^{-2}	1.4×10^{-5}, 5.8×10^{-2}	1.7×10^{-5}, 3.6×10^{-2}	1.3×10^{-5}, 4.8×10^{-2}	5.5×10^{-6}, 6.5×10^{-2}
	7.0×10^{-2}	4.6×10^{-4}, 5.6×10^{-2}	5.8×10^{-4}, 2.3×10^{-2}	4.1×10^{-4}, 3.3×10^{-2}	1.9×10^{-4}, 4.4×10^{-2}
	7.6×10^{-2}		1.0×10^{-2}		
	8.3×10^{-2}		4.0×10^{-3}		
	1.0×10^{-1}	1.7×10^{-3} , 3.9×10^{-2}			1.0×10^{-2}
	1.1×10^{-1}				4.0×10^{-3}

HAPTER 5

Measuring Slow Heteroaggregation Rates with Time-Resolved Multi-Angle Dynamic Light Scattering

Cao, T.; Trefalt G.; Borkovec, M.

Abstract

Heteroaggregation rate coefficients can be monitored by time-resolved multi-angle dynamic light scattering. However, the measured heteroaggregation rates are in a narrow range, typically over one order of magnitude. In the present work, we propose an approach to enhance the range of measured heteroaggregation rates by enlarging the contrast of the scattering profiles between the different aggregates. In the new system of AL particles (302 nm in diameter) and SL particles (250nm in diameter) containing anionic surfactant—sodium n-octyl sulfate (SOS), one observes that the scattering profiles of hetero-aggregates (AL-SL) and homo-aggregates (SL-SL) exhibit a similar characteristic peak, while homo-aggregates (AL-AL) have a different one. Thus, the contrast between the scattering profiles can be increased by suppressing the homoaggregation of SL particles in the presence of SOS. As a result, the heteroaggregation rates between AL particles and SL particles in the SOS solution are measured in a much wider range, namely over two orders of magnitude.

Introduction

Numerous studies focus on colloidal aggregation, but one normally investigates the aggregation of the same kind (or very similar) particles, referred to as homoaggregation.[1-5] Such investigations are surely important, as many applications involve precisely such systems, for example, in the formulation of drugs, fabrication of paints, or food processing. However, at least as many applications concern aggregation in systems involving two or more types of particles, referred to as heteroaggregation. Notable examples are ceramic processing, papermaking, water treatment, or groundwater remediation. Aggregation processes in such mixed particle systems are much less understood.

The simplest example of such a mixed system consists of a binary suspension involving two types of particles. The initial states of particle aggregation are governed by the formation of particle dimers, and larger aggregates form at later stages of aggregation. In the early stages of aggregation in a binary suspension, three types of dimers may form, namely two types of symmetric homoaggregates, and one type of heteroaggregate.

While many experimental techniques to probe homoaggregation processes are available, the choices are rather limited concerning heteroaggregation processes. The main challenge in such studies is to distinguish the formation of homoaggregates and heteroaggregates. One approach is single particle counting.[6,7] Thereby, one forces the aggregating suspension

through a narrow capillary, and then one is able to probe one particle aggregate after another, typically through conductivity or light scattering. While this technique normally achieves an excellent resolution, and is often able to distinguish various types of aggregates, it is very slow and may disrupt the aggregates though the high shear rates present.

The other approach is to use time-resolved light scattering techniques.[8-12] While such techniques are well established to probe homoaggregation processes, they have not been used to investigate heteroaggregation processes widely. One possible approach is to measure an apparent aggregation rate, and to vary the fractions of the two types of particles.[8,9] The presence of heteroaggregation leads to a characteristic dependence of the apparent aggregation rate on this fraction, from which the heteroaggregation rate can be extracted. However, this approach is very laborious, as for each condition different suspensions must be prepared and analyzed.

Here we take another approach, and exploit the different angular dependencies of the scattering profiles of the different aggregates.[10-12] In particular, when the size of the particles involved is chosen to be somewhat different, the different dimers can be distinguished through the angular variation of the scattering signal. Such studies were already carried out in the past, and it was indeed possible to extract heteroaggregation rates over a wide range of conditions. However, the drawback of these approaches is that the contrast between the different aggregates was poor, and therefore heteroaggregation rates were not accessible over a very wide range, typically over one order of magnitude or less.

In the present study we will demonstrate that by appropriate choice the particles involved, the contrast between the different aggregates can be substantially enhanced. This approach enables us to measure heteroaggregation rates over a much wider range, and as we shall see, the heteroaggregation rates can be measured over more than two orders of magnitude.

Experimental

Materials. Monodisperse amidine and sulfate latex were purchased from Invitrogen corporation, denoted as AL300 and SL200. These abbreviations indicate the approximate diameters of these particles in nm, which are 302 nm and 250 nm. The same batches of particles were extensively characterized as described in a previous study.[13] Before use, the particle suspensions were dialyzed for about one week in Milli-Q water (Millipore) until the conductivity of the surrounding solution dropped below 80 mS/m. For the dialysis,

polyvinylidene fluoride and cellulose ester membranes were used for the AL200 and sulfate SL200 particles, respectively. Analytical grade sodium n-octyl sulfate (SOS) (Alfa Aesar) and NaCl (Sigma-Aldrich) were dissolved with Milli-Q water and adjusted to pH 4.0 with HCl.

Electrophoresis. The electrophoretic mobility was measured with Zetasite Nano ZS (Malvern Instruments). Suspensions were prepared by adding a small aliquot of the dialyzed latex suspension to the solution containing the appropriate amount of SOS and NaCl. The particle concentrations were 0.50 mg/L (3.4×10^{14} m^{-3}) for the AL300 particles and 0.23 mg/L (3.3×10^{14} m^{-3}) for SL200.

Light scattering. A multi-angle light scattering goniometer (ALV CGS-8F) was used to measure the aggregation rates. The goniometer uses 8 fiber-optic detector and a solid-state laser operating at a wavelength of 532 nm with an angular resolution of 4.25°. Borosilicate cuvets were used to carry out the experiments, which were first cleaned with hot piranha solution, which was prepared by mixing concentrated H_2SO_4 and 30% H_2O_2 in a volume ratio 3:1. Then they were washed in plenty of Milli-Q water and dried at 60°C in a dust-free oven. The aggregation process was initiated by injecting the respective particle suspensions into the solutions containing SOS and NaCl, and subsequent rapid mixing. For each time point, the light scattering signals were measured during 20 s, and the hydrodynamic radii were extracted from the second cumulant fit of the correlation function by means of the Stokes-Einstein relation. The aggregation was typically monitored over 30 min. From these experiments, the apparent dynamic rate is extracted

$$\Delta(\theta) = \frac{1}{R(\theta,0)} \cdot \left.\frac{dR(\theta,t)}{dt}\right|_{t\to 0} \qquad (1)$$

This rate is obtained for each θ scattering angle by fitting the time dependence of the apparent hydrodynamic radius $R(\theta,t)$ with a straight line, and dividing its slope by the intercept at the beginning of the experiment. All experiments were carried out in the early stages of the aggregation process. This condition was ensured that the hydrodynamic radius did not increase by more than 30% during the overall measurement time. In suspensions of one particle type, homoaggregation stability ratios were determined in a similar fashion, but only carrying out measurements at one scattering angle of 90°. These types of measurements were described in detail earlier.[3,13]

Evaluation of heteroaggregation rates. The early stages of the aggregation are governed by the formation of particle dimers from particle monomers. In a binary mixture of colloidal particles of type A and B, three possible pairs may form. There are two types of homoaggregates

$$\begin{aligned} \mathrm{A} + \mathrm{A} &\rightarrow \mathrm{AA} \\ \mathrm{B} + \mathrm{B} &\rightarrow \mathrm{BB} \end{aligned} \tag{2}$$

and one type of heteroaggregate

$$\mathrm{A} + \mathrm{B} \rightarrow \mathrm{AB} \tag{3}$$

One can show that that these three aggregation processes contribute to the apparent dynamic rate in an additive fashion, namely[10,12]

$$\Delta(\theta) = k_{\mathrm{AA}} H_{\mathrm{AA}}(\theta) + 2k_{\mathrm{AB}} H_{\mathrm{AB}}(\theta) + k_{\mathrm{BB}} H_{\mathrm{BB}}(\theta) \tag{4}$$

where k_{ij} are the aggregation rate coefficients for the reactions given in eqs. (2) and (3) and $H_{ij}(\theta)$ are characteristic functions that are dependent of the scattering angle. The subscripts *i* and *j* refer to the particles A and B. This angle-dependence will enable us to separate the contributions from the different aggregation processes, and thus enable us to extract the heteroaggregation rate coefficient k_{AB} . The characteristic functions are somewhat complicated and given here without derivation. We refer to the literature for further details.[10-12] This function is best represented as the difference of two other functions

$$H_{ij}(\theta) = F_{ij}(\theta) - G_{ij}(\theta) \tag{5}$$

where

$$F_{ij}(\theta) = \frac{N_0 x_i x_j}{2} \cdot \frac{I_{ij}(\theta) - I_i(\theta) - I_j(\theta)}{x_{\mathrm{A}} I_{\mathrm{A}}(\theta) + x_{\mathrm{B}} I_{\mathrm{B}}(\theta)} \tag{6}$$

and

$$G_{ij}(\theta) = \frac{N_0 x_i x_j}{2} \cdot \frac{I_{ij}(\theta)/R_{ij} - I_i(\theta)/R_i - I_j(\theta)/R_i}{x_{\mathrm{A}} I_{\mathrm{A}}(\theta)/R_{\mathrm{A}} + x_{\mathrm{B}} I_{\mathrm{B}}(\theta)/R_{\mathrm{B}}} \tag{7}$$

Here, $I_i(\theta)$ is the scattering intensity and R_i the hydrodynamic radius of the particle monomer of type *i*, and $I_{ij}(\theta)$ is the scattering intensity and R_{ij} hydrodynamic radius of the

particle dimer of type *ij*. The quantities x_i are the number fractions of the particles of type *i* and N_0 is the total particle number concentration of both types of particles. Note that $x_A + x_B = 1$. Thus, the characteristic functions also depend on the number fraction of one particle type. This dependence is essential, since one needs both types of particles to make heteroaggregation possible. In a suspension where only one type of particle is present, say A, one has $x_A = 1$ and $H_{AB} = H_{BB} = 0$. The expression for H_{AA} then becomes identical to the know relation for homoaggregation, and one can extract the homoaggregation rate coefficient.[14] The mixture is then used to obtain the heteroaggregation rate coefficient k_{AB}. An appropriate number fraction to obtain the best contrast is chosen for all experiments.

When one uses spherical and monodisperse particles, the scattering intensities and hydrodynamic radii can be calculated. The scattering intensities of the particle monomers can be evaluated with Mie theory and the ones of the particle dimers with T-matrix theory.[15,16] Minor polydispersity effects can also be included in the calculation. The hydrodynamic radii of the dimers can be obtained from the empirical formula [12,17]

$$\alpha_{ij} = \frac{2R_{ij}}{R_i + R_j} = 1.392 + 0.608 \cdot \left(\frac{R_i - R_j}{R_i + R_j} \right)^2 \tag{8}$$

This formula accurately represents the exact results obtained from the analysis of the diffusion coefficients at low Reynolds numbers of pairs of unequal spheres. For the particles used, the theoretical hydrodynamic radii were used in the data analysis.

To align with previous studies, we report the aggregation rate coefficients in terms of the stability ratios defined as

$$W_{ij} = \frac{k_{ij}^{(\text{fast})}}{k_{ij}} \tag{9}$$

where k_{ij} and $k_{ij}^{(\text{fast})}$ are the experimental and fast aggregation rate coefficients, respectively. We choose 0.8 M NaCl to define the fast aggregation conditions.

Results and Discussion

Heteroaggregation rate coefficients were measured with time-resolved multi-angle dynamic light scattering in the past.[10-12] In all these studies, however, the rate coefficients of homoaggregation and heteroaggregation were quite comparable. In consequence, highest

measured heteroaggregation stability ratios remained low, below 10 at best. In the present study, we show how to extend this restriction, and will report reliable measurements of heteroaggregation stability ratios exceeding 100.

To this aim we study aggregation in mixed latex particles suspensions with amidine and sulfate surface functionalities. These particles will be denoted AL300 and SL200, since their diameters are very close to 300 nm and 200 nm, respectively. The same particles were used in a previous study, where extensive characterization is reported.[13] Their polydispersity is below 6%. The pH of all suspensions was adjusted to 4.0.

Behavior in NaCl solutions. Figure 1 shows the electrophoretic mobility of these particles in NaCl solutions. One observes that the AL300 particles are positively charged, while the SL200 particles negatively. The sign of the charge can be easily understood by considering the chemical nature of the surface groups. The magnitude of the mobility of the AL300 particles is higher, suggesting that the magnitude of the charge is higher for AL300 particles than for SL300. Moreover, the mobility of Al300 particles goes through a maximum, as suggested by the standard electrokinetic model due to O'Brien and White.[18,19] The SL200 particles do not show this maximum, which is also consistent with a lower magnitude of the charge density.

We have first studied homoaggregation in separate suspensions of particles AL300 and SL200 in NaCl solutions. Such investigations were already described in a previous study[13], but we present these results here as well. Here their analysis will be further extended with T-matrix theory.

The stability ratios for homoaggregation are shown in Fig. 2a and 2b. One observes the typical behavior reported for charged latex particles in earlier studies.[10] At high salt concentrations, the aggregation rate is fast, and independent of the salt concentration. By definition, the stability ratio is set to unity in this regime. With decreasing salt concentration, the stability ratio increases steeply and the aggregation becomes slow. At 10 mM and below, the suspensions are perfectly stable. The transition between slow and fast aggregation is referred to as the critical coagulation concentration (CCC). For both systems, the CCC is around a NaCl concentration of 0.15 M.[13]

Let us now focus on the analysis of the absolute homoaggregation rates under fast conditions. These conditions were realized in 0.8 M NaCl. The rate coefficients were extracted with T-

matrix theory. These results are summarized in Fig. 3a and 3b. These figures show the apparent dynamic rates for the homoaggregation process in suspensions containing AL300 or SL200 particles, respectively. One observes that the T-matrix theory describes the measured angle dependence perfectly well. One should note that the fit involves only one adjustable parameter, namely the respective aggregation rate coefficient. Adjusting this coefficient only changes the overall magnitude of the apparent rate, but not its characteristic angular dependence. We also remark that for the AL300 and SL200 particles the angular dependence of the apparent dynamic rates is very different.

The fitted homoaggregation rate coefficients are shown in Table 1. One observes that these coefficients are very similar. In particular, these numbers agree with the fast aggregation rate coefficients for the same particles measured in 0.6 M NaCl solutions within experimental error.[13] However, the latter number were determined without making any assumptions about the actual optical response of the particles, and it is most comforting to see that both approaches yield the same results.

Let us now focus on the heteroaggregation process, where a mixed suspension of AL300 and SL200 particles was investigated in 10 mM NaCl solution. Fig. 2a and 2b show that the stability ratios are way above 100, and these processes can be thus perfectly neglected. Since the particles are oppositely charged, however, at these conditions only heteroaggregation occurs. Figure 3c confirms that this is indeed the case. This figure compares the measured apparent dynamic rate with the T-matrix theory calculation for the heteroaggregates. The very good agreement indicates that only these aggregates form. One can again adjust the heteroaggregation rate coefficient, and one finds that this coefficient is $(4.6\pm0.2)\times10^{-18}$ m^3/s. This experiment confirms that the T-matrix theory described the optical response of the heteroaggregates very well. Note however that the respective rate coefficient does not correspond to fast aggregation conditions.

To determine the heteroaggregation rate coefficient in the fast aggregation conditions, a similar experiment was carried out in 0.8 M NaCl solution. The result is shown in Fig. 3d. Now both homoaggregation processes occur together with the heteroaggregation. However, the homoaggregation rate coefficients are known under these conditions, and thus the only unknown is the heteroaggregation rate coefficient. Adjusting this parameter one obtains an excellent fit of the experimental data, and the respective rate coefficient can be extracted.

This number is reported in Table 1, and is very comparable to the homoaggregation rate coefficients.

With this number at hand, one can also calculate the stability ratios for heteroaggregation. The available values are reported in Fig. 2c. The observed decrease can be explained by the salt dependence of the double layer attraction between two oppositely charged surfaces. This attraction strengthens with decreasing ions strength, which results in decreasing stability ratio with decreasing salt concentration. The same trends in the heteroaggregation between oppositely charged particles were already described in the literature earlier.[10-12]

Behavior in SOS solutions. The aggregation behavior of these latex particles was further studied in solutions containing the short-chain anionic surfactant sodium octyl sulfate (SOS). This additive was chosen as it strongly adsorbs to positively charged surfaces and thereby inducing a charge reversal.

Fig. 4a illustrates this behavior for the AL300 particles. At low SOS concentrations, the particles are positively charged. Within increasing SOS concentration, the charge decreases, and vanishes at a concentration around 0.3 mM. Upon further addition of SOS, the charge decreases further, thereby making the particles negatively charged. This behavior is due to the adsorption of the negatively charged SOS on the positively charged particle surface. When NaCl is being added, the magnitude of the charge decreases somewhat, but the overall behavior remains the same.

Fig. 4b shows the corresponding electrophoretic mobility results for the SL200 particles. The particles are negatively charged, but addition of SOS increases the magnitude of their charge, which suggests that SOS also adsorbs to these negatively charged particles. Adding NaCl, the magnitude of the mobility decreases.

Let us now focus on the aggregation behavior in the presence of SOS. Given the high charge density of the SL200 particles, these suspensions remain stable for all conditions investigated. On the other hand, the AL300 particles aggregate rapidly near the charge reversal point. This situation is illustrated in Fig. 5a. When one plots the stability ratio versus the SOS concentration, one observes a pronounced minimum near 0.3 mM. The aggregation is fast near this minimum, and slows down substantially when one moves away from it. Moreover, this minimum widens with the addition of NaCl.

This behavior is easily understood since the particles are neutral near the charge reversal point, and thus they interact with attractive van der Waals forces only. These forces induce fast aggregation. Away from the charge reversal point, the particles become charged, and their aggregation is slowed down by repulsive double layer forces. Adding a monovalent electrolyte screens the double layer forces, thereby making them less repulsive, and thus reducing the stability ratio. Very similar type of stability behavior was already observed in other systems, for example, for hematite particles versus pH[5], for amidine latex particles in the presence of tetraphenylborate or polystyrene sulfonate[13,20] or sulfate latex particles in the presence of aliphatic polyamines or polyethyleneimine.[12,21,22]

Let us now focus on the aggregation in the mixed suspension containing AL300 and SL200 particles. Fig. 6 illustrates the angular dependence of the apparent dynamic rates for different SOS concentrations. Fig. 6a shows the situation at the charge reversal point. One observes that heteroaggregation dominates the signal, as evident from the peak near 100°. As the SOS concentration is being increased, homoaggregation becomes increasingly important. This fact can be inferred from Figs. 6b and 6c, as the maximum is reduced, and is replaced by a minimum near 120°, which is characteristic for homoaggregation. Fig. 6d illustrates the extreme situation, where the signal is almost fully dominated by homoaggregation, but the contribution from heteroaggregation can be still detected, albeit barely. By fitting these apparent dynamic rates, the heteroaggregation rate coefficients can be extracted.

The respective heteroaggregation stability ratios are shown versus the SOS concentration in Fig. 5b. At low SOS concentrations, these ratios are below unity, since the heteroaggregation is enhanced by attractive double layer forces. When one adds NaCl to the system, the stability ratio becomes unity. The same situation was already encountered in the absence of SOS, and is illustrated in Fig. 2c. As the SOS concentration is being increased, the heteroaggregation stability ratio starts to increase steeply.

This increase can be explained by the onset of repulsive double layer forces between negatively charged surfaces. In this situation, however, one deals with an asymmetric situation where a strongly charged surface of the SL200 particles interacts with a weakly charged surface of the AL300 particle, which is decorated with adsorbed SOS molecules. For this reason, the onset of the increase in the heteroaggregation stability ratios occurs at lower SOS concentrations than for homoaggregation shown in Fig. 5a. For homoaggregation, one deals with a symmetric situation, where the two decorated AL300 particles interact. In this

case, the double layer repulsion is weaker, and thus the onset is shifted to higher concentrations. A similar shift between the onset between slow heteroaggregation and slow homoaggreation was already observed in similar binary suspensions containing amidine and sulfate latex particles in the presence of cationic polyamines.[12] In the latter situation, however, the polyamines induced the charge reversal of the negatively charged sulfate particles.

The novel aspect of this study is the present measurement of heteroaggregation stability ratios up to 100, see Fig. 5b. One observes that the dependence of these stability ratios on the SOS concentration is similar as for homoaggregation. However, it appears that the slope of the homoaggregation stability plots in the slow regime remains the same for different NaCl concentrations, while for heteroaggregation the slope is being modified. This observation is novel, since such high heteroaggregation stability ratios were not reported in the literature so far. The only comparable data is the mentioned study by Cao et al.[12] However, that study only reports heteroaggregation stability ratios up to 10, and based on these data considerations concerning the slope of the stability plots is hardly possible.

Conclusions

This study investigates heteroaggregation between amidine and sulfate latex particles in the presence of a short chain anionic surfactant SOS by time-resolved multi-angle dynamic light scattering. This surfactant strongly adsorbs to the amidine particles, which induces their charge reversal. The homoaggreagtion of these particles was equally studied, as they aggregate rapidly near the charge reversal point. The sulfate particles remain negatively charged and stable. The heteroaggregation process is probed in mixed suspensions of amidine and sulfate latex particles, whereby one can clearly separate the contributions between homoaggreagtion and heteroaggregation. In this fashion, the heteroaggregation rate can be measured. The heteroaggregation rate is fast at low SOS concentrations, where the two particles are oppositely charged. This rate slows down at higher SOS concentrations due to double layer repulsion between the negatively particles. However, the onset of this slow heteroaggregation occurs at lower SOS concentrations than for homoaggregation. The reason for this shift is that the double layer repulsion between two SOS-decorated amidine particles is weaker than between one sulfate particle and one SOS-decorated amidine particle.

Acknowledgements

This work was supported by the Swiss National Science Foundation through awards 178759 and 159874 and the University of Geneva.

Table 1. Absolute aggregation rate coefficients in 0.8 M NaCl.

System	Fast rate coefficient ($\times 10^{-18}$ m^3/s)
AL300-AL300	3.1±0.2
SL200-SL200	2.8±0.2
AL300-SL200	3.1±0.2

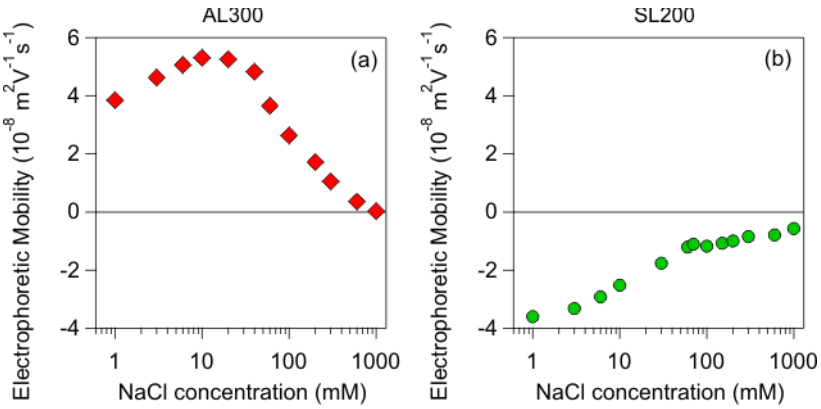

Figure 1. Electrophoretic mobility versus the NaCl concentration for the latex particles investigated at pH 4.0. (a) AL300 and (b) SL200.

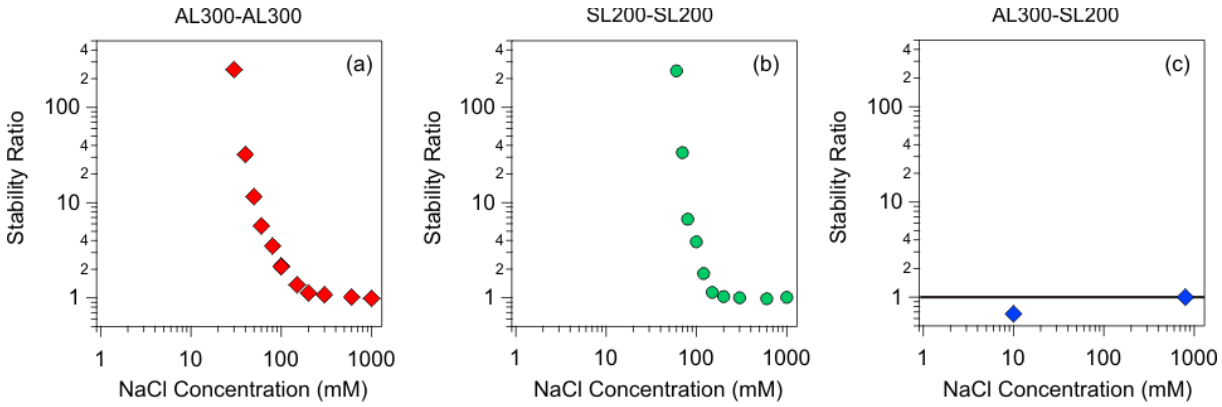

Figure 2. Stability ratios for the different aggregation processes versus the NaCl concentration at pH 4.0. Homoaggregation for (a) AL300-AL300 and (b) SL200-SL200. (c) Heteroaggregation for AL300-SL200.

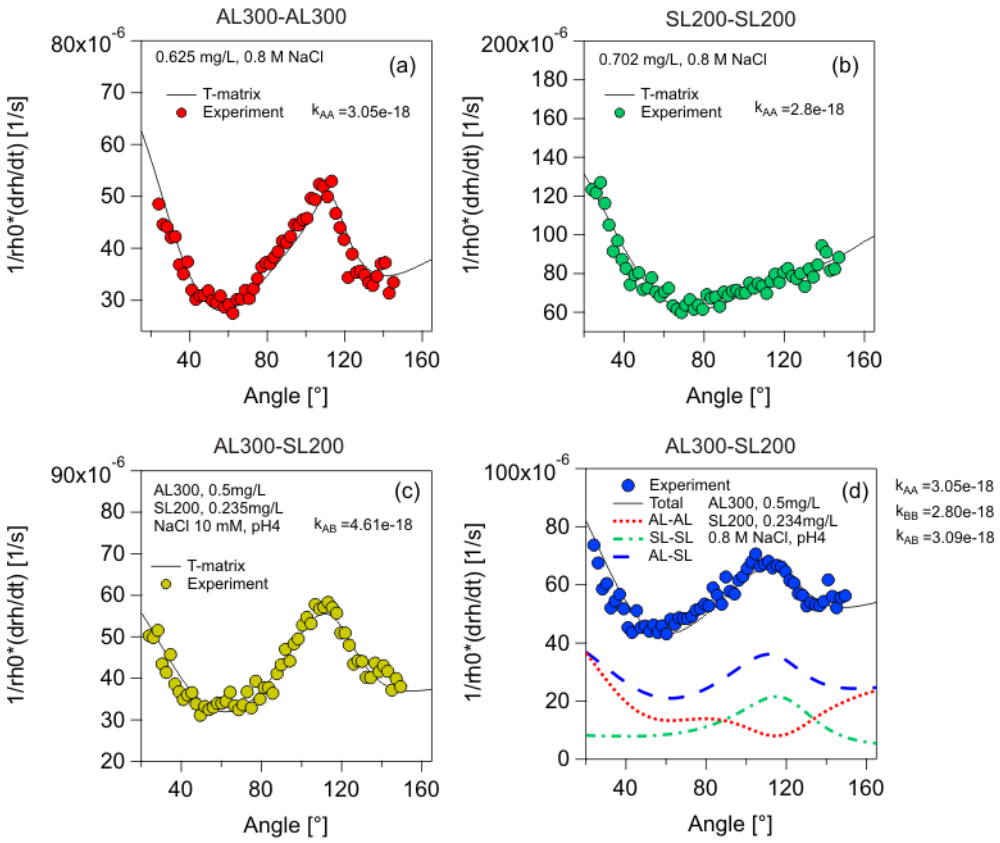

Figure 3. Apparent dynamic rates versus the scattering angle at pH 4.0. The points are the experimental results and the solid lines best fits with T-matrix theory. Homoaggregation in (a) AL300 and (b) SL200 suspensions with 0.8 M NaCl. (c) Pure heteroaggregation in 10 mM NaCl suspension. (d) Mixed homoaggregation and heteroaggregation in 0.8 M NaCl.

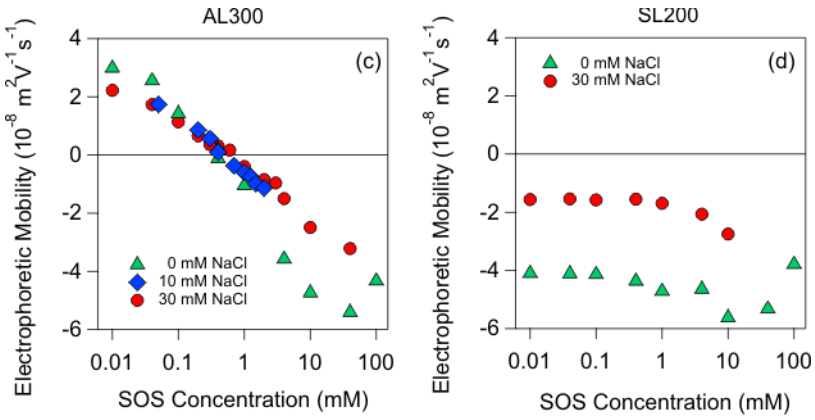

Figure 4. Electrophoretic mobility versus the SOS concentration at different levels of added NaCl for the latex particles investigated at pH 4.0. (a) AL300 and (b) SL200.

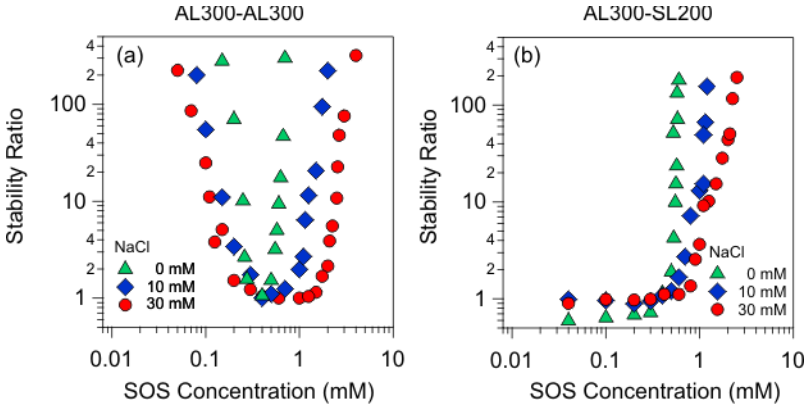

Figure 5. Stability ratios versus the SOS concentration at different levels of added NaCl for the latex particles investigated at pH 4.0. (a) Homoaggregation AL300-AL300 and (b) heteroaggregation AL300-SL200.

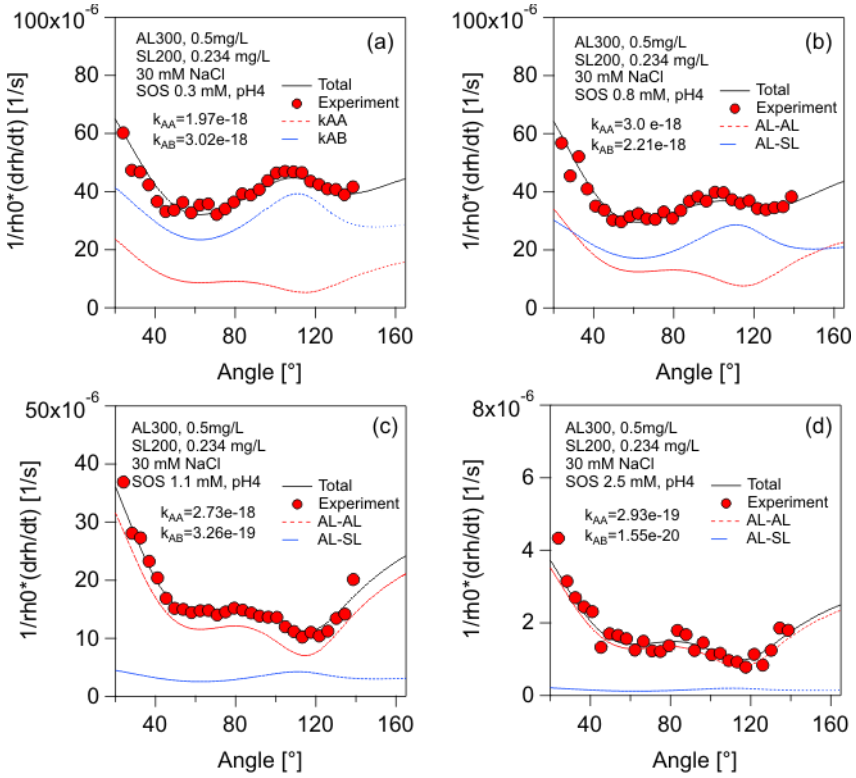

Figure 6. Apparent dynamic rates versus the scattering angle in solutions containing 30 mM NaCl and pH 4.0. The points are the experimental results and the solid lines best fits with T-matrix theory. SOS concentration (a) 0.3 mM, (b) 0.8 mM, (c) 1.1 mM, and (d) 2.5 mM.

References

(1) Elimelech, M.; Gregory, J.; Jia, X.; Williams, R. A., *Particle Deposition and Aggregation: Measurement, Modeling, and Simulation*. Butterworth-Heinemann Ltd.: Oxford, 1995.

(2) Chen, K. L.; Mylon, S. E.; Elimelech, M. *Environ. Sci. Technol.* **2006,** 40, 1516-1523.

(3) Cao, T.; Szilagyi, I.; Oncsik, T.; Borkovec, M.; Trefalt, G. *Langmuir* **2015,** 31, 6610–6614.

(4) Szilagyi, I.; Sadeghpour, A.; Borkovec, M. *Langmuir* **2012,** 28, 6211-6215.

(5) Schudel, M.; Behrens, S. H.; Holthoff, H.; Kretzschmar, R.; Borkovec, M. *J. Colloid Interface Sci.* **1997,** 196, 241-253.

(6) Lichtenfeld, H.; Shilov, V.; Knapschinsky, L. *Colloids Surf. A* **1998,** 142, 155-163.

(7) Holthoff, H.; Schmitt, A.; Fernandez-Barbero, A.; Borkovec, M.; Cabrerizo-Vilchez, M. A.; Schurtenberger, P.; Hidalgo-Alvarez, R. *J. Colloid Interface Sci.* **1997,** 192, 463-470.

(8) Kihira, H.; Matijevic, E. *Langmuir* **1992,** 8, 2855-2862.

(9) Kim, A. Y.; Berg, J. C. *J. Colloid Interface Sci.* **2000,** 229, 607-614.

(10) Lin, W.; Kobayashi, M.; Skarba, M.; Mu, C.; Galletto, P.; Borkovec, M. *Langmuir* **2006,** 22, 1038-1047.

(11) Yu, W. L.; Borkovec, M. *J. Phys. Chem. B* **2002,** 106, 13106-13110.

(12) Cao, T.; Sugimoto, T.; Szilagyi, I.; Trefalt, G.; Borkovec, M. *Phys. Chem. Chem. Phys.* **2017,** 19, 15160 - 15171.

(13) Cao, T.; Trefalt, G.; Borkovec, M. *Langmuir* **2018,** 34, 14368-14377.

(14) Holthoff, H.; Egelhaaf, S. U.; Borkovec, M.; Schurtenberger, P.; Sticher, H. *Langmuir* **1996,** 12, 5541-5549.

(15) Mishchenko, M. I.; Mackowski, D. W. *J. Quant. Spectrosc. Radiat. Transf.* **1996,** 55, 683-694.

(16) Mishchenko, M. I.; Travis, L. D.; Lacis, A. A., *Scattering, Absorption, and Emission of Light by Small Particles* University Press: Cambridge 2002.

(17) Yu, W. L.; Matijevic, E.; Borkovec, M. *Langmuir* **2002,** 18, 7853-7860.

(18) O'Brien, R. W.; White, L. R. *J. Chem. Soc. Farad. Trans. II* **1978,** 74, 1607-1626.

(19) Borkovec, M.; Behrens, S. H.; Semmler, M. *Langmuir* **2000,** 16, 5209-5212.

(20) Gillies, G.; Lin, W.; Borkovec, M. *J. Phys. Chem. B* **2007,** 111, 8626-8633.

(21) Szilagyi, I.; Polomska, A.; Citherlet, D.; Sadeghpour, A.; Borkovec, M. *J. Colloid Interf. Sci.* **2013,** 392, 34-41.

(22) Szilagyi, I.; Rosicka, D.; Hierrezuelo, J.; Borkovec, M. *J. Colloid Interf. Sci.* **2011,** 360, 580-585.

CHAPTER 6

Conclusions

Throughout the present thesis I investigated homo- and hetero-aggregation processes of colloidal particles in the solution containing various charged species. Light scattering gave the access to the aggregation rate coefficient either for homoaggregation or for heteroaggregation. Electrophoresis measurements provided insight concerning the charging properties of particle surfaces, which can also be used to calculate the aggregation rate by means of DLVO theory. This thesis contributes towards the better understanding of particle aggregation.

The effect of multivalent counterions on the colloidal stability of particle suspension was studied for more than one century. The well-known *Schulze-Hardy rule* was proposed to rationalize these findings, stating that multivalent counterions destabilize the particle suspension much more effectively than the monovalent ones. We studied the effect of multivalent co-ions on the homoaggregation of particles for the first time. It was found that the CCCs of particle suspension are inversely proportional to the valence of the co-ions. The DLVO theory calculations also revealed the same dependence. We proposed the *inverse Schulze–Hardy rule* to summarize this dependence.

DLVO theory is powerful in predicting the aggregation behavior of colloidal particles. However, we described a colloidal system where DLVO theory is only partially valid in quantifying the aggregation behavior. In suspensions of AL particles or SL particles in the presence of Ph_4B^- anions and NaCl, Ph_4B^- anions were found to adsorb strongly on both types of particle surfaces. This leads to an accumulation of negative charge on the particle surfaces, and induces a slow aggregation regime for both AL and SL particles. DLVO theory predicted this aggregation behavior successfully. Furthermore, for both types of particles, an additional region of fast aggregation at intermediate concentrations of Ph_4B^- was observed. DLVO theory failed to predict this intermediate fast aggregation region. We suspect that this region of fast aggregation results from additional attractive non-DLVO forces, which might be induced by surface charge heterogeneities within the adsorbed layer on the particle surfaces. When adding such additional forces into DLVO theory, the updated calculations can reflect the intermediate fast aggregation region reasonably well.

Heteroaggregation processes in mixtures of AL particles (300 nm in diameter) and SL particles (600 nm in diameter) were investigated in the presence of multivalent ions with multi-angle light scattering. Two patterns of heteroaggregation between these two types of particles were identified. In monovalent salt solutions, fast heteroaggregation occurred under all the conditions since these two types of particles were oppositely charged. In solutions containing multivalent ions, one type of particles remained the same charge sign, while the other type of particles reversed their charge. As a result, intermediate region of slow heteroaggregation was observed. This behavior was reproduced by DLVO theory reasonably well. The calculations of the stability ratios for heteroaggregation process were sensitive to the boundary conditions, which were used to calculate double layer forces. The experimental results were close to the calculations for constant potential boundary conditions.

Considering that the heteroaggregation rate measured by multi-angle light scattering was in a narrow range, an approach was proposed to improve the range of measured heteroaggregation rates by increasing the contrast of the scattering profiles between the different aggregates. In the new system of AL particles (302 nm in diameter) and SL particles (250nm in diameter) containing anionic surfactant—sodium n-octyl sulfate (SOS), it was found that the scattering profiles of hetero-aggregates (AL-SL) and homo-aggregates (SL-SL) presented a similar characteristic peak, while homo-aggregates (AL-AL) had a different one. Therefore, the contrast between the scattering profiles can be enlarged by suppressing the homoaggregation of SL particles in the presence of SOS. As a result, the heteroaggregation rates between AL particles and SL particles in the SOS solution could be measured in a much wider range, namely over two orders of magnitude.

Acknowledgement

First of all, I would like to express my deep gratitude to my supervisor, Professor Michal Borkovec, for accepting me as a PhD student in his research group as well as for his advice, guidance, patience and encouragement. He always supported me as much as possible whenever I had difficulties and needs.

I am very grateful to Professor Istvan Szilagyi from the University of Szeged and Professor Gérard Hopfgartner from the University of Geneva for accepting to review my thesis and to be a member of the committee for my PhD defense.

I would like to express my very special thanks to Dr. Gregor Trefalt for teaching me the operation and the theory of light scattering instruments, for the tremendous support and fruitful discussions throughout my PhD studies. I am grateful to Dr. Takuya Sugimoto for his collaboration on *Chapter 4*, whereby he carried out the experiments described in the subsector entitled "Effects of simple salts containing multivalent anions", while my results are described in the subsector entitled "Effects of an aliphatic polyamine and monovalent salt". I would like to thank Dr. Tamás Oncsik for his helps during the days when I started working in the group.

I specially thank our group secretary—Anne-Marie Loup, for her passionate helps, taking care of all the paper work, and a lot of lovely and warm moments she created. Also thanks to our lab technician—Olivier Vassalli, for all his helps like the purchase of experimental materials and TOC measurements. I am grateful to Dr. Plinio Maroni for his friendliness, and his enthusiasm and passion in science, which impressed me a lot.

I would like to thank all current and former members of the research group. It is them who build such a nice atmosphere for study and work. It is impossible to forget our scientific discussions, our lunch chats and hangout times. I am also very grateful to my friends in Geneva. They made my life in Geneva wonderful.

At the end, I would like to express my deepest gratitude to my family. The weekly voice and video chats with my parents make me feel that I am not alone and not far away from home. The greetings and messages from my older brother and younger brother are always arrived just in time, which lightened up my mood over and over. Without their infinite love and support, nothing of this would be happened.